Aurora A regulation by reversible cysteine oxidation reveals evolutionary-conserved redox-control of Ser/Thr protein kinase activity.

Dominic P. Byrne[1*], Safal Shrestha[2,3], Martin Galler[4], Min Cao[4], Leonard Daly[1,5], Amy E. Campbell[1,5], Claire E. Eyers[1,5], Elizabeth A. Veal[4], Natarajan Kannan[2,3] and Patrick A. Eyers[1*]

[1] Department of Biochemistry, Institute of Integrative Biology, University of Liverpool, Liverpool, L69 7ZB, UK

[2] Institute of Bioinformatics, University of Georgia, Athens, GA 30602, USA

[3] Department of Biochemistry & Molecular Biology, University of Georgia, Athens, GA 30602, USA

[4] Institute for Cell and Molecular Biosciences and Institute for Ageing, Newcastle University, Newcastle upon Tyne, NE2 4HH, UK

[5] Centre for Proteome Research, University of Liverpool, Liverpool, L69 7ZB, UK

* Correspondence to dominic.byrne@liverpool.ac.uk or Patrick.eyers@liverpool.ac.uk

ONE-SENTENCE SUMMARY: The catalytic activity of multiple Ser/Thr kinases is regulated through a conserved Cys-based mechanism.

ABSTRACT:

Reactive oxygen species (ROS) are recognized physiological mediators of cellular signaling, and also play potentially-damaging roles in human diseases. In this study, we demonstrate that the catalytic activity of the Ser/Thr kinase Aurora A is inhibited by oxidation of a conserved cysteine residue (Cys 290), which lies adjacent to Thr 288, the activating site of phosphorylation in the activation segment. We find that ~100 human Ser/Thr kinases possess a Cys at this position, which is important not only for the regulated activity of Aurora A, but also fission yeast MAPK-activated kinase (Srk1) and PKA (Pka1). Moreover, the equivalent cysteine is prognostic for biochemical redox-sensitivity amongst a cohort of human CAMK, AGC and AGC-like kinases, including PKA, AKT, AMPK, CAMK1, MAPKAP-K2/3, MELK, SIK1-3 and PLK1/4. We predict that redox modulation of the Cys 290 equivalent may be an underappreciated regulatory mechanism that is widespread amongst subsets of eukaryotic protein kinases. Given the key biological roles of these kinases, our work has important implications for understanding physiological and pathological responses to ROS, and highlights the importance of multivalent activation segment regulation in Ser/Thr kinases.

INTRODUCTION:

Reactive oxygen species (ROS), the collective term for reactive oxygen-derived radicals including superoxide and peroxide, were originally regarded as side-products of oxygen metabolism, but are now recognised as key players in eukaryotic signal transduction [1, 2]. Endogenous redox signaling in cells is induced in response to growth factors such as EGF [1, 3], and ROS are important regulators of cell migration, differentiation and the proliferative cell cycle [4-6]. The sulfur atom of Cys residues, the predominant intracellular redox-signaling molecule, can exist in a variety of oxidation states (fig. S1). In ROS-targeted signaling of proteins, oxidation of a reactive Cys thiolate anion ($Cys\text{-}S^-$) results in the formation of the transient sulfenic acid species (Cys-SOH), which can either undergo further (irreversible) oxidation to sulfinic ($Cys\text{-}SO_2H$) or sulfonic ($Cys\text{-}SO_3H$) acid. The sulfenic species can be stabilised by formation of a disulfide with another Cys or through formation of a cyclic sulfenamide, as established in the case of the tyrosine phosphatase PTP1B, which can be recycled to the thiolate in vivo by glutaredoxin or thioredoxin [7-11]. The reduced glutathione (GSH) pool serves to buffer the cellular environment, with physiological concentrations ranging from ~1 to 10 mM [12-16]. In the cytosol, glutathione exists as both oxidized (GSSG) and reduced (GSH) species, and the GSSG/GSH ratio changes as a function of redox stress [15]. Reversible modification of protein cysteine thiol groups through disulfide bond formation with GSH is therefore considered to be a defence mechanism, protecting proteins against proteotoxic stress caused by irreversible oxidation [17].

Protein phosphorylation on Ser/Thr and Tyr residues controls multiple aspects of eukaryotic life [18]. In order to regulate the precise flow of signaling information, the enzymes that catalyse the addition and removal of phosphate groups are themselves subject to reversible regulation. In the case of Ser, Thr and Tyr kinases, this often involves phosphorylation-based mechanisms in which conserved residues are cyclically phosphorylated and dephosphorylated to control catalysis. A well-known example is the reversible phosphorylation of Ser/Thr and Tyr residues in the conformationally-flexible 'activation segment', which can either be liberated or folded-back onto the kinase to inhibit substrate binding and phosphorylation [19]. The activation segment, also known as the T-loop, is located between the DFG and APE motifs [20], two highly-characteristic regions found in canonical eukaryotic protein kinases (ePKs) [21]. In the case of pTyr regulation, redox control of Tyr phosphatases is well-documented [9, 10, 22], providing an extra layer of regulation in addition to reversible phosphorylation of Tyr kinases such as EGFR [23].

For ePKs, several examples of redox-associated mechanisms have been reported, although the lack of a catalytic Cys in the active-site means that these mechanisms have been centred on

other regulatory regions of the kinase domain, most notably modification of conserved Cys residues in the Gly-rich P-loop. Well-characterized examples of redox-sensitive Tyr kinases regulated by this mechanism include ABL, SRC, EGFR and FGFR [24-27]. In addition, several examples of Ser/Thr kinase regulation through redox-active Cys residues exist, although no overarching evolutionary-based mechanism has been proposed. Examples of eukaryotic redox-regulated proteins containing Ser/Thr kinase domains include ASK1, MEKK1, MELK, PKA, PKG, ERK, JNK and p38 MAPK-family members [28-43].

The discovery of chemically-accessible (and redox-sensitive) Cys residues in protein kinases has created new opportunities for the design of chemical reagents and covalent clinical compounds to target these residues with impressive specificity [44-48]. However, without a common set of biochemical reagents and reliable real-time assay conditions, it is currently challenging to define a common theme or mechanism for redox-based regulation amongst protein kinases, which are assayed under a variety of different biochemical conditions.

Aurora A is an oncogenic Ser/Thr protein kinase [49], which is subject to multi-level, reversible regulation in human cells including phosphorylation/dephosphorylation in the activation segment and allosteric control by accessory factors such as TPX2, TACC3 and protein phosphatases [50-53]. Aurora A activation controls the G2/M transition [54] and is also required for centrosome separation and mitotic spindle assembly [55, 56]. Furthermore, Aurora A-dependent signaling is also implicated in mitochondrial dynamics and metabolism, which are closely associated with the production of ROS [57].

In this study, we report that the catalytic activity of Aurora A is acutely controlled by a specific Cys-based oxidation mechanism. DTT-reversible Aurora A oxidation by a variety of chemical agents occurs through modification of Cys 290, which lies adjacent to Thr 288, the well-established activating 'T-loop' site of phosphorylation. This Cys has been conserved in all Aurora kinases throughout eukaryotic evolution, and we propose that redox modulation of the Cys 290-equivalent in distinct eukaryotic kinases might be a dominant, evolutionary-conserved, mechanism, since ~10% of 285,479 protein kinase-related sequences in the non-redundant (NR) sequence database contains a Cys at this position. In addition, we show that this Cys residue is important for the *in vivo* activity of PKA and a MAPK-activated kinase in fission yeast. We then go on to establish that the presence of a Cys residue is prognostic for redox-sensitivity amongst many human CAMK and AGC-like kinases, but not Tyr kinases, which lack conserved Cys residues in the activation segment. Important examples of redox-regulated Ser/Thr kinases include PKA, PLK1/4, AKT, SIK, AMPK, MAPKAP-K2/3 and CAMK1. Overall, our study demonstrates that redox modification of the activation segment might represent an extra conserved layer of regulation for subsets of eukaryotic protein

kinases, including a significant proportion of the human kinome. These findings have implications for understanding physiological and pathological responses to ROS in cells, and help rationalise numerous lines of experimental evidence demonstrating that reducing agents are often required for the catalytic activity of many Ser/Thr kinases *in vitro*.

RESULTS:

Redox regulation of Aurora A

Human Aurora A was purified to homogeneity in the presence or absence of the reductant DTT, and immunoblotting with a phosphospecific antibody confirmed similar levels of pThr 288 in enzyme preparations, as expected for active, autophosphorylated, Aurora A (fig. S2A). Regardless of whether it was purified under our standard reducing conditions (+DTT) or not, Aurora A activity was inhibited by H_2O_2 in a concentration dependent manner, with ~70 % inhibition observed at 100 μM H_2O_2, even when the ratio of enzyme:peroxide was increased 1000-fold (Fig. 1A and fig. S2B-C). Diamide, which also oxidizes exposed cysteine residues in proteins [58, 59], also inhibited Aurora A activity in a dose-dependent manner (Fig. 1A and Fig.S2C).

A similar degree of inhibition was observed when much higher concentrations of Aurora A were exposed to a gradient of peroxide for 16h, in order to mimic chronic physiological exposure to oxidation (fig. S2B). In contrast, exposure of Aurora A to increasing concentrations of DTT progressively enhanced catalytic activity, regardless of the purification protocol employed (compare Fig. 1A and fig. S2C). To further evaluate the redox response of Aurora A towards a substrate, we employed the physiological Aurora A target TACC3, and confirmed that phosphorylation at Ser 558 was inhibited in a dose-dependent manner by H_2O_2, similar to the Aurora A inhibitor MLN8237 (Fig. 1B). In marked contrast, DTT increased phosphotransferase activity towards TACC3 (Fig. 1B). A prerequisite for Aurora A activation is autophosphorylation on Thr 288 in the activation loop [60, 61], which is generated in this experiment during bacterial maturation prior to purification. Importantly Thr 288 was highly phosphorylated under all of the tested conditions, regardless of the presence of DTT and/or H_2O_2, suggesting that oxidative inhibition of Aurora A was not a result of peroxide-induced dephosphorylation at this regulatory site (Fig. 1B). Next, we sought to establish if H_2O_2 exposure led to irreversible inhibition of Aurora A. We quantified the real-time phosphorylation of a substrate peptide by Aurora A that had been previously exposed to H_2O_2. When H_2O_2 was included in the reaction, only ~15 % of the peptide substrate was phosphorylated after 25 mins, compared to ~60% in its absence (Fig. 1C, left panel). However, supplementing the reaction with DTT restored H_2O_2 –inhibited Aurora A activity, resulting in an immediate increase in the rate of substrate phosphorylation comparable to a control maintained in an oxidized (inhibited) state (Fig. 1C, left panel). Similarly, the activity of Aurora A purified in the presence of DTT, then inhibited by H_2O_2 was also rescued in real-time by the addition of DTT (fig. S2D). In contrast, DTT was ineffective at reactivating Aurora A inhibited by MLN8237 (Fig. 1C, right panel). These findings indicate that the

catalytic activity of Aurora A is reversibly inhibited by oxidation. Importantly, the inclusion of H_2O_2 did not affect the amount of Aurora phosphorylated on Thr 288, although we noted that H_2O_2-treatment did cause a slight increase in the electrophoretic mobility of Aurora A (Fig. 1D, asterisk). This mobility shift was abolished by DTT, consistent with the presence of a reversibly oxidized Cys residue (or residues) in Aurora A [62, 63].

To rule out 'non-specific' kinase inactivation as a result of oxidative protein unfolding or multi-site oxidation, we performed thermal stability measurements for Aurora A incubated in the presence of H_2O_2. The unfolding profile obtained for Aurora A was unaltered by inclusion of H_2O_2, DTT or reduced glutathione (GSH), with T_m values of ~40°C observed under test conditions (fig. S3A). In order to evaluate the consequences of Aurora A oxidation on the ability to bind Mg-ATP, we measured the rate of phosphate incorporation into the peptide substrate in the presence of different H_2O_2 concentrations. Michaelis-Menten kinetic analysis revealed that H_2O_2 treatment significantly reduced the catalytic constant, K_{cat}, of Aurora A, without affecting the affinity for ATP at the highest concentrations tested (inferred from $K_{M[ATP]}$ values) (fig. S3B). Consistent with a lack of direct effects on the nucleotide-binding site, DSF analysis demonstrated that almost identical ΔT_m values were calculated after binding of ATP or the inhibitor MLN8237 in the presence of H_2O_2, DTT or GSH (fig. S3C). Together, these data indicate that oxidation inhibits the ability of Aurora A to drive substrate (peptide and protein) phosphorylation without affecting the affinity for ATP or the thermal stability (unfolding) profile of the enzyme.

Aurora A autoactivation is stimulated by DTT and inhibited by H_2O_2

As an additional measure of the ability of H_2O_2 to inhibit Aurora A activity we investigated the rate of autophosphorylation in Aurora A generated by bacterial co-expression with lambda phosphatase (λPP), which removes all activating phosphate from Thr 288, then subsequently re-purified it to remove residual phosphatase. Accumulation of pThr 288 was then assessed by immunoblotting following the addition of Mg-ATP in the presence and absence of the known allosteric activator TPX2. Under standard assay conditions, Aurora A autophosphorylation was extremely slow, and only trace amounts of pThr 288 Aurora A were detected after 60 mins (Fig. 1E). As predicted, inclusion of DTT and/or TPX2 markedly increased the rate of Aurora A autophosphorylation, whereas no phosphorylation was detected in the presence of H_2O_2, even in the presence of TPX2 (Fig. 1E). These data confirm that, although peroxide treatment does not lead to loss of Thr 288 phosphorylation in phosphorylated Aurora A, reducing conditions are required to stimulate efficient autoactivation of the unphosphorylated 'ground-state' form of the enzyme *in vitro*.

Identification of Cys 290 as the site of Aurora A redox regulation

The observation that Aurora A is reversibly inhibited by H_2O_2 *in vitro* and that this inhibition is associated with a reversible mobility shift (Fig. 1D) raised the possibility that ROS may directly regulate Aurora A activity *in vivo*. The reversible oxidative modification of signaling proteins is associated with oxidation of the sulfur-containing amino acids cysteine and methionine, with the initial oxidation of a specific cysteine-thiol generating a reversible sulfenyl (SOH) derivative (Fig. S1) [64]. To investigate the presence of Cys-SOH in Aurora A, we exploited an antibody that detects SOHs that have been selectively and covalently derivatized with dimedone [5, 6, 65]. Sulfenylated Aurora A was readily detected (Fig. 2A), with the signal increasing progressively after exposure to increasing concentrations of H_2O_2 (Fig. 2B). Incubation of Aurora A with DTT markedly-reduced dimedone-labelling (Fig. 2B), consistent with the regeneration of Cys thiols, which are refractory to dimedone adduct formation. Importantly, no labelling of the protein was detected in the absence of dimedone, confirming antibody specificity (Fig. 2A).

To identify potential redox-sensitive Aurora A residues, we employed the bioinformatics tool Cy-preds [66], which highlighted the surface residue Cys 290 as a potential target for oxidative modification of the seven human Aurora A Cys residues. Cys 290 is highly conserved, and lies within the canonical activation segment, in very close proximity to the regulatory Thr 288 side-chain. Interestingly, the equivalent Cys in PKA has previously been analysed in terms of redox regulation, with a role for Cys 200 established *in vitro* [59, 67]. To assess whether regulatory oxidative modification of Aurora A could be specifically assigned to Cys 290, we generated Aurora A containing a Cys to Ala substitution at this position (fig. S4A). When compared to WT Aurora A, incorporation of the C290A mutation had no effect on protein thermostability (T_m ~40°C, fig. S4B) measured by DSF [68, 69] or ΔT_m values induced by ATP or inhibitor (MLN8237) binding (fig. S4C). Furthermore, $K_{M[ATP]}$ values obtained in peptide-based kinase assays were virtually identical for both kinases, although the C290A mutant exhibited decreased activity (~50 % of WT, fig. S4D). This latter observation is consistent with previous analysis of a C290A Aurora A mutation [70], and emphasizes the potential importance of this residue as a regulatory hot-spot within the activation loop.

We next tested whether Cys 290 might be prone to oxidation by comparing the H_2O_2-induced sulfenylation of WT and C290A Aurora A. Immunoblotting revealed dimedone labelling was greatly diminished in C290A Aurora A compared to WT, indicative of a reduction in the number of Cys residues undergoing sulfenylation (Fig. 2C). Critically, mutation of Cys 290 protected Aurora A from inhibition by H_2O_2 (Fig. 2D). This manifested as an increase in the half-maximal inhibitory concentration (IC_{50}) of H_2O_2 from ~35 μM for WT Aurora A to ~10 mM for C290A Aurora A. Concomitantly, C290A mutation abolished DTT dependent activation of Aurora A (Fig. 2E). Finally, we investigated C290A Aurora A-dependent

phosphorylation of TACC3, observing that catalytic activity towards this physiological substrate was unaffected by the presence of either reducing or oxidizing agents (fig. S4E). Together these results confirm that Cys 290 plays a central role in a new regulatory mechanism that underpins Aurora A kinase activity *in vitro*, and suggests that this may be a direct result of a switch between oxidized 'inactive' and reduced 'active' catalytic states.

The reduced C290A phosphotransferase activity in comparison to WT Aurora A (fig. S4) indicated that an Ala substitution was not optimal in terms of catalysis. Based on its similar size, structure and hydrophilic properties, Ser is potentially a better-suited (non-redox-sensitive) mimic of this Cys residue. However, introduction of a Ser (or Asp) residue at the Cys 290 position generated Aurora A that was devoid of Thr288 phosphorylation (fig. S5A) despite no detectable changes in protein stability (as judged by T_m values, fig. S5B) or binding to ATP or MLN8237 (fig. S5C), confirming an inability of the kinase to autophosphorylate and autoactivate. Consistently, both C290S and C290D mutants were also completely catalytically inactive when evaluated real-time (fig. S5D). These observations reveal the extraordinary sensitivity of Aurora A to modest structural perturbations at the Cys 290 position, and further establishes the potential regulatory role of this conserved site in the activation segment. In agreement with published findings, PKA activity was also inhibited in a concentration dependent manner by H_2O_2 [59, 67, 71] whereas DTT modestly stimulated kinase activity (Fig. 2F). Importantly, and in agreement with previous findings [59], the inhibitory effect of H_2O_2 was completely abrogated in the site-specific cysteine mutant PKA C200A (Fig. 2G). Moreover, inhibition of PKA by H_2O_2 was due to the reversible oxidation of a sulfhydryl residue, since activity could be fully restored in real-time by DTT exposure (Fig. 2F).

TPX2 protects Aurora A from inactivating oxidation

In addition to autophosphorylation of Thr 288 in the activation loop, which lies adjacent to Cys 290 (Fig. 2H), Aurora A can be activated allosterically by interaction(s) with the spindle assembly factor TPX2 [50, 72-75]. Given that binding to TPX2 and phosphorylation of the activation loop are complementary mechanisms for Aurora A activation, we investigated redox regulation of Aurora A in the context of TPX2. First we considered the effect of redox state on the interaction between Aurora A and TPX2. Aurora A was exposed to increasing concentrations of H_2O_2 or DTT and then evaluated for its ability to interact with GST-tagged TPX2. GST pull-down assays revealed that Aurora A remained associated with GST-TPX2 even at the highest concentrations of H_2O_2 and DTT employed (fig. S6A). Thus, the redox state of Aurora A had no detectable effect on binding to TPX2 in vitro. Next, we examined inhibition of Aurora A by H_2O_2 in the presence of TPX2. The phosphorylated activation loop

of Aurora A has recently been shown to adopt a range of conformations in solution, only becoming highly ordered in a stable 'DFG-in' conformation upon TPX2 binding [75]. Furthermore, both 'inactive' unphosphorylated and 'active' phosphorylated Aurora A adopt similarly well-defined structures upon TPX2 binding, resulting in an increase in kinase activity [51, 75]. We found that TPX2 increased the resistance of Aurora A to inhibition by H_2O_2, increasing the IC_{50} [H_2O_2] value to > 1 mM (Fig. 2I). Importantly, the modest inhibitory effect of H_2O_2 on the TPX2-Aurora A complex could be completely reversed in real-time upon addition of DTT (Fig. 2J). Allosteric activation of Aurora A by TPX2 is therefore sufficient to overcome kinase inactivation by oxidation under these conditions. It is possible that oxidation of Aurora A at Cys 290 alters the structural dynamics of the activation loop and stabilizes a less active subpopulation, with activity being recapitulated following binding to, and structural reorganization by, TPX2. This is supported by the observation that C290A Aurora A, which displays lower kinase activity compared to the WT protein, is also strongly activated by TPX2 binding, but unlike WT Aurora A remains resistant to inhibition by H_2O_2 when TPX2-bound (fig. S6B, C). Importantly activities of WT and C290A Aurora A were unaffected by GST (fig. S6C). Furthermore, C290S (but not C290D) Aurora A, which lacks kinase activity (and phosphorylation at Thr288) when evaluated in isolation, was partially activated in the presence of TPX2 (but not DTT) in our peptide assay, and displayed clear phosphotransferase activity towards TACC3 (fig. S6D, and E).

Aurora A can also be activated by glutathionylation on Cys290

Sulfenylated cysteines are susceptible to further, irreversible, oxidation. In vivo, reversibility can be ensured by formation of a disulphide with a cysteine in glutathione or another protein (fig. S1). We therefore investigated the influence of reduced (GSH) or oxidized (GSSG) glutathione alongside a panel of other redox-active compounds on Aurora A activity. Aurora A activation by the reducing agents DTT, tris(2-carboxyethyl)phosphine (TCEP) and 2-mercaptoethanol (2-ME) was confirmed by enhanced rates of peptide substrate phosphorylation compared to control assays (Fig. 3A). Notably, the inclusion of GSH (or GSSG) in the assay also induced a measurable increase in activity (Fig. 3A). This increased Aurora A activity is in contrast to PKA, which is reported to be inhibited by GSH [59]. Consistently, C290A Aurora A was more resistant to activation by these reducing agents (Fig. 3B). Importantly, and in contrast to WT Aurora A, which demonstrated concentration-dependent activation by GSH, C290A Aurora A only exhibited modest increases (~1.5-fold) in activity at the highest tested GSH concentrations (Fig. 3C). Next we investigated whether modulation of Aurora A activity was a consequence of mixed disulfide formation between Cys 290 and glutathione. To probe for glutathionylation, we employed an antibody that specifically reacts to protein-glutathione complexes (Fig. 3D). PKA was included as a

positive control as it has previously been shown to be glutathionylated [59]. Glutathionylation was readily detected for WT Aurora A incubated with GSSG, but not for the C290A mutant, suggesting that changes in Aurora A activity were a direct result of glutathionylation of this cysteine (Fig. 3D)(fig. S7A). However, despite stimulating Aurora A activity, addition of GSH alone was insufficient to restore the activity of oxidized Aurora A (Fig. 3E), which required reduction by DTT (fig. S7B) or enzymatic deglutathionylation by glutaredoxin-1 (GRX) (fig. S7C) to restore Aurora A catalytic activity. The AGC kinase AKT has previously shown to be regulated by glutathione-dependent mechanisms [36]. To confirm AKT glutathionylation using real-time assay, PDK1-phosphorylated S473D AKT was incubated with GSH in the presence and absence of H_2O_2. Similar to Aurora A, AKT was covalently modified by glutathione (Fig. 3F). The catalytic activity of AKT was enhanced several hundred-fold by GSH exposure in the absence of H_2O_2 (fig. S7D). Furthermore, the activity of AKT was rapidly inhibited by oxidation, and could be restored by the addition of DTT. The subsequent addition of GSH did not rescue activity (Fig. 3G), as demonstrated for Aurora A.

Oxidative stresses inhibits Aurora A substrate phosphorylation in human cells

To validate our *in vitro* findings, we next investigated whether Aurora A activity is redox-regulated in human cells, employing the endogenous substrate TACC3 phosphorylation as an intracellular read-out for Aurora A activity [76, 77]. HeLa cells were initially synchronized with nocodazole, and then exposed to H_2O_2 or DTT for 30 mins. Western blotting revealed a dose-dependent decrease in TACC3 phosphorylation at Ser 558 in cells treated with H_2O_2 compared both to control cells, and those treated with DTT (Fig. 4A-B). As expected, cells incubated with the Aurora A inhibitor MLN8237 demonstrated complete loss of TACC3 phosphorylation (Fig. 4A), whereas nocodazole exposure alone, which has recently been shown to enhance the oxidation of Cys residues [5], did not lead to net Aurora A inhibition. We next determined the effects of the cell-permeable oxidant diamide [58]. Strikingly, the extent of TACC3 phosphorylation was inversely proportional to the diamide concentration, analogous to observations with H_2O_2 (Fig. 4C). Menadione is a quinone oxidant that stimulates rapid generation of cellular ROS through redox-cycling [78]. Menadione exposure also caused a concentration-dependent inhibition of TACC3 phosphorylation (Fig. 4D). Aurora A protein levels were not affected by H_2O_2, diamide or menadione eliminating the possibility that degradation was the cause of reduced TACC3 phosphorylation. (Fig. 4A-D). Finally, we investigated the effect of chronic oxidative stress on Aurora A activity. Glucose oxidase (GO) was added to nocodazole-containing culture medium at a non-toxic concentration (2 U/ml) to facilitate the generation of peroxide. At this level of enzyme activity, GO is reported to generate intracellular steady-state levels of H_2O_2 of 1-2 μM [79-

81]. As shown in Fig. 4E, GO also resulted in a time-dependent decrease in TACC3 phosphorylation. To evaluate the physiological relevance of Aurora A redox regulation as a signaling mechanism, we also investigated the reversibility of inactivation. Cells were exposed to H_2O_2 prior to incubation with DTT or the cellular antioxidants GSH and N-acetyl-L-cysteine (NAC). Under these conditions, TACC3 phosphorylation was restored to basal levels by both GSH and NAC, presumably due to ROS scavenging (Fig. 4F). However, in the presence of H_2O_2, DTT was unable to rescue TACC3 phosphorylation.

Next, we analyzed Cys 290-based regulation in Aurora A. HeLa cells were transiently cotransfected with GFP-tagged TACC3 in the presence or absence of either WT or C290A Myc-tagged Aurora A, and synchronised with nocodazole in order to activate Aurora A. GFP-tagged TACC3 became phosphorylated at Ser 558 by endogenous Aurora A following nocodazole treatment, with a concomitant decrease of phosphorylation at this site in the presence of diamide (Fig. 4G). Transient overexpression of either WT or C290A Myc-tagged Aurora A also led to an increase in GFP-TACC3 phosphorylation at Ser 558. Importantly, we detected a diamide-induced, dose-dependent decrease in GFP-TACC3 phosphorylation co-transfected with WT Aurora A, consistent with inhibition of Aurora A by oxidation. In contrast, the inhibitory effect of diamide on GFP-TACC3 phosphorylation was blunted in cells expressing C290A Aurora A (Fig. 4G). Taken together, these data suggest that C290 in Aurora A is important for inhibition of Aurora A kinase activity in response to oxidants in cells.

Cys residues are evolutionary conserved in a variety of ePK activation segments

Cys is the second least-common amino acid in vertebrate proteomes [82], and although >200,000 Cys residues are present in the human proteome, they are often conserved in redox 'hot-spots' [83]. Reactive Cys side chains, especially those lying on surface-exposed regions of proteins [66], are often susceptible to redox modification (fig. S1). To investigate the potential generality of Cys-based redox mechanism in protein kinases that possess an activation segment, we analyzed >250,000 protein kinase related sequences, confirming that ~11.5% of ePKs found across the kingdoms of life possess the Cys 290 equivalent of Aurora A (Fig. 5A). This number reduced to 1.4% of all ePKs when the co-conservation of Cys residues at the DFG +2 and 'T-loop +2' positions, which individually are the most prevalent in these kinases, were considered side-by-side (Fig. 5A, bottom). Strikingly, the Cys 290-equivalent residue (see Table 1) was very strongly associated with two of the seven human kinase groups: the AGC kinases and the CAMKs (Fig. 5B), and this pattern was also observed in kinomes from all the kingdoms of life, including model genetic organisms such as fungi (fig. S8A-E). Intriguingly, Cys residues are encoded locally in eukaryotic kinomes at

every possible position within the conserved activation segment (fig. S8F and Table 2). However, analysis of all canonical human kinases and pseudokinases demonstrated that most of the Cys-containing kinases belong to families encoding Ser/Thr kinases, notably stress-activated protein kinase kinases such as MAPKAP-K2/3, MKK3, MKK4, MKK6 and MKK7 and Cys-rich pseudokinases such as Tribbles 1-3 [69], all of which possess a conserved Cys at the DFG + 4 position [84].

The conserved redox-sensitive cysteine is important for the *in vivo* activities of the fission yeast PKA, Pka1, and the MAPK-activated kinase, Srk1

Having established that C290 is important for the activity and redox-sensitivity of human Aurora kinase, we investigated whether the equivalent Cys was important for the *in vivo* activity of well-characterised examples of the AGC and CAMK groups in the fission yeast *Schizosaccharomyces pombe*, by studying the single PKA catalytic subunit (Pka1) and the MAPK activated kinase, Srk1, which is a homologue of human MAPKAP-K2[85, 86].

Initially, we examined whether C358, equivalent to C200 in human PKA (Fig. 5C & 6A), was important for the activity of the single catalytic subunit of PKA, termed Pka1, by ectopically expressing wild-type Pka1 or Pka1 in which C358 was substituted with serine (C358S) or alanine (C358A) in Δ*pka1* mutant cells. Immunoblotting with antibodies that recognise cellular phosphorylated PKA substrates [87] detected fewer bands in *pka1* mutant cells than wild-type (*pka1*$^{+}$) cells, confirming that these bands represented substrates of Pka1. Notably, high-level ectopic expression of wild-type Pka1 restored the missing phosphorylated Pka1 substrate signals, increasing their intensity to wild-type levels, and confirming that Pka1 substrate phosphorylation was restored. In contrast, despite similar expression (Fig. 6B) Pka1^{C358S} and Pka1^{C358A}, only partially restored Pka1 activity (Fig. 6B). Pka1 has a number of well-established roles in regulating *S. pombe* growth and survival under stress conditions. For example, Δ*pka1* mutant cells are unable to adapt and grow in high salt conditions [88] (Fig. 6C). We therefore examined whether C358 in Pka1 was important for adaptation to high salt by comparing the growth of Δ*pka1* mutant cells expressing wild-type Pka1, Pka1^{C358S} or Pka1^{C358A} on plates containing 1M KCl. Consistent with C358 playing an important role in Pka1 activity, neither Pka1^{C358S} and Pka1^{C358A} was able to restore growth to the same extent as wild-type Pka1 (Fig. 6C).

Next we examined whether the equivalent conserved cysteine was important for the activity of the MAPK-activated kinase Srk1. Srk1 expression delays entry to mitosis by phosphorylating the dual-specificity phosphatase CDC25 [89]. Accordingly, in cells ectopically over-expressing Srk1 from a multi-copy plasmid CDC25 is excluded from the

nucleus, causing a G2 delay that results in some substantially elongated cells (Fig. 6D), and increases the mean length of cells at mitosis (Fig. 6D). In contrast, despite similar expression levels (Fig. 6E), ectopic expression of Srk1^{C324S} or Srk1^{C324A} produced a much more modest increase in cell length (Fig. 6D) and failed to block nuclear localisation of CDC25 (Fig. 6F). This permits us to conclude that C324 in Srk1 is important for the *in vivo* activity of Srk1 in delaying mitotic entry by phosphorylating CDC25 [89]. Together these data establish that the T-loop +2 Cys plays an important role in the in vivo activity of both these kinases, raising the possibility that redox modification of this cysteine may regulate the roles of these kinases in controlling cell division and stress resistance.

Analysis of human MAPKAP-K2 and Polo-like kinases.

To further investigate the importance of the T-loop +2 Cys in redox regulation, we analysed a variety of T-loop + 2 Cys-containing kinases (Fig. 5C), beginning with MAPKAP-K2, PLK1, and PLK4, which were assayed using the redox microfluidic kinase assay developed for Aurora A, but individually modified to include kinase-specific peptide substrates (Table 2). To aid comparison, the activity of each kinase was measured in the presence or absence of increasing concentrations of H_2O_2 or DTT and the reversibility of redox-dependent modulation measured using the H_2O_2 and DTT 'rescue' procedure developed for Aurora A.

Recombinant bacterially-expressed GST-tagged MAPKAP-K2 was activated by DTT, and inhibited by peroxide, but was reactivated by subsequent exposure to DTT (Fig. 7A). To evaluate this effect in MAPKAP-K2 purified from human cells, we generated 3C protease-cleavable MYC-tagged constructs of WT and C244A MAPKAP-K2 and purified them from HEK 293T cells (Fig. 7B). Following immunoprecipitation, bound proteins were eluted using 3C protease, and then assayed in real-time the presence of DTT or diamide. Strikingly, the inhibitory effect of diamide on WT MAPKAP-K2 activity was reduced in the C244A MAPKAP-K2 mutant (Fig. 7C), confirming this cysteine is required for full oxidative inhibition of this kinase.

The Aurora kinases and Polo-like kinases (PLKs) both perform complementary mitotic roles [90]. The PLK family are stringently regulated multifaceted modulators of mitosis and cytokinesis [91], and the close regulatory relationship between PLK1 and Aurora A in mitosis [54, 92] led us to investigate potential redox regulation for PLK1 and PLK4. [93]. We demonstrated dose-dependent activation and inhibition of bacterially-expressed truncated PLK1 by DTT and H_2O_2 respectively (Fig. 7D), and inhibitory oxidation was completely reversed in real-time by subsequent exposure to DTT (Fig. 7E). However, mutation of the T-loop +2 Cys residue of truncated PLK1 (amino acids 1-361) purified from *E.coli* resulted in a kinase that was catalytically inactive, which prohibited further analysis. We next

immunoprecipitated full-length PLK1 from human cells (Fig. 7F) and compared WT and C212A PLK1 using the same substrate peptide (Fig. 7G). Consistently, full length PLK1 was inhibited by both diamide and the inhibitor BI2536 (Fig. 7G). Interestingly, not only was full-length C212A PLK1 catalytically active, but peptide phosphorylation was preserved under experimental conditions that led to the complete inactivation of WT PLK1 (Fig. 7G). Additionally, we evaluated the related Ser/Thr kinase PLK4, a 'master' centrosomal kinase [94, 95], which possesses a conserved Cys residue (Cys 172), +2 residues from the T-loop autophosphorylation site (Thr 170). Consistently, PLK4 was reversibly inhibited by H_2O_2 and activity was both rescued and stimulated under reducing conditions (Fig. 7H). Moreover, C172A PLK4 was refractory to inhibition by oxidation, confirming the role of this Cys residue as a central regulator of catlalytic activity (Fig. 7I). Supporting the evolutionary relevance of these novel findings, analysis of homologous kinases demonstrated that the Cys 290-equivalent was conserved across all known eukaryotic Aurora, PKA and Polo-like kinases (fig. S8A-E)

The presence of a Cys at residue DFG + 2 converts Aurora A into an enzyme that requires DTT for activity.

To help understand the mechanism of redox regulation in Aurora A, we investigated the DFG +2 amino acid in Aurora A, which is a Ser or Ala in all multicellular vertebrates (Fig. 8A), but which is a Cys in many apicomplexan and fungal species. We first analysed purified Aurora A DFG +2 mutants side-by-side (fig. S10A). The presence of an Ala residue at position 278 did not change thermal stability (fig. S10B, C) or alter the redox-sensitive catalytic output of Aurora A (Fig. 7B, left and middle), whereas introduction of a Cys residue had a dramatic effect, with S278C exhibiting a ΔTm of 5°C and an absolute requirement for DTT in order to drive catalytic activity (Fig. 8B, right and Fig. 8C and 8D). Like WT Aurora A, S278A was still reversibly inhibited by peroxide and activated by DTT, in contrast to S278C, which was inactive until DTT was spiked into the assay (Fig. 8E, right panel). Immunoblotting confirmed that S278C contained lower levels of Thr288 autophosphorylation after purification (fig. S10D), which likely contributes to lower activity, but which cannot explain the dramatic, and instantaneous, effect of DTT on catalysis. We predicted that the obligate requirement for DTT to activate S278C Aurora A was due to an inhibitory intermolecular disulfide bond forming between Cys 290 and the newly introduced Cys 278, in a manner analogous to other DFG 2+ cysteine containing kinases that also possess cysteines at the T-loop +2 position, such as AKT and MELK (see below). This hypothesis was confirmed by inspection of peptides derived from S278C Aurora A by liquid chromatography-tandem mass spectrometry (LC-MS/MS), which revealed the presence of a

DTT-reversible intramolecular disulfide bond formed between Cys 278 and Cys 290 that was absent in WT Aurora A (Fig. 8F).

AKT and MELK require the presence of a reducing agent for catalysis.

Under identical assay conditions to those described above, we next confirmed that the inclusion of DTT in the buffer enhances AKT catalytic activity several hundred-fold (Fig. 8G). In contrast, oxidation completely prevents AKT-dependent substrate peptide phosphorylation, although activity can be restored, or even enhanced, by subsequent DTT exposure, similar to our findings with S278C Aurora A. Consistently, both of these proteins contain spatially-related Cys residues in the activation segment (Fig. 5A and Fig. 8A). Maternal embryonic leucine zipper kinase (MELK) is a member of the CAMK kinase grouping, and is closely related to the AMPK-related kinases [96, 97]. Redox regulation of MELK has previously been reported, although precise regulatory mechanisms remains unclear [98]. Interestingly, the activation segment of MELK contains two consecutive Cys residues (Fig. 5C), one of which might form an intermolecular disulfide bond with a Cys supplied by the DFG +2 Cys, as previously described for an inhibited oxidized state of AKT[36, 99]. MELK exhibited very low activity in the absence of DTT, with activity increasing several hundred-fold after inclusion of DTT in the assay (Fig. 8H). H_2O_2 inhibited MELK activity in a dose-dependent manner, and DTT-dependent activation was so pronounced that MELK activity rapidly surpassed control levels when DTT was used to 'rescue' H_2O_2-inhibition (Fig. 8I). Individual C168A and C169A point mutation blocked DTT-dependent MELK activation, but neither mutation in isolation completely abrogated MELK redox-sensitivity, particulary oxidation by peroxide (Fig. 8I). However, combined mutation (C168A/C169A MELK) abolished DTT-dependent activation, and these Cys mutations diminished dimedone adduct formation, especially under control conditions in the absence of peroxide (fig. S9B), extending previous findings [98].

Evaluation of redox regulation in a Cys-containing CAMK and AGC kinase panel

To establish generality for a Cys-based mechanism of Ser/Thr kinase regulation, we increased the scope of our analysis to incorporate a panel of protein kinases containing an evolutionary-conserved Cys residue in the T-loop +2 position of the activation segment (Fig. 5C). All enzymes were purified (or supplied) in the presence of 1 mM DTT, and assayed in real-time using peptide substrates. Catalytic activity was quantified in the presence of additional DTT, H_2O_2 or H_2O_2 followed by DTT. Remarkably, the majority of kinases tested displayed redox-dependent regulation. Redox analysis of MAPKAP-K3 demonstrated potent inhibition of enzyme by peroxide (Fig. 9A). Consistent, with our observations with GST-MAPKAP-K2 (Fig. 7A), DTT also activated and restored activity to peroxide-treated MAPKAP-K3 (Fig.

9A). The removal of the GST tag in the MAPKAP-K3 preparation eliminating any possibility that the redox regulation of kinase activity was mediated by the affinity tag (Fig. 7A).

The 5'-AMP-activated protein kinase holoenzyme complex (AMPK, comprised of α1, β2 and γ1 subunits) is a member of the CAMK family and was also inhibited by H_2O_2 in a DTT-reversible manner (Fig. 9B). These findings support a growing body of evidence that ROS participate in the regulation of AKT and AMPK activity, although the precise mechanisms remain controversial. Interestingly, direct activation of AMPKα catalytic subunits in the presence of H_2O_2 has previously been described [100], whereas inhibition of AMPKα activity through Cys130/174 oxidation has also been reported [34]. Cys174 in AMPKα is analogous to Cys 290 of Aurora A, and is situated two amino acids C-terminal to the Thr172 phosphorylation site, the critical positive modulator of AMPK activity by 'upstream' kinases. The salt-inducible kinases (SIK1-3) are members of the AMPK-related family of CAMKs [101] and all contain a T-loop + 2 Cys residue. Consistently, purified SIK1-3 were all reversibly inhibited after H_2O_2 exposure (Fig. 9C-E). Interestingly, H_2O_2 was also weakly- and reversibly inhibitory towards phosphorylase kinase, PHKγ, a member of the CAMK group (fig. S11A).

Protein Kinase G (PKG) belongs to the AGC group of kinases, although its mechanism of regulation is distinct from that of closely related PKA and PKC isozymes. However, and in contrast to other T-loop Cys-containing AGC kinases tested (including PKA and AKT), there was no evidence for oxidative inhibition of the PKG1 splice variants PKG1-1 or PKG1-2, when they were assayed in either the absence, or presence, of cGMP (fig. S11B-E), which is consistent with recent findings [38]. In contrast, oxidative modification of PKG1-1 (but not PKG1-2) was previously suggested to result in activation of the kinase in a cGMP-independent manner [31], but we were unable to detect such an effect using our assay system (fig. S11).

CAMK1 has been reported to be inhibited by glutathionylation of Cys179 in the activation segment [102]. Consistently, we found that oxidation was sufficient to inactivate two isoforms of CAMK1, CAMK1A and CAMK1D, both of which were assayed in an identical fashion (Fig. 9F-G). Inactivation is potentially as a consequence of Cys179 oxidation, and likely independent of the GST affinity tag, since it was proteolytically excised in the CAMK1A sample, but still present in CAMK1D. Consistently, DTT exposure reversed H_2O_2-dependent inhibition of both CAMK1 isoforms (Fig. 9F-G). The related kinase CAMK2 lacks an activation segment T-loop + 2 Cys residue, but redox-regulation of dual-Met residues has been reported to promote CAMK2 activation by stabilizing a calcium/calmodulin-independent species [103]. Consistently, CAMK2G, was robustly activated by DTT, and

inhibited reversibly by H_2O_2 (Fig. 9H), suggesting a non Cys-activation segment mechanism of redox regulation for this kinase. In contrast, CAMK2D was completely resistant to changes in redox when assayed in the presence of Ca^{2+} and calmodulin (Fig. 9I), demonstrating that neither peroxide nor DTT act as non-specific regulatory factors for these recombinant kinases under our experimental conditions. Taken together, our data suggest that redox regulation is a conserved, reversible mechanism for multiple Ser/Thr protein kinases in vitro.

Finally, we examined redox regulation in Tyr kinases, which with a few exceptions (Table 2), do not contain any conserved Cys residues in the activation segment, and as a family possess none at-all at the T-loop +2 position (Fig. 5B). The EPHA3 Tyr kinase domain was completely resistant to inhibition or activation by peroxide and DTT respectively (fig. S12A). ABL also lacks a T-loop Cys residue but is known to be susceptible to alternative modes of redox-dependent regulation [104]. Reversible inactivation of ABL by peroxide was also readily observed in our assays (fig. S12B). We next attempted to sensitize EPHA3 to Cys-based redox regulation by incorporating Cys residues at equivalent positions in the activation segment (Fig. 5C). However, both G784C and a double mutant EPHA3 protein containing G783C and G784C substitutions remained unresponsive to peroxide or DTT (fig. S12D, E), whereas G783C EPHA3 lacked any detectable phosphotransferase activity (fig. S12C), suggesting that this Gly residue is critical for activity.

DISCUSSION:

Aurora A is a redox-sensitive Ser/Thr kinase

In this study, we demonstrate that Aurora A is susceptible to reversible, oxidative-inactivation in vitro and in cells, by a mechanism that involves cysteine (Cys 290) located in the conserved activation loop, two amino acids C-terminal to the regulatory site of T288 autophosphorylation.

The nature of the oxidation events(s) in Aurora A are currently unclear. We employed an antibody with specificity towards Cys-SOHs that have been covalently derivatized with dimedone, to monitor alterations in Aurora A SOH content. These data unequivocally demonstrated direct oxidative modification of Aurora A at Cys residues after exposure to H_2O_2 resulting in an increase in total protein sulfenylation (Fig. 2). Interestingly, not all Cys residues are equally susceptible to oxidation in proteins, with those that have a functional role in redox-dependent signaling often possessing a low pKa value of approximately 5.0 [105]. Moreover, the solvent accessibility and the structural micro-environment impact the reactivity of Cys-residues [66, 105]. In addition to SOH, reversible Cys-sulfenamides have also been implicated as targets of dimedone adduct formation, and we are currently undertaking detailed investigation to formally distinguish between these two reversibly oxidized thiol species [11] in Aurora A. Direct *S*-glutathionylation of Aurora A was also detected at Cys 290 (Fig. 3), which is consistent with disulfide exchange between GSSG and reactive Cys thiolates in the kinase that can stabilize the partially oxidized sulfenic form by formation of a disulfide with Cys in glutathione ion order to prevent irreversible oxidation (fig. S1). The presence of sulfenylated (or sulfenamide) Cys in Aurora A was of particular interest, since this is a reversible Cys-modification and might therefore function as a bona fide signaling mechanism in response to cellular oxidative stress, as previously described PTP1B [22]. Our observation that C290A Aurora A was still modified by dimedone, albeit to a lesser extent than for control Aurora A (Fig. 2C), provides evidence for the existence of additional redox active Cys residues, although their relevance for regulating catalytic activity appears to be minor and we establish here that Cys290 is required for oxidation and inhibition of Aurora A. Interestingly, a very recent study found that Aurora A can be covalently modified by the sulfhydryl moiety of the Cys-containing metabolite CoA under appropriate redox conditions, and that an intermolecular disulfide bond with Cys 290 in an adjacent Aurora A might contribute to an oxidative mechanism of inhibition [106]. Future work will evaluate the relative contribution of disulfide bond formation in this, and other, redox-sensitive Ser/Thr kinases analysed in this paper.

584 Using Cy-preds [66], which combines structural energetics and similarity-based
585 considerations, we identified Cys 290 in Aurora A as a very high-probability target for
586 oxidation. The location of this residue on the activation loop (or T-loop) of Aurora A is
587 notable, as this region is a well-known regulatory locus for the modulation of catalytic
588 activity in many eukaryotic protein kinases [107, 108]. We propose that Cys 290 in Aurora A
589 is strategically positioned to trigger a regulatory response to ROS, or for protection from
590 over-oxidation by covalent glutathionylation. This hypothesis has previously been explored
591 for equivalent activation loop Cys residues including Cys 200 of PKA [59, 71], Cys 310 of
592 AKT [109], Cys174 of AMPK [34], and Cys179 of CAMK1 [102]. Structural analyis of AKT
593 previously described an oxidized intramolecular species, likely to be the catalytically-inactive
594 version present upon exposure to peroxide in our studies (Fig. 8A and fig. S13). Together, our
595 findings establish Cys 290 as a likely target of oxidative modification and a dominant
596 coordinator of redox regulation in Aurora A. Although it is unlikely that Cys 290 directly
597 participates in substrate phosphorylation by Aurora A, maintaining a reduced sulfhydryl at
598 this position appears to be required for enzyme activity in the absence of allosteric regulators
599 such as TPX2, which serve to protect Aurora A from oxidative inhibition in vitro (Fig. 2).

600 **Cellular modulation of Aurora A activity by reversible oxidation.**

601 The findings from our biochemical studies are strongly supported by cellular data. We
602 observed inhibition of TACC3 Ser558 phosphorylation (a physiological marker of Aurora A
603 activity) in cells exposed to both oxidants and inducers of oxidation (Fig. 4). In addition,
604 inhibition of Aurora A by H_2O_2 could be blocked by including ROS-scavengers such as NAC
605 and GSH in the culture medium, either restoring oxidized Aurora A back to a reduced,
606 catalytically-active state or by protection of Aurora A from over-oxidation (Fig. 2). The
607 inability of DTT to restore Aurora A activity in vivo likely reflecting its profound cellular
608 effects on the oxidation state of ER proteins and subsequent enhanced ROS generation as part
609 of the unfolded protein response[110]. Furthermore, phosphorylation of exogenous TACC3
610 under highly oxidative conditions could be induced through transient co-expression with a
611 'redox-resistant' C290A Aurora A mutant, supporting a physiological regulatory role for the
612 T-loop +2 Cys residue in a cellular context. Interestingly, oxidative stress has been shown to
613 impede mitotic progression of cells via a number of different mechanisms [111, 112]. To
614 ensure that changes in signaling were a direct consequence of oxidative modification of
615 Aurora A, and not just due to cell cycle inactivation of the kinase, all of our experiments were
616 performed using synchronized cells arrested in mitosis with nocodazole [5]. Previous
617 observations demonstrated hyperphosphorylation of Aurora A at Thr 288 in HeLa cells under
618 oxidative stress [113], which was proposed as a mechanism for ROS-induced mitotic arrest.
619 Although Thr 288 autophosphorylation is a kinase-activating prerequisite (Figure 1), a

growing body of evidence suggests that monitoring this phosphorylation site is not ideal for reporting Aurora A catalytic activity in cells [114]. In this regard, it is noteworthy that phosphorylated Thr 288 can also potentially be generated by non-autophosphorylation mechanisms [115, 116], whose sensitivity to redox regulation may differ. Furthermore, Aurora A regulation is a dynamic, multi-layered process involving several regulatory steps that are uncoupled from autophosphorylation, including allosteric activating complexes formed with non-catalytic protein binding partners [117]. Based on our data, we propose that Aurora A-dependent phosphorylation of TACC3 at Ser 558 is an ideal biomarker for reporting Aurora A redox-regulated activity, since Aurora A is the only kinase known to target this site physiologically. In support of this finding, an increase in Aurora A autophosphorylation and CoAlation is also found in cells treated with inducers of oxidative stress [118]. Regardless of the mechanism, complex spatio-temporal regulation means that caution should be applied when interpreting changes in cellular Aurora A catalytic outputs, especially if changes in the redox environment are induced or suspected.

A conserved propensity for Ser/Thr kinase regulation by redox?

The redox regulation of signaling enzymes is a rapidly expanding field of study. Whereas the majority of early research focused on the indirect targeting of kinases through oxidative inhibition of protein tyrosine phosphatases [105], there is now a wealth of evidence detailing direct oxidation of Cys and Met residues in protein kinases, where diversity within kinase groups and subfamilies has been reported [119, 120]. However, although Cys-dependent redox regulation has been described within stress-activated protein kinase modules, including thioredoxin-regulated ASK1 [32, 121, 122], MEKK1 [123], MKK6 [124], and glutathione-responsive JNK and p38α-MAPK [125], to our knowledge, no conserved mechanism has been described. Moreover, none of these redox-regulated human MAPK, MAPKK and MAPKKKs contain this conserved activation segment Cys residue (Table 2), in contrast to the p38-MAPK targets MAPKAP-K2 and MAPKAP-K3, which we demonstrate are rapidly inactivated by oxidation in vitro (Fig. 8).

Evolutionary bioinformatics reveals that Cys is widespread in ePKs.

Our comparative evolutionary analysis of protein kinomes revealed that ~11.5 % of all protein kinases contain an analogous Cys residue to Cys 290 in Aurora A (equivalent to Cys 200 in PKA) at the 'T-loop +2 position' in the activation segment (Fig. 5). However, only specific members of the AGC and CAMK sub-families were enriched for this conserved Cys residue. This prompted us to investigate redox-sensitivity in a selection of kinases containing a conserved T-loop Cys. Of 17 'T-loop +2 Cys'-containing kinases investigated, 13 were

susceptible to reversible oxidative modulation. These included kinases for which redox-sensitivity had previously been noted, including AKT, AMPK, MELK and CAMK1, as well as totally novel targets of oxidative modification, including SIK1-3, PLK1, PLK4 and MAPKAP-K2/3. We were also able to directly attribute redox-inhibition in the T-loop + 2 Cys residue in MAPKAP-K2 and PLK1 through comparative analysis of WT and Cys-Ala mutant proteins purified from human cells (Fig. 7). Intriguingly, some kinases that were predicted to be redox-sensitive based on the presence of the appropriate Cys-residue in the activation segment, such as Protein Kinase G (PKG) and Phosphorylase Kinase (PhK), were resistant to peroxide inhibition, under identical experimental redox conditions that led to reversible modulation of other kinases. However, these (and other) kinases may still be sensitive to oxidation in cells, where peroxiredoxins have been shown to act as peroxide signal relays for kinases [126] and other proteins [127] A lack of chemical reactivity in an activation segment Cys might partially explain this observation, as observed for GAPDH [128], and also nicely demonstrates that the concentrations of redox reagents in our standard assay do not induce effects through a non-specific mechanism, such as protein denaturation. The intrinsic pKa value of individual Cys residues, and their susceptibility to oxidation, is influenced by networks of interacting amino acids, solvent accessibility, protein-protein interactions and structural dynamics [66, 129]. In this context, artificial incorporating of a Cys residue at the equivalent position in EPHA3 did not sensitize this Tyr kinase to oxidation (fig. S12), suggesting that the EPHA3 activation loop is potentially in an unfavourable environment to stabilize reactive Cys residues. Moreover, the relative reactivity of a Cys-residue is likely to be context-specific and could vary between different allosteric activation states. In this regard, it is noteworthy that Cys 290 transitions from being exposed, to buried, in TPX2-bound Aurora A [118], although it is not immediately obvious to what extent this reconfiguration translates to a reversible change in Cys reactivity.

The Cys-containing regulatory activation segment in ePKs.

The conserved location of the specific Cys residue studied in this study is rather specific to CAMK and AGC families of ePKs, although well-studied groups of kinases in these families such as G-protein coupled kinases (GPRKs), PDK1, NDR/LATS kinases, MLCKs or DAPKs, do not possess an evolutionary-conserved Cys at the Cys 290 equivalent of Aurora A. Closer inspection of the activation segment confirms that although Cys is present at all possible positions in the activation segment across various kinomes (fig. S8F), two sites, DFG +2 (5.1%) and T-loop +2 (11.5%) dominate evolutionary Cys conservation in this region. Interestingly, *both* Cys residues acids are co-conserved in ~1.4% of all ePKs in our database (Fig. 5A, bottom panel), where in the context of redox regulation, they are believed to support

intramolecular and/or intermolecular disulfide bonds in AKT, MELK (and perhaps PAKs, p70S6k and PKC isozymes Table 2 and fig. S13). Consistent with this prediction, the introduction of a Cys residue at the DFG + 2 position in Aurora A changed both thermal stability and redox regulation so that it behaved much more like AKT and MELK. Moreover, we obtained MS data that confirmed the formation of an intermolecular disulfide bond between Cys 290 and the newly introduced Cys 278 (Fig. 7G), which likely explains the acquired obligate dependency on reducing agents to activate S278C Aurora A.

The kinase activation segment contains multiple conserved residues available for post-translational phosphorylation in protein kinases [130-133], and serves as a critical regulatory structure for the modulation of catalytic activity [19]. The activation loop of Aurora A itself undergoes dynamic conformational changes in response to phosphorylation and interactions with allosteric binding-partners, enabling Aurora A to transition between alternate active states [134]. This structural plasticity is perhaps most apparent when considering the number of distinct Aurora A conformations that have been captured in complex with small molecule inhibitors by crystallographic and NMR based techniques [135-138]. Even in an active, phosphorylated form, the activation loop of Aurora A possesses a dynamic conformational ensemble of 'DFG-in' sub-states [75, 139]. We postulate that oxidation of Cys 290, or equivalent Cys residues in the activation segment. Alternatively, their oxidation could generate higher-order molecular species such as inhibitory dimers. The observation that activation by TPX2 binding to Aurora A supersedes oxidative inhibition is consistent with this explanation, given that inactive (e.g Thr 288 dephosphorylated) Aurora A assumes an active conformation when it is bound to TPX2 [75]. Aurora A activity is also reversibly inhibited by CoAlation on Cys 290, and this modification has also been reported in human cells exposed to a variety of oxidative stresses, where Aurora A dimerization represents a potential mechanism for redox regulation [118].

Further structural and proteomics efforts are required to decipher the molecular and structural processes involved in oxidative regulation of protein kinases and to assess the relative contribution of different reversible Cys oxidized states (e.g sulfenic acids, sulfenyl-amides, intra-and intermolecular disulfide bonds) in modulating function. The proximity of conserved Cys residues in ePKs is known to enable a regulatory intramolecular disulfide bond to form, including Cys296 and Cys310 in the auto-inhibited conformation of AKT and Cys153 and Cys 168 of MELK [99, 109, 140]. Our studies with MELK also point to a plausible mechanistic explanation for the oxidative inactivation of structurally homologous kinases through dimerization (fig. S13), as observed for the S278C mutant of Aurora A. Although

MELK activity exhibits an obligate dependence on the presence of reducing agents [97], elimination of the intramolecular disulfide bond by double mutation of both Cys residues releases MELK from this regulatory requirement [140]. Interestingly, in our experiments removal of either Cys168 or Cys169 (the latter of which represents the T+2 Cys) was insufficient to abolish redox dependent activation of MELK, which potentially indicates a redundancy in the ability of both residues to form a disulfide bond with Cys153. This was substantiated with a double Cys168/169 MELK mutant, which was no longer activated by DTT. For T-loop +2 Cys kinases that lack a complementary Cys residues with which an intramolecular disulfide bond could form, the molecular mechanisms of redox based regulation are less apparent, although we cannot discount inter- or intradisulfide bond formation between other, as yet uncharacterized Cys residues in the activation segment (Table 2) or beyond. Finally, our recent work demonstrates that the evolutionary-related prokaryotic and eukaryotic Fructosamine 3 kinases (FN3Ks), which lack the conventional activation segment found in the Ser/Thr kinases described here, also employ reversible Cys regulatory mechanisms to control catalytic output [141]. Indeed, like many human Tyr kinases, FN3K's possess conserved redox-active Cys residues in the Gly-rich loop that function as oxidizable switches to co-ordinate reversible dimerization and control enzymatic (in)activation.

CONCLUSIONS:

In this paper, we describe a new mechanism for the oxidative modulation of Aurroa A kinase activity involving a structurally-conserved redox active Cys residue located on the activation loop. Due to a central role in controlling catalytic output through phosphorylation, this region of kinases has been heavily investigated as a regulatory hot-spot. Our new findings suggest that Cys oxidation and reduction can act dominantly over T-loop phosphorylation, providing an additional phosphorylation-independent layer of control over enzyme activity that might be important in eukaryotic cells. The activation segment has been exploited for the generation of many phosphospecific antibodies for biological evaluation of CAMK and AGC kinases. To our knowledge, the effects of Cys redox status have not been tested in the context of phosphospecific antibody protocols, and in most cases, Cys residues in proteins are reduced by boiling in buffer containing a reducing agent prior to SDS-PAGE. However, our work demonstrates the vulnerability of Cys residues to redox modification in human AGC and CAM kinases, which impinges directly on catalytic output, and that might also impact on the ability of antibodies to accurately monitor phosphorylation status of the activation segment under certain circumstances.

This study opens new investigative avenues to explore the functional relationship between physiological ROS-based signaling networks and the broader redox-regulated kinome,

759 especially mechanisms that occur through conserved activation-segment Cys residues in
760 eukaryotic kinases. Mitochondrial damage and the associated elevation of ROS is implicated
761 in a range of human diseases including ageing [142], cancer [143] and neural degenerative
762 disorders such as Parkinson's disease [144] and a multitude of factors, including hypoxia,
763 contribute to sustained high ROS levels in tumours [145]. A key line of enquiry, therefore,
764 will be to explore the impact of chronic oxidative stress and increased sulfenylated-protein
765 populations on both normal and pathological Ser/Thr kinase function. The extent to which
766 oxidation of kinases may influence the therapeutic efficacy of inhibitor compounds in a
767 cellular context is also of interest, especially for kinases targeted by Cys-based covalent
768 mechanisms. Indeed, different Aurora A inhibitors target distinct conformational species,
769 which can be broadly separated into compounds with preferences for the DFG-in or DFG-out
770 states [75, 137, 138]. The ability of oxidative modifications in the activation segment to alter
771 this 'DFG equilibrium' may also have implications for the selectivity of inhibitors in cells,
772 where the propensity of redox-active Cys residues in Ser/Thr kinases to undergo sulfenylation
773 could be exploited for the rationale design new classes of covalent inhibitors. This strategy
774 has been adapted to great success to generate clinical compounds with potency and selectivity
775 towards tyrosine kinases, such as afatinib and neratinib, which target Cys797 of the redox-
776 regulated tyrosine kinase EGFR for the treatment of non-small cell lung cancer [146]. Finally,
777 a deeper mechanistic understanding of the dynamics of Ser/Thr kinase redox regulation, may
778 reveal Cys residues that are differentially exposed in active and inactive kinase conformations
779 and potentially lead to a diverse and versatile reservoir of specific drug targets [147].

780

MATERIALS AND METHODS:

Commercial recombinant protein kinase fusion proteins were purchased from MRC PPUU reagents (University of Dundee), and were purified from Sf21 cells or *E. coli*. Full details are provided in Table 2. GST and 6His-tagged kinases were purified using standard procedures, prior to storage in 1 mM DTT (except where indicated) at -80°C. All kinases were assayed using standard enzyme preparations [148]. Bacterially-expressed GST-MAPKAP-K2 and GST-MAPKAP-K3 were activated in vitro by incubation with catalytically-active p38α, which was removed by re-purification prior to assay. General biochemicals and all redox reagents, including glutaredoxin (GRX), were purchased from Sigma-Aldrich.

Protein kinase assays

Kinase assays were performed using non-radioactive real-time mobility shift-based microfluidic assays, as described previously [68, 93, 130, 149] in the presence of 2 μM of the appropriate fluorescent-tagged peptide substrate (Table 2) and 1 mM ATP. Pressure and voltage settings were adjusted manually to afford optimal separation of phosphorylated and non-phosphorylated peptides. All assays were performed in 50 mM HEPES (pH 7.4), 0.015% (v/v) Brij-35, and 5 mM $MgCl_2$, and the real-time or endpoint degree of peptide phosphorylation was calculated by differentiating the ratio of the phosphopeptide:peptide present in the reaction. Kinase activity in the presence of different redox reagents was quantified by monitoring the generation of phosphopeptide during the assay, relative to controls. Data were normalised with respect to control assays, with phosphate incorporation into the peptide generally limited to <20% to prevent depletion of ATP and to ensure assay linearity. ATP K_M and the concentration of a compound that caused 50% inhibition (IC_{50}) values were determined by nonlinear regression analysis using Graphpad Prism software. Where specified, kinase assays employing Aurora A were supplemented with 100 nM GST-TPX2 or GST alone. Assays for CAMK kinases included 5 mM $CaCl_2$ and 2 μM Calmodulin as standard. Where appropriate, PKG1 assays were performed in the presence of 1 mM cGMP. Recovery of Aurora A activity from oxidative inhibition was assessed by monitoring substrate phosphorylation in the presence of peroxide in real time, followed by subsequent introduction of DTT or GSH. To standardize this assay for all kinases, enzymes were pre-incubated in the presence or absence of 5 mM H_2O_2 on ice for 30 mins and then substrate phosphorylation was initiated with the addition of 1 mM ATP and the appropriate substrate peptide in the presence (where indicated) of 10 mM DTT. Aurora A kinase assays were also developed with recombinant GST-TACC3 as a substrate. TACC3 Ser 558 phosphorylation was detected by immunoblotting with a pSer 558 TACC3 antibody, as previously described [77].

817 Aurora A autophosphorylation after phosphatase-treatment was detected using a Thr 288
818 phosphospecific antibody [77].
819
820 **Cloning and Recombinant Protein purification**

821 For enzyme and DSF assays, murine or human Aurora A, MELK (1-340), PLK1 (1-364),
822 PLK4 (1-369), full-length PKA, EPHA3 (kinase domain and juxtamembrane region), ABL
823 (46-515), TACC3 and TPX2(1-43) were produced in BL21 (DE3) pLysS *E. coli* cells
824 (Novagen) with expression induced with 0.5 mM IPTG for 18 h at 18°C and purified as *N*-
825 terminal His6-tag or *N*-terminal His6-GST tag fusion proteins by affinity chromatography
826 and size exclusion chromatography using a HiLoad 16/600 Superdex 200 column (GE
827 Healthcare) equilibrated in 50 mM Tris/HCl, pH 7.4, 100 mM NaCl and 10 % (v/v)
828 glycerol. Where appropriate, recombinant protein was purified in the presence of 1 mM
829 DTT. Ser278Ala, Ser278Cys, Cys290Ala Aurora A and equivalent Cys-Ala mutants of
830 other kinases were generated using standard mutagenic procedures, and purified as
831 described above [68]. To generate a phosphorylation-depleted kinase, Aurora A was co-
832 expressed with lambda phosphatase in BL21 (DE3) pLysS *E. coli* cells prior to
833 purification; lambda phosphatase was subsequently removed by IMAC.

834 **Differential Scanning Fluorimetry**

835 Thermal-shift assays were performed with a StepOnePlus Real-Time PCR machine (Life
836 Technologies) using Sypro-Orange dye (Invitrogen) and thermal ramping (0.3 °C in step
837 intervals between 25 and 94°C). All proteins were diluted to a final concentration of 5 μM
838 in 50 mM Tris/HCl, pH 7.4 and 100 mM NaCl in the presence or absence of the indicated
839 concentrations of ATP, H_2O_2, DTT, GSH or MLN8237 (final DMSO concentration no
840 higher than 4 % v/v) [150] and were assayed as described previously [69]. Normalized
841 data were processed using the Boltzmann equation to generate sigmoidal denaturation
842 curves, and average $T_m/\Delta T_m$ values calculated as previously described [151] using
843 GraphPad Prism software.

844 **Human cell culture and cell treatments**

845 HeLa cells were cultured in Dulbecco's Modified Eagle Medium (DMEM) (Lonza)
846 supplemented with 10% foetal bovine serum (FBS) (Hyclone), 50 U/ml penicillin and 0.25
847 μg/ml streptomycin (Lonza) and maintained at 37 °C in 5 % CO_2 humidified atmosphere.
848 To examine the effects of oxidative stress on Aurora A kinase activity, cells were arrested
849 in mitosis with 100 nM nocodazole for 16h, then treated with a range of concentrations of
850 H_2O_2, menadione, or diamide for 30-60 min. To stimulate chronic oxidative stress,

arrested HeLa cells were collected, washed in PBS, and fresh culture medium containing glucose oxidase at a non-toxic concentration (2 U/ml) and 100 nM nocodazole was added. Subsequently, cells were collected and harvested periodically over a 2 h time period. To investigate reversible inactivation of Aurora A by peroxide, arrested cells were incubated for 10 mins with 10 mM H_2O_2, and then peroxide-containing medium was removed and replaced with fresh culture medium containing 10 mM DTT, NAC or GSH or buffer control. To examine TACC3 phosphorylation by exogenous Aurora A, HeLa cells were transfected with pcDNA3 encoding full length WT or C290A N-terminal Myc-tagged Aurora A and pBrain-GFP-TACC3KDP-shTACC3 (to simultaneously express N-terminal tagged GFP-TACC3 and supress expression of endogenous TACC3, Addgene), using Lipofectamine 3000 (ThermoFisher), and to simultaneously express N-terminal tagged GFP-TACC3 and supress expression of endogenous TACC3. 3 μg of DNA (for each plasmid) was used to transfect six well plate dishes of HeLa cells and the media was changed after 3 h. Equal volumes of transfection reagent were used for both single- and cotransfections. Transfected HeLa cells were synchronized with nocodazole as previously described 24 h after transfection. In all assays cells were subsequently washed in PBS and harvested in bromophenol blue-free SDS sample buffer supplemented with 1% Triton X-100, protease inhibitor cocktail tablet and a phosphatase inhibitor tablet (Roche) and sonicated briefly prior to immunoblotting.

Human cell lysis, immunoprecipitation and Western blot analysis

Total cell lysates were centrifuged at 20817*x* g for 20 min at 4˚C and the supernatant was preserved for further analysis. Samples were initially diluted 50-fold and protein concentration was measured using the Coomassie Plus staining reagent (Bradford) Assay Kit (Thermo Scientific) and processed for immunblotting with TACC3 or Aurora A antibodies as described [77, 92]. To assay the kinase activity of T-loop + 2 Cys containing kinases immunoprecipitated from human cells, WT and Cys-Ala full length variants of MAPKAP-K2 and PLK1 (C244A and C212A respectively) were cloned into a pcDNA3 vector and expressed with a 3C-protease cleavable, N-terminal Myc tag. All immunoprecipitation experiments utilised HEK 293T cells transfected using a 3:1 Polyethylenimine (PEI, average Mw ~25,000 Da, Sigma) to DNA ratio (60:20 μg, for a single 10 cm culture dish). Cells were treated with 4 mM Valproic acid 24 h after transfection and proteins were harvested the following day using a lysis buffer containing 50 mM Tris/HCl, pH 7.4, 150 mM NaCl, 0.1 % (v/v) Triton X-100, and 5 % (v/v) glycerol and supplemented with a protease inhibitor cocktail tablet and a phosphatase inhibitor tablet (Roche). Lysates were briefly sonicated on ice, clarified by centrifuged at 20817*x* g for 20 min at 4˚C and the resulting supernatants were incubated with Pierce Anti-c-Myc-

887 Agarose resin (ThermoFisher) for 1 h with gentle end-over end mixing at 4˚C. Agarose
888 beads containing bound protein were collected and washed three times in 50 mM
889 Tris/HCl, pH 7.4, and 500 mM NaCl and then equilibrated in storage buffer, 50 mM
890 Tris/HCl, pH 7.4, 100 mM NaCl and 5 % (v/v) glycerol. The purified kinases were then
891 proteolytically eluted from the beads over a 3 h period using 3C protease (0.5 μg) at 4˚C
892 with gentle agitation, and then assayed as previously described.

893 **Detection of sulfenylated and glutathionylated proteins by immunoblotting**

894 Recombinant Aurora A was incubated with 50 mM Tris/HCl, pH 7.4, and 100 mM NaCl
895 in the presence of different concentrations of H_2O_2 or 10 mM DTT for 10 min. Cysteine
896 sulfenic acid was detected by SDS-PAGE and immunoblotting after adduct formation with
897 1 mM dimedone for 20 mins at RT. Dimedone stocks were prepared in DMSO with a final
898 assay DMSO concentration no higher than 4 % (v/v). To detect glutathionylation of
899 proteins, proteins were incubated with 10 mM GSSG or GSH for 30 mins and glutathione-
900 protein complexes were detected by immunoblotting after non-reducing SDS-PAGE.

901 **MS analysis of intermolecular disulfide bond formation in S278C Aurora A**

902 **Aurora A sample preparation**

903 5 μg of Aurora A purified in the absence of DTT was heated at 80 ^{o}C in 0.06% (w/v)
904 RapiGest SF (Waters), dissolved in 25 mM ammonium bicarbonate, for 10 min. Sample was
905 digested overnight at 25 ^{o}C using a 20:1 (w/w) ratio of Aurora A:Chymotrypsin (Promega),
906 with 600 rpm shaking. The sample was equally split into 2, one aliquot of which was reduced
907 with dithiothreitol (DTT) (3 mM) at 60 ^{o}C for 10 min, cooled and alkylated with
908 iodoacetamide (IAA) (10 mM) at room temperature for 30 min in dark. Excess IAA was
909 quenched by addition of DTT to a final concentration of 7 mM. The second sample was left
910 on ice. RapiGest hydrolysis was induced in both samples by the addition of 1.5% (v/v)
911 trifluoroacetic acid (TFA), 3% (v/v) acetonitrile, shaking at 600 rpm, 37 ^{o}C for 2 hr. Insoluble
912 products were removed by centrifugation (13 000 g, 15 min 4 ^{o}C). Samples were subjected to
913 strong cation exchange using in-house packed stage tips (Empore™ Supelco 47 mm Cation
914 Exchange disc #2251), 3 discs per 200 μL tip. All centrifugation steps were performed at
915 2000 g for 3 min, or until all liquid had passed through the stage tip. Briefly, tips were
916 equilibrated by the sequential washing of 2X 200 μL of each: acetone, methanol, water, 5%
917 (v/v) ammonium hydroxide (in water) and water. Peptide samples were passed through the
918 equilibrated stage tip 3X and washed with 250 μL 1.5% (v/v) TFA in water, before eluting in
919 250 μL of 5% (v/v) ammonium hydroxide (in water). Eluted material was dried to completion
920 under cooled vacuum centrifugation. Peptides were solubilised in 20 μL 97% water, 3% (v/v)

acetonitrile, 0.1% (v/v) TFA and sonicated for 10 min before centrifugation (13 000 g, 15 min 4 ^{o}C) to remove insoluble material prior to liquid chromatography-tandem mass spectrometry analysis.

Liquid chromatography mass spectrometry analysis of WT and S278C Aurora A

Peptides were separated on a Ultimate 3000 nano system (Dionex), by reverse-phase HPLC, using a trapping column (PepMap100, C18, 300 µm x 5 mm) in loading buffer (3% (v/v) acetonitrile, 0.1% (v/v) TFA) at a flow rate of 9 µL/min for 7 minutes. Chromatographic separation was performed using Easy Spray C18 column (75 µm x 500 mm, 2 µm bead diameter) at a flow rate of 0.3 µL/min over a 30 min gradient of 3% buffer A (0.1% (v/v) Formic acid in water): 97% buffer B (80% (v/v) acetonitrile, 0.1% (v/v) Formic acid in water) to 20% buffer A: 80% buffer B. Data was acquired using a Thermo Orbitrap Fusion Lumos Tribrid mass spectrometer (Thermo Scientific). All spectra were acquired in the Orbitrap in a data-dependent analysis mode using a top speed approach (cycle time 3 s), with ions being subjected to HCD (normalised collision energy (NCE) of 32%). MS1 parameters: 60K resolution at 200 m/z, automatic gain control (AGC) = $4e^5$, maximum injection time = 50 ms, mass range = 350 – 2000, charge stated 2+ - 6+. MS2 parameters: 30K resolution at 200 m/z, AGC = $5e^4$, maximum injection time = 54 ms. A dynamic exclusion window was applied for 60 s at a tolerance of 10 ppm.

MS Data analysis

pLink-SS software was used to initially identify spectra containing disulfide linked peptides, as described [152]. Precursor and fragment tolerances were set to 10 ppm, variable modifications of Cys carbamidomethylation and Ser/Thr phosphorylation. Once a spectra containing a disulfide linked peptide was identified, the spectra was redrawn using a custom R script and manually annotated to include disulfide fragmentation mass shifts (-33.987 amu (dehydroalanine) and +31.971 amu (disulfohydryl) at both Cys residues [153].

Identification, alignment and visualization of protein kinase-related sequences

The MAPGAPS procedure [154] was employed alongside a variety of curated eukaryotic protein kinases profiles [130, 155-157] to identify and align eukaryotic protein kinase-related sequences from the non-redundant (NR) sequence database and UniProt reference proteome [158] databases (Release 2018_09). Sequences with a Cys residue at the Aurora A Cys290 equivalent position were retrieved and used for further taxonomic analysis. Taxonomic information was based on NCBI Taxonomy database [159]. Weblogo's [160] and were

generated using Weblogo Version 2.8. Amino acids were coloured based on their chemical properties. Polar amino acids (G,S,T,Y,C,Q,N) are colored green, basic (K,R,H) blue, acidic (D,E) red, and hydrophobic (A,V,L,I,P,W,M) black.

Yeast strains and growth conditions

S. pombe cells (Table 4) were transformed with the indicated plasmids and grown at 30^{o}C in synthetic minimal medium (Edinburgh minimal medium 2) supplemented with 100 mg/l histidine, 87-100 mg/l adenine, 75 mg/l uracil and, where indicated, 20 μg/ml thiamine [PMID: 2995825].

Plasmids

The wild-type *srk1* gene (including intron) was amplified from *S. pombe* genomic DNA by pcr and *srk*^{C324A}, and *srk1*^{C324S} were generated synthetically, PCR-amplified and ligated into NdeI and BamHI sites in pRep41HM [161] to generate pRep41HM*srk1*, pRep41HM*srk*^{C324A}, and pRep41HM*srk*^{C324A} expressing HisMyc-tagged Srk1, Srk1^{C324A} or Srk1^{C324S} from the nmt41 promoter. Wild type *pka1* open reading frame, without the stop codon, was amplified from *S. pombe* genomic DNA and cloned into pJet1.2. *pka1*^{C358S} was amplified from genomic DNA by a two-step overlapping PCR to introduce the mutation. Pka1^{C358A} was generated synthetically. Wild-type and *pka1* mutant genes were then subcloned into NdeI and BamHI sites in pRep41pkC [161] to generate pRep41Pka1pkc, pRep41Pka1^{C358S}pkc and pRep41Pka1^{C358A}pkc expressing C-terminally Pk-tagged Pka1, Pka1^{C358S} or Pka1^{C358A} from the nmt41 promoter. All primer sequences are available upon request.

Analysis of *S. pombe* proteins by immunoblotting

Equal amount of exponentially growing cells (9×10^{6}-1×10^{7}cells) were added to 20% trichloroacetic acid (TCA), harvested by centrifugation at 3000rpm for 1min and then snap frozen in liquid nitrogen. Protein was extracted as described previously (Delaunay et al., 2000) but without phosphatase treatment. Proteins were resuspended in 1% SDS, 1mM EDTA, 100mM Tris-HCL pH 8.0 containing 10mM NEM (*N*-Ethymaleimide). Protein concentrations were estimated using the bicinchoninic acid protein assay (Thermo scientific) and equal amounts of protein (5-10μg) resolved on 8% SDS-PAGE gels, followed by transferred to nitrocellulose membrane and analysed as described [162] 6His-Myc-tagged Srk1 protein was detected using anti-myc antibodies (9E10, Santa Cruz). Anti-tubulin antibody (anti-Tat1) was used as a loading control. For detecting Pka1 phosphorylated substrates, membranes were blocked with 10% (w/v) BSA in TBST, incubated with Phospho PKA substrate (RRXS*/T*) (Cell signaling 100G7E) primary antibody diluted 1:1000 in TBST containing 5% (w/v) BSA and probed with HRP-conjugated anti rabbit (cell signaling)

secondary antibody, diluted 1:3000. For Pka1-Pk detection, anti-pk (Sigma-Aldrich V8012) primary antibody (1:1000) was applied followed by HRP-conjugated anti mouse antibody (Sigma) diluted 1:3000. Enhanced chemiluminescence (Pierce™ ECL Plus, Thermo Scientific) and ImageQuant Software (Typhoon FLA9500) or Vilber Fx6 / Fx7 Chemiluminescent System (Labtech) was used to image fluorescence.

Analysis of *S. pombe* cell length at division and CDC25GFP localisation

Exponentially growing *S. pombe* were resuspended in phosphate-buffered saline, and mounted onto poly-L-lysine coated slides. DIC images were taken using a Zeiss Axioscope and cell lengths compared by measuring >94 newly divided cells for each sample. For analysis of fluorescence (CDC25GFP localisation), cells were mounted in Vectashield containing 1.5µg/ml DAPI to visualise DNA, and observed on a Zeiss Axioscope fluorescence microscope using appropriate filters.

Assessing growth and salt stress sensitivity of *S. pombe*

Equal numbers of exponentially growing WT(JX333) or Δ*pka1*(JX384) cells transformed with pRep41pkc(vector), pRep41Pka1pkc, pRep41Pka1^{C358S}pkc or pRep41Pka1^{C358A}pkc grown in EMM supplemented with 100mg/l adenine and 20µg/ml thiamine (EMMAT) were serially diluted (10-fold dilutions then spotted onto EMMAT agar plate or EMMAT agar plates containing 1M KCl). Plates were incubated at 30°C for 2-5 days and imaged at 24h intervals until comparable levels of growth were observed for the WT cells on each plate.

Statistical analysis

All experimental procedures were repeated in at least 3 separate experiments with matched positive and negative controls (unless stated otherwise). Results are expressed as mean ± SD for all in vitro experiments and data are expressed as the mean ± standard deviation. When applied, statistical significance of differences (*P ≤0.05) was assessed using a Students t-test for normally-distributed data. All statistical tests were performed using Prism 7 (GraphPad Software).

FIGURE LEGENDS:

Figure 1. Redox-dependent regulation of Aurora A activity *in vitro.*

(A) Dose response curves for the reducing reagent DTT (red) and the oxidizing agents H_2O_2 (blue) and diamide (green) with 6 nM recombinant Aurora A in the presence of 1 mM ATP. Aurora A activity was assessed by monitoring phosphorylation of a fluorescent peptide substrate, and normalized to controls after 30 min assay. **(B)** Immunoblot of an *in vitro* kinase assay using recombinant GST-TACC3 as a substrate for Aurora A. Aurora A (3 ng) was incubated with the indicated concentrations of H_2O_2 and DTT or 0.1 mM of the Aurora A-specific inhibitor MLN8237 for 30 mins at 20 °C. The kinase assay was then initiated following the addition of GST-TACC3 (1 μg) and Aurora A-dependent phosphorylation of TACC3 (pSer558, top panel) was detected after 15 mins. 0.5 mM ATP and 5 mM $MgCl_2$ were included in the reaction. Reactions were terminated by the addition of SDS loading buffer. Equal loading of TACC3 substrate was confirmed with anti-TACC3 antibody (second panel from top). Also shown is total (second panel from bottom) and phosphorylated Aurora A (pThr 288, bottom panel). **(C)** Oxidative-inhibition of Aurora A is reversible. Aurora A (12.5 nM) activity was monitored in real time in the presence (blue) or absence (black) of 1 mM H_2O_2 (left panel) or 10 μM MLN8237 (right panel). After 25 mins, reactions were supplemented (where indicated) with 2 mM DTT (red). Aurora A dependent phosphorylation of the fluorescent peptide substrate was monitored using assay conditions described in **(A)**. **(D)** Immunoblot demonstrating reversible increase in the electrophoretic mobility of Aurora A, presumably due to oxidation by H_2O_2. Aurora A (0.5 μg) was incubated with the indicated concentrations of H_2O_2 for 10 mins at 20°C and analysed after non-reducing or reducing SDS-PAGE. Asterisk denotes the reversibly oxidized species found in the absence of DTT; the identity of the more slowly migrating pT288-containing species in these samples is unknown. Total Aurora A (upper panel) and pThr 288 Aurora A (lower panel) blots are also shown. **(E, F)** Immunoblot demonstrating redox-dependent Aurora A autophosphorylation at Thr 288. Dephosphorylated Aurora A (1 μg) was produced by co-expression with lambda

phosphatase in *E. coli* and then incubated with 1 mM ATP and 10 mM $MgCl_2$ for the indicated time periods under reducing (+ 1 mM DTT) or oxidizing (+ 1 mM H_2O_2) conditions in the presence and absence of TPX2 or MLN8237. Reactions were terminated by the addition of SDS loading buffer.

Figure 2. Conserved Cys 290 residue in the Aurora A activation loop is reversibly oxidized *in vitro*: effect of TPX2.

(A) Detection of reactive cysteine oxidation in Aurora A with an antibody with specificity towards cysteine sulfenic acids that have been derivatised by dimedone (SOH-Aurora A). Aurora A (0.5 μg) was incubated with 1 mM H_2O_2 in the presence or absence of 1 mM dimedone for 20 mins (all incubations performed at 20°C). Total Aurora A loading is also shown (bottom panel). **(B)** Concentration dependent oxidation of Aurora A detected by dimedone. Aurora A (0.5 μg) was incubated with an increasing concentration of H_2O_2,10 mM DTT or buffer alone for 10 min and then all samples were exposed to 1 mM dimedone for a further 20 mins (all incubations performed at 20°C). **(C)** Immunoblot demonstrating depleted total SOH content in Aurora A C290A compared to WT enzyme. Assay conditions are as described for **(B)**. **(D)** Comparative analysis of WT (red) and C290A (blue) Aurora A activity in the presence of a fixed amount of ATP (1mM) and varying concentrations of H_2O_2 or **(E)** DTT. Assays were performed using 6 nM Aurora A, and the extent of substrate phosphorylation (presented here as activity normalized to controls containing buffer alone) was determined after 60 mins assay time. **(F)** Redox regulation of PKA catalytic domain. WT or C200A His-PKA (0.3 nM) were assayed with the indicated concentration of H_2O_2 or DTT and activities were normalized relative to controls. **(G)** Reversible redox regulation of PKA. **(H)** Structural disposition of the Aurora A activation segment (red). Cys 290 lies adjacent to Thr 288, the site of Aurora A autophosphorylation. **(I)** Binding of TPX2 protects Aurora A from inactivation by H_2O_2. H_2O_2 dose response curves are shown for Aurora A (6 nM) pre-incubated for 10 mins at 20 °C with or without 100 nM GST-TPX2 prior to oxidation with the

indicated concentration of H_2O_2. Aurora A activity in the presence of 1 mM ATP was normalised to buffer controls after 40 mins assay time. **(J)** TPX2-Aurora A kinase activity is restored by DTT following oxidative-inhibition by H_2O_2. Substrate phosphorylation by Aurora A (1 nM, with 100 nM GST-TPX2) was monitored in real time in the presence or absence of 1 mM H_2O_2 for 50 mins prior to the addition of 2mM DTT to the indicated reactions. Assays were started simultaneously with 100 μM ATP.

Figure 3. Aurora A is activated by modification of Cys 290.

(A) Redox-dependent activation of Aurora A or **(B)** C290A Aurora A by a panel of reducing agents. WT and C290A Aurora A proteins (12.5 nM) were incubated with 1 mM ATP in the presence of 1 mM of the appropriate reducing agent and fluorescent peptide substrate. Activity was calculated relative to a control (buffer only) after 40 mins assay time. **(C)** Dose response curves for GSH. The activity of WT and C290A Aurora A (12.5 nM) was monitered in the presence of increasing concentrations of GSH and 1 mM ATP. Aurora A activity was normalised to buffer controls after 40 min assay time. **(D)** Immunoblot demonstrating in vitro glutathionylation of Aurora A at Cys 290. 1 μg of recombinant purified WT and C290A Aurora A proteins were incubated in the presence or absence of 10 mM GSSG for 30 mins at 20°C. Western blots were probed with an antibody with specificity towards glutathione-conjugated proteins. Equal loading of protein was confirmed using an antibody for Aurora A. PKA (1 μg) was also included as a positive control. SDS-PAGE was performed under non-reducing conditions**. (E)** Inhibition of Aurora A by H_2O_2 is relieved by DTT but not GSH. Aurora A (12.5 nM) activity was assayed in real time in the presence or absence of 1 mM H_2O_2 for 50 mins and reactions were supplemented (where indicated) with 2 mM DTT (left panel) or GSH (right panel). Aurora A-dependent phosphorylation of the fluorescent peptide substrate was initiated by the addition of 1 mM ATP. **(F)** Immunoblot demonstrating glutathionylation of AKT. 1 μg PDK1 phosphorylated S473D AKT was incubated with 100 μM H_2O_2 for 10 mins prior to the application of 1 mM GSH (30 mins at 20°C). SDS-PAGE was performed under non-reducing conditions and 1 μg Aurora A was used as a positive

control. **(G)** Activity of AKT is recapitulated by DTT but not GSH. The activity of PDK1 phosphorylated S473D AKT (7 nM) with 1 mM ATP was monitored in the presence of 1 mM H_2O_2 for 40 mins prior to the addition of 2mM DTT (left panel) or GSH (right panel).

Figure 4. Oxidation inhibits endogenous Aurora A activity in human cells.

(A) Treatment of HeLa cells with H_2O_2 results in a loss of TACC3 phosphorylation at Ser558. Immunoblot shows a loss of Aurora A-dependent phosphorylation of TACC3 (pTACC3) in HeLa cells untreated or treated with 10 mM H_2O_2 or 1 μM MLN8237 for 30 mins. **(B)** Concentration dependent inhibition of endogenous Aurora A activity by H_2O_2. Immunoblots show a loss of pTACC3 in HeLa cells incubated with the indicated concentration of H_2O_2 for 30 mins. A representative western blot of two independent experiments is shown. **(C)** Concentration dependent inhibition of endogenous Aurora A activity by the oxidizing reagent diamide and (**D**) redox-cycling quinone menadione. Loss of pTACC3 in HeLa cells incubated with the indicated concentration of diamide for 30 mins or menadione for 60 mins. **(E)** Loss of pTACC3 in HeLa cells exposed to glucose oxidase (GO). Immunoblots show time-dependent inhibition of TACC3 phosphorylation in HeLa cells cultured in the presence of 2 U/ml GO and nocodazole for the indicated time periods. **(F)** Aurora A oxidative-inhibition is reversed by the peroxide scavengers, NAC and GSH. Immunoblots of HeLa cells treated with 10 mM H_2O_2 for 10 mins prior to the addition of fresh culture medium containing 10 mM DTT, NAC or GSH or buffer control. Cells were then cultured for an additional 20 mins prior to the extraction of whole cell lysates. In all experiments described here, HeLa cells had been blocked in mitosis by nocodazole (100 ng/mL) for 16 h. Whole cell lysates were analysed by western blot and probed with anti-TACC3 or anti-pSer558-TACC3 antibodies. Equal loading was confirmed using antibodies against Aurora A and GAPDH. **(G)** Immunoblots showing phosphorylation of GFP-TACC3 by Myc-Aurora A in co-transfected HeLa cells. Transiently transfected HeLa cells containing plasmids for expression of EGFP, GFP-TACC3 and WT or C290A Myc-Aurora A were cultured for 24 h and then arrested in mitosis with 100 nM

nocodazole for 16h. HeLa cells were then incubated with the indicated concentration of diamide for 30 mins and whole cell lysates were collected.

Figure 5. Bioinformatic analysis of Aurora A Cys 290-equivalent in all ePKs.

(A) Analysis of ePKs, centered on the activation segment between the canonical DFG and APE motifs. The amino acid distribution (percentage of all kinases) is shown on right, data presented as HMM Sequence Logos. **(B)** Human Kinome dendrogram, showing highly skewed distribution of kinases containing a Cys residue at the T-loop +2 residue in AGC and CAML groups. **(C)** Activation segment alignment of human kinases analysed in this study.

Figure 6. Cys 358 of *S. pombe* PKA (Pka1) is required for growth in high salt conditions and Cys 324 is important for the anti-mitotic activity of *S. pombe* MAPKAP-K2/Srk1 in promoting nuclear exclusion of CDC25.

(A) Sequence comparison between *S. pombe* Pka1 and MAPKAP-K2/Srk1, showing the presence of the conserved activation loop Cys residue; C358 in Pka1 and C324 in Srk1. **(B-C)** Analysis of exponentially growing wild-type; WT(JY333) or Δ*pka1* (JX384) *S. pombe* expressing pk-tagged wild type Pka1, Pka1^{C358S} or Pka1^{C358A} compared with vector control(Rep41pkc) suggests that **(B)** C358 is important for the kinase activity of Pka1. Pka1-dependent phosphorylated substrates, detected using Phospho PKA substrate (RRXS*/T*) antibodies in samples from wild-type (WT) but not Δ*pka1* cells, are indicated by arrows on the upper panel. Anti-Pk antibodies were used to show that wild type Pka1-Pk, Pka1^{C358S}–Pk and Pka1^{C358A}-Pk proteins are expressed at similar levels in these samples. Tubulin antibodies were used to confirm similar loading. *indicates a band that is increased in cells lacking Pka1. **(C)** C358 in Pka1 is dispensable for growth under control conditions but required for the growth of *S. pombe* on plates containing 1M KCl.. **(D-E)** Analysis of exponentially growing wild-type *S. pombe* (AD38) expressing wild-type Myc-tagged Srk1, Srk1^{C324S} or Srk1^{C324A} compared with vector control (Rep41HM) reveals **(D)** that mutants in which cysteine 324 is substituted are less effective at delaying mitotic entry (increasing cell length) than wild-type

Srk1. The graph shows the cell length of >94 newly divided cells (such as those indicated by arrowheads in images). **(E)** wild-type myc—tagged Srk1^{C324S} and Srk1^{C324A} Srk1 proteins are expressed at similar levels, relative to a tubulin loading control. **(F)** Analysis of Cdc25-GFP-expressing cells (KGY4337) co-expressing wild-type Srk1, Srk1^{C324S} or Srk1^{C324A}, compared with vector control (Rep41HM) using fluorescence microscopy. In the right panel, cells were stained with DAPI to visualise DNA (blue), confirming that wild-type Srk1 promotes the nuclear exclusion of CDC25GFP much more effectively than Srk1^{C324S} or Srk1^{C324A}.

Figure 7. Analysis of redox regulation in human MAPKAP-K2, PLK1 and PLK4

(A) 10 nM GST-MAPKAP-K2 was incubated on ice for 30 mins in the presence or absence of 5 mM H_2O_2. Reactions were then initiated with the addition 1 mM ATP and substrate peptide in the presence (where indicated) of 10 mM DTT. **(B)** Immunoprecipitations of N-terminal Myc-tagged WT and C244A MAPKAP-K2 from HEK 293T cells from two independent transfection experiments. Western blots of lysates were probed for transient overexpression of Myc-MAPKAP-K2 using an antibody for Myc-tagged proteins (top panel). Purified MAPKAP-K2 was detected following 3C protease dependent elution by western blotting followed by Ponceau staining (bottom panel). EGFP transfections were used as a negative control **(C)** The activity of immunoprecipitated WT and C244A MAPKAP-K2 was measured in the presence of 1 mM DTT (red), 1 mM diamide (blue), or buffer control (black), with 1 mM ATP. MAPKAP-K2-dependent phosphorylation of fluorescent substrate peptide was monitored in real time. The data shown is the average and SD of two independent immunoprecipitation experiments each assayed in duplicate. Equal volumes of eluted protein were used in each assay for WT and mutant proteins. **(D)** Redox regulation of PLK1catalytic domain. GST-PLK1 (160 nM) was assayed as for PKA, in the presence of the indicated concentration of H_2O_2 or DTT and activity was normalized relative to buffer control. **(E)** Reversible redox regulation of PLK1. **(F)** Immunoprecipitations of N-terminal Myc-tagged WT and C212A PLK1 from HEK 293T cells from two independent transfections. Overexpressed Myc-PLK1 was detected in lysates using anti-Myc antibody (top panl) and

1184 purified PLK1 was confirmed using anti-PLK1 antibody (bottom panel). EGFP control data
1185 also shown. **(G)** The activity of immunoprecipitated WT and C212A PLK1 was measured in
1186 the presence of 1 mM DTT (red), 1 mM diamide (blue), or 100 μM of the PLK-specific
1187 inhibitor BI 2536 (black) with 1 mM ATP. Activity was calculated relative to a control
1188 (buffer only) after 2 h assay time. **(H)** Redox regulation of WT and C172A His-PLK4. His-
1189 PLK4 (4 μM) was assayed with H_2O_2 or DTT and activity was normalized relative to control.
1190 **(I)** Reversible redox regulation of WT PLK4.
1191
1192 **Figure 8. Redox response of an engineered Ser/Thr kinase: A DFG+2 Cys residue**
1193 **generates an obligate DTT requirement for catalytic activity in Aurora A.**

1194 **(A)** Activation segment amino acid conservation in 2,285 Aurora kinase-like AGC family
1195 members from diverse eukaryotic kinomes. Human Aurora A sequence annotation is used to
1196 highlight Asp274 and Glu299, which encompass the activation segment. The T-loop residue
1197 (Thr288) is highlighted. The height of the letters indicates the relative frequency of the amino
1198 acid at each position. **(B)** The activity of Aurora A and DFG +2 point mutants, S278A and
1199 S278C (25 nM) was measured in the presence (red) or absence (black) of 10 mM DTT.
1200 Aurora A-dependent phosphorylation of fluorescent substrate peptide was monitored in real
1201 time. **(C)** Comparison of WT (red bars), S278A (green bars) and S278C (black bars) Aurora
1202 A catalytic activity (pmoles of phosphate incorporated into substrate per minute) at 10 min
1203 time point. (**D)** Direct comparison of Aurora A DFG+2 mutants. S278A (green bars) and
1204 S278C (black bars). 25 nM of each enzyme was assayed with the indicated concentration of
1205 H_2O_2 or DTT. Data is presented as rate of peptide phosphorylation (pmol phosphate/min). **(E)**
1206 Reversible redox regulation of Aurora A DFG+2 mutants. Aurora A (25 nM) activity was
1207 monitored in real time in the presence (blue) or absence (black) of 2 mM H_2O_2. After 30
1208 mins, reactions were supplemented (where indicated) with 5 mM DTT (red). Aurora A
1209 dependent phosphorylation of the fluorescent peptide substrate was monitored using assay
1210 conditions described in **(B)**. **(F)** Disulfide bonding of a S278C mutant to C290 in the active
1211 site of Aurora kinase A. MS/MS spectrum of the triply charged peptide ion of m/z 593.9391,

fragmented using HCD. Peptide sequence is displayed with the annotated HCD product ions labelled, including the position of the Cys1 (278) – Cys13 (290) disulfide bond. HCD resulted in peptide backbone fragmentation and cleavage of the disulfide bond (producing dehydroalanine or disulfohydryl cysteine with mass shifts of -33.987 and +31.971 amu respectively[153]. a/b ions (red), y ions (blue), internal ions (green) and precursor derived product ions (orange) are annotated, including charge state and neutral losses. MS1 mass is equivalent to a singly phosphorylated peptide, however the specific site(s) of phosphorylation could not be localised in the spectrum. **(G)** 7 nM PDK1 phosphorylated His-S473D AKT was incubated on ice for 30 mins in the presence or absence of 5 mM H_2O_2. Reactions were initiated with 1 mM ATP and substrate peptide in the presence (where indicated) of 10 mM DTT. **(H)** Reversible redox regulation of MELK. Peroxide-mediated inhibition of MELK activity is reversed by addition of DTT. **(I)** Redox regulation of MELK and mutants. WT and activation loop Cys mutants (50 nM) were assayed with H_2O_2 (left) or DTT (right), and activities normalized relative to controls. In these assays, kinases were incubated on ice for 30 mins in the presence or absence of 5 mM H_2O_2. Reactions were then initiated with the addition of 1 mM Mg-ATP and substrate peptide in the presence or absence of 10 mM DTT. In all experiments, kinase-optimised fluorescent peptide substrates were used (see Table 3).

Figure 9. Reversible oxidation of a conserved Cys residue regulates the activity of multiple Ser/Thr kinases.

A panel of AGC and CAMK-related kinases were probed for reversible oxidation-dependent inhibition using real time phosphorylation of kinase specific peptide substrates (Table 3). In all assays, kinases were incubated on ice for 30 mins in the presence or absence of 5 mM H_2O_2. Reactions were then initiated with the addition 1 mM ATP and substrate peptide in the presence (where indicated) of 10 mM DTT. Kinases were assayed at the following final concentrations: **(A)** 15 nM MAPKAP-K3, **(B)** 24 ng His-AMPK $\alpha1 + \beta2 + \gamma1$, **(C)** 0.5 μM MBP-SIK1, **(D)** 2 nM GST-SIK2, **(E)** 2 nM GST-SIK3, **(F)** 0.7 μM CaMK1A, **(G)** 60 nM

GST-CaMK1D, **(H)** 0.6 µMCaMK2G and **(I)** 0.6 µM CaMK2D. All assays including CaMKs were supplemented with 5 mM $CaCl_2$ and 2 µM Calmodulin.

Table 1. Human protein kinases containing the Aurora A Cys 290 equivalent in the Activation Segment. Human kinases (Uniprot ID) and sequence of the activation segment.

Protein Kinase Gene Name (UniProt ID)	Activation Segment Sequence (Cys)
TSSK1 (Q9BXA7)	DFSFSKRCLRDDSGRMALSKTFCGSPAYAAPE
TSSK2 (Q96PF2)	DFGFSKRCLRDSNGRIILSKTFCGSAAYAAPE
TSSK3 (Q96PN8)	DFGFAKVLPKSHRELSQTFCGSTAYAAPE
TSSK4 (Q6SA08)	DFGFAKMVPSNQPVGCSPSYRQVNCFSHLSQTYC GSFAYACPE
TSSK6 (Q9BXA6)	DFGFGRQAHGYPDLSTTYCGSAAYASPE
KS6B1 (P23443)	DFGLCKESIHDGTVTHTFCGTIEYMAPE
KS6B2 (Q9UBS0)	DFGLCKESIHEGAVTHTFCGTIEYMAPE
KS6A1 (Q15418) #1	DFGFAKQLRAENGLLMTPCYTANFVAPE
KS6A2 (Q15349) #1	DFGFAKQLRAGNGLLMTPCYTANFVAPE
KS6A3 (P51812) #1	DFGFAKQLRAENGLLMTPCYTANFVAPE
KS6A6 (Q9UK32) #1	DFGFAKQLRGENGLLLTPCYTANFVAPE
KS6A1 (Q15418) #2	DFGLSKEAIDHEKKAYSFCGTVEYMAPE
KS6A2 (Q15349) #2	DFGLSKEAIDHDKRAYSFCGTIEYMAPE
KS6A3 (P51812) #2	DFGLSKESIDHEKKAYSFCGTVEYMAPE
KS6A4 (O75676)	DFGLSKEFLTEEKERTFSFCGTIEYMAPE
KS6A5 (O75582)	DFGLSKEFVADETERAYSFCGTIEYMAPD
KS6A6 (Q9UK32) #2	DFGLSKESVDQEKKAYSFCGTVEYMAPE
AKT1 (P31749)	DFGLCKEGIKDGATMKTFCGTPEYLAPE
AKT2 (P31751)	DFGLCKEGISDGATMKTFCGTPEYLAPE
AKT3 (Q9Y243)	DFGLCKEGITDAATMKTFCGTPEYLAPE
PLK1 (P53350)	DFGLATKVEYDGERKKTLCGTPNYIAPE
PLK2 (Q9NYY3)	DFGLAARLEPLEHRRRTICGTPNYLSPE
PLK3 (Q9H4B4)	DFGLAARLEPPEQRKKTICGTPNYVAPE
PLK4 (O00444)	DFGLATQLKMPHEKHYTLCGTPNYISPE
MAST1 (Q9Y2H9)	DFGLSKMGLMSLTTNLYEGHIEKDAREFLDKQVC

	GTPEYIAPE
MAST2 (Q6P0Q8)	DFGLSKIGLMSLTTNLYEGHIEKDAREFLDKQV**C**GTPEYIAPE
MAST3 (O60307)	DFGLSKIGLMSMATNLYEGHIEKDAREFIDKQV**C**GTPEYIAPE
MAST4 (O15021)	DFGLSKVGLMSMTTNLYEGHIEKDAREFLDKQV**C**GTPEYIAPE
KAPCA/PKAα (P17612)	DFGFAKRVKGRTWTL**C**GTPEYLAPE
KAPCB/PKAβ (P22694)	DFGFAKRVKGRTWTL**C**GTPEYLAPE
KAPCG/PKAγ (P22612)	DFGFAKRVKGRTWTL**C**GTPEYLAPE
PRKX (P51817)	DFGFAKKLVDRTWTL**C**GTPEYLAPE
PRKY (O43930)	DFGFAKKLVDRTWTL**C**GTPEYLAPE
KGP1/PKG1 (Q13976)	DFGFAKKIGFGKKTWTF**C**GTPEYVAPE
KGP2/PKG2 (Q13237)	DFGFAKKIGSGQKTWTF**C**GTPEYVAPE
PKN1 (Q13976)	DFGLCKEGMGYGDRTSTF**C**GTPEFLAPE
PKN2 (Q13237)	DFGLCKEGMGYGDRTSTF**C**GTPEFLAPE
PKN3 (Q6P5Z2)	DFGLCKEGIGFGDRTSTF**C**GTPEFLAPE
JAK1 (P23458)	DPGIPITVLSRQE**C**IERIPWIAPE
SGK494 (Q96LW2)	DFGLSRHVPQGAQAYTI**C**GTLQYMAPE
SGK1 (O00141)	DFGLCKENIEHNSTTSTF**C**GTPEYLAPE
SGK2 (Q9HBY8)	DFGLCKEGVEPEDTTSTF**C**GTPEYLAPE
SGK3 (Q96BR1)	DFGLCKEGIAISDTTTTF**C**GTPEYLAPE
AAPK1 (Q13131)	DFGLSNMMSDGEFLRTS**C**GSPNYAAPE
AAPK2 (P54646)	DFGLSNMMSDGEFLRTS**C**GSPNYAAPE
BRSK1 (Q8TDC3)	DFGMASLQVGDSLLETS**C**GSPHYACPE
BRSK2 (Q8IWQ3)	DFGMASLQVGDSLLETS**C**GSPHYACPE
KPCA/PKCα (P17252)	DFGMCKEHMMDGVTTRTF**C**GTPDYIAPE
KPCB/PKCβ (P05771)	DFGMCKENIWDGVTTKTF**C**GTPDYIAPE
KPCD/PKCδ (Q05655)	DFGMCKENIFGESRASTF**C**GTPDYIAPE
KPCE/PKCε (Q02156)	DFGMCKEGILNGVTTTTF**C**GTPDYIAPE
KPCG/PKCγ (P05129)	DFGMCKENVFPGTTTRTF**C**GTPDYIAPE

KPCI/PKCι (P41743)	DYGMCKEGLRPGDTTSTFCGTPNYIAPE
KPCL/ PKCλ (P24723)	DFGMCKEGICNGVTTATFCGTPDYIAPE
KPCT/PKCτ (Q04759)	DFGMCKENMLGDAKTNTFCGTPDYIAPE
KPCZ/ PKCζ (Q05513)	DYGMCKEGLGPGDTTSTFCGTPNYIAPE
AURKA (O14965)	DFGWSVHAPSSRRTTLCGTLDYLPPE
AURKB (Q96GD4)	DFGWSVHAPSLRRKTMCGTLDYLPPE
AURKC (Q9UQB9)	DFGWSVHTPSLRRKTMCGTLDYLPPE
CHK1 (O14757)	DFGLATVFRYNNRERLLNKMCGTLPYVAPE
CHK2 (O96017)	DFGHSKILGETSLMRTLCGTPTYLAPE
STK35 (Q8TDR2)	DFGLSKVCAGLAPRGKEGNQDNKNVNVNKYWL SSACGSDFYMAPE
PDK1L (Q8N165)	DFGLSKVCSASGQNPEEPVSVNKCFLSTACGTDF YMAPE
HUNK (P57058)	DFGLSNCAGILGYSDPFSTQCGSPAYAAPE
MARK1 (Q9P0L2)	DFGFSNEFTVGNKLDTFCGSPPYAAPE
MARK2 (Q7KZI7)	DFGFSNEFTFGNKLDTFCGSPPYAAPE
MARK3 (P27448)	DFGFSNEFTVGGKLDTFCGSPPYAAPE
MARK4 (Q96L34)	DFGFSNEFTLGSKLDTFCGSPPYAAPE
SGK196/POMK (Q9H5K3)	DLDALPLVNHSSGMLVKCGHRELHGDFVAPE
ULK1 (O75385)	DFGFARYLQSNMMAATLCGSPMYMAPE
ULK2 (Q8IYT8)	DFGFARYLHSNMMAATLCGSPMYMAPE
BUB1 (O43683)	DLGQSIDMKLFPKGTIFTAKCETSGFQCVE
MELK (Q14680)	DFGLCAKPKGNKDYHLQTCCGSLAYAAPE
NIM1 (Q8IY84)	DFGFSTVSKKGEMLNTFCGSPPYAAPE
NUAK1 (O60285)	DFGLSNLYQKDKFLQTFCGSPLYASPE
NUAK2 (Q9H093)	DFGLSNLYHQGKFLQTFCGSPLYASPE
SIK1 (P57059)	DFGFGNFYKSGEPLSTWCGSPPYAAPE
SIK2 (Q9H0K1)	DFGFGNFFKSGELLATWCGSPPYAAPE
SIK3 (Q9Y2K2)	DFGFSNLFTPGQLLKTWCGSPPYAAPE
SIK1B (A0A0B4J2F2)	DFGFGNFYKSGEPLSTWCGSPPYAAPE

SNRK (Q9NRH2)	DFGFSNKFQPGKKLTTS**C**GSLAYSAPE
KCC1A/CAMK1A (Q14012)	DFGLSKMEDPGSVLSTA**C**GTPGYVAPE
KCC1B/CAMK1B (Q6P2M8)	DFGLSKIQAGNMLGTA**C**GTPGYVAPE
KCC1D/CAMK1D (Q8IU85)	DFGLSKMEGKGDVMSTA**C**GTPGYVAPE
KCC1G/CAMK1G (Q96NX5)	DFGLSKMEQNGIMSTA**C**GTPGYVAPE
KCC4/CAMK4 (Q16566)	DFGLSKIVEHQVLMKTV**C**GTPGYCAPE
CAMKV (Q8NCB2)	DFHLAKLENGLIKEP**C**GTPEYLAPE
DCLK1 (O15075)	DFGLATIVDGPLYTV**C**GTPTYVAPE
DCLK2 (Q8N568)	DFGLATVVEGPLYTV**C**GTPTYVAPE
DCLK3 (Q9C098)	DFGLAKHVVRPIFTV**C**GTPTYVAPE
MKNK1/MNK1 (Q9BUB5)	DFDLGSGMKLNNSCTPITTPELTTP**C**GSAEYMAPE
MKNK2/MNK2 (Q9HBH9)	DFDLGSGIKLNGDCSPISTPELLTP**C**GSAEYMAPE
PASK (Q96RG2)	DFGSAAYLERGKLFYTF**C**GTIEYCAPE
PHKG1 (Q16816)	DFGFSCQLEPGERLREV**C**GTPSYLAPE
PHKG2 (P15735)	DFGFSCHLEPGEKLREL**C**GTPGYLAPE
KPSH1/PSKH1 (P11801)	DFGLASARKKGDDCLMKTT**C**GTPEYIAPE
KPSH2/PSKH2 (Q96QS6)	DFGLAYSGKKSGDWTMKTL**C**GTPEYIAPE
STK33 (Q9BYT3)	DFGLAVKKQSRSEAMLQAT**C**GTPIYMAPE
RSK KS6A4 (O75676)	DFGFARLRPQSPGVPMQTP**C**FTLQYAAPE
RSK KS6A5 (O75582)	DFGFARLKPPDNQPLKTP**C**FTLHYAAPE
MAPKAP-K2 (P49137)	DFGFAKETTSHNSLTTP**C**YTPYYVAPE
MAPKAP-K3 (Q16644)	DFGFAKETTQNALQTP**C**YTPYYVAPE

1247

1248

1249

Table 2. Positional evaluation of all human kinases that contain Cys residues in the Activation Segment. The location of the Cys residue relative to the end of the DFG motif is shown and includes the total number of kinases at each position and the commonly used names of each kinase.

Cys Position	Number in human kinome	Human kinase/pseudokinase name
DFG + 1	5	MAP3K4/MEKK4, MAP3K8/COT, MOS, PINK1, HSER/GUCY2C
DFG +2	43	p70S6K, p70S6Kb, PKCα, PKCβ, PKCγ, PKCδ, PKCε, PKCι, PKCλ, PKCτ, PKCζ, PKN1, PKN2, PKN3, AKT1, AKT2, AKT3, SGK1, SGK2, SGK3, MRCKa, MRCKb, DMPK1, DMPK2, ROCK1, ROCK2, IRE1, IRE2, LATS1, LATS2, MELK, MOK, NDR1, NDR2, PAK1, PAK2, PAK3, PAK4, PAK5, PAK6, PINK1, SGK496, SCYL2
DFG +3	15	BARK1, BARK2,PHKγ1, PHKγ2, DYRK1A, DYRK1B, DYRK2, DYRK3, DYRK4, SRPK1, SPRK2, MSSK1, TAK1, SCYL3, TRIB3
DFG +4	4	ANK3RD, HUNK, NIK, LMR1
DFG +5	4	TSSK1, TSSK2, IRAK2, LRRK2
DFG +6	2	MPSK1/STK16, LRRK2
DFG +7	1	JNK2
DFG +8	4	MNK1, MNK2, GCN2, SGK069/SBK
DFG +9	5	LATS1, LATS2, PSKH1, RYK, DRAK2/STK17B
DFG +10	4	CDK5, MAP3K5/ASK1, MAP3K6/ASK2, MAP3K7/TAK1
DFG +11	12	NRBP1, RSKL1, RSKL2, LKB1, HIPK1, HIPK2, HIPK3, ILK, FGR/SRC2, IKKα, IKKβ, IRE2
DFG +12	5	ROCK1, ROCK2, NEK3, TYRO3, RSKL2
DFG +13/ T-LOOP	3	SPEG, VRK1, PBK/TOPK
DFG +14/ T-LOOP +1	6	ADCK5, ALK, NEK1, NEK5, SCYL2, MELK
DFG +15/ T-LOOP +2	99	Described in detail in Table 1
DFG +16/ T-LOOP +3	3	GSK3α, GSK3β, MPSK1
DFG + 17/ T-LOOP +4	8	EPHB6, MAP2K3/MKK3, MAP2K4/MKK4, MAP2K6/MKK6, MAP2K7/MKK7, TRIB1, TRIB2, TRIB3

DFG +18	2	RIOK1, HRI/eIF2αK
DFG + 19	7	KSR1, KSR2, NEK8, OSR1, PINK1, PIK3R4, STLK3
DFG +20	1	Haspin
DFG + 21 (APE-1)	7	ADCK1, ACK, CAMKIV, TEC, TNK1, PASK,RSKL1

1254

1255

Table 3. Protein kinase enzymes and substrates. Sequence of recombinant protein kinases and peptide substrates employed for assay of purified human protein kinases. Sources of enzymes (insect cell or bacteria) are included. 5FAM=5-carboxyfluorescein

Purified recombinant Protein Kinase	Peptide substrate sequence
MBP-SIK1 (2-783) Sf21 cells (DU40321)	5FAM-ALNRTSSDSALHRRR-$CONH_2$
GST-SIK2 (2-926) Sf21 cells (DU16623), GST-SIK3 (2-1369) Sf21 cells (DU 16624)	5FAM-KKVSRSGLYRSPSMPENLNRPR-$CONH_2$
His-AMPK α1 (11-559) + β2 (1-272) + γ1 (1-331) Sf21 cells (DU32489)	5FAM-AMARAASAAALARRR-$CONH_2$
Full length human myc-3C-PLK1 or GST-PLK1 (1–369) *E. coli*	5FAM-AEEISDELMEFSLKDQEA-$CONH_2$
His-PLK4 (1-269) *E. coli*	5FAM-FLAKSFGSPNRAYKK-$CONH_2$
His-ABL (46-515) *E. coli*	5FAM-EAIYAAPFAKKK-$CONH_2$
(GST-cleaved) PHK (1-297) *E. coli* (DU733)	5FAM-KRKQISVRGL-$CONH_2$
His-AKT (118-470) Sf21 cells	5FAM-GRPRTSSFAEG-$CONH_2$
(GST-cleaved) CAMK1A (2-369) *E. coli* (DU1148), GST-CAMK1D (1-385) *E. coli* (DU37123)	5FAM-KKLNRTLSVA-$CONH_2$
(GST- cleaved) CAMK2D (1-478) *E. coli* (DU33795), (GST- cleaved) GST-CAMK2G (1-527) *E. coli* (DU51376)	5FAM-KKLNRTLSVA-$CONH_2$
Full length human myc-3C-MAPKAP-K2, GST-MAPKAP-K2 (46-400) *E. coli* (DU1714), (GST-cleaved) MAPKAP-K3 (2-382) *E. coli* (DU929),	5FAM-KKLNRTLSVA-$CONH_2$
His-Aurora A (Full length, 1-403) *E. coli*, His-PKA (Full length,1-351) *E. coli*, His-PKG1-1 (Full length, 1-671) Sf21 (DU26285), His-PKG1-2 (Full length, 1-686) Sf21 (DU26299)	5FAM-LRRASLG-$CONH_2$
GST-MELK (1-340) *E. coli*	5FAM-AMARAASAAALARRR-$CONH_2$
His-EPHA3 (kinase domain) *E. coli*	5FAM-EFPIYDFLPAKKK-$CONH_2$

Table 4. Yeast strains described in this study

Strain	Genotype	Source or reference
AD38	*h⁻ ade6-M216 leu1-32 ura4-D18 sty1::his7⁺ sty1⁺:ura4⁺*	[162, 163]
KGY4337	*h⁻ cdc25-GFP:KanR ura4-D18 ade6-M210 leu1-32*	[164]
JX333	*h⁻ ade6-M216 leu1-32*	[165]
JX384	*h⁻ ade6-M216 leu1-32 ura4-D18 pka1::ura4⁺*	[165]

SUPPLEMENTARY MATERIALS:

fig. S1. Chemical routes for Cys redox modifications in proteins, and their detection with commercial reagents.

fig. S2. Variation of oxidant:protein ratio, and real-time redox analysis of Aurora A purified in the presence of DTT.

fig. S3. Biochemical analysis of Aurora A oxidation.

fig. S4. Analysis of Aurora A and a redox-resistant C290A mutant.

fig. S5 Comparison of Aurora A containing Ala, Ser or Asp at position 290.

fig. S6. WT and C290A Aurora A both bind to TPX2.

fig. S7. Reversible glutathionylation of Aurora A and AKT; effects of glutaredoxin.

fig. S8. Taxonomic analysis of conserved Cys residues within the activation segment of all ePKs.

fig. S9. Biochemical comparison of Cys-containing protein Ser/Thr and Tyr kinases.

fig. S10. Thermal profiling and immunoblotting-based redox analysis of Aurora A 'DFG +2' kinase mutants; comparison of S278A with S278C

fig. S11. Kinases possessing a T-loop +2 Cys residue that are insensitive to redox-dependent regulation in standard real-time redox assay.

fig. S12. Real-time redox analysis of model Tyr kinases and Cys mutants.

fig. S13. Structural-models of disulphide-based mechanisms involving activation segment Cys in Ser/Thr kinases.

SUPPLEMENTARY FIGURE LEGENDS:

Supplementary Figure 1. Chemical routes for Cys redox modifications in proteins, and their detection with commercial reagents. A redox flow-chart is presented. Note the DTT reversibility of the sulfenic Cys and disulfide species and detection of glutathionylated and dimedone-conjugated sulfenylated cysteines using commercial antibodies.

Supplementary Figure 2. Analysis of Aurora A purified in the presence of DTT.
(A) Recombinant Aurora A (0.5 µg each) purified in the presence or absence of DTT and resolved by SDS-PAGE and visualised by Coomassie blue staining (top panel). Phosphorylation (pThr 288) of each protein (20 ng) was also analysed by immunoblotting (bottom panel). **(B)** Dose response curves for H_2O_2 incubated for 16 h (left panel) or 2 h (right panel) with 5 µM recombinant Aurora A in the presence of 1 mM ATP and 2.5 mM $MgCl_2$. Aurora A was then diluted to 50 nM and the enzymes activity was assessed by monitoring phosphorylation of a fluorescent peptide substrate, and normalized to controls as previously described. Half-maximal inhibitory concentration (IC_{50}) of H_2O_2 under these conditions was calculated to be <10 µM.**(C)** Dose response curves for the reducing reagent DTT (red) and the oxidizing agents H_2O_2 (blue) and diamide (green) with 6 nM recombinant Aurora A purified in the presence of DTT. Aurora A activity was assessed by monitoring phosphorylation of a fluorescent peptide substrate using 1 mM ATP, and normalized to control experiments containing buffer alone after 30 min assay time. **(D)** Oxidative-inhibition of Aurora A purified in the presence of DTT is reversible. Assay conditions are as described in Fig. 1C.

Supplementary Figure 3. Biochemical analysis of Aurora A oxidation.
(A) Aurora A stability is unaffected by redox state. Thermal denaturation profiles of recombinant Aurora A (5 µM) in the presence of 1 mM of the indicated redox-reagent. Representative unfolding profiles of two independent experiments shown. **(B)** $K_{M[ATP]}$ determination for Aurora A (12.5 nM) in the presence of H_2O_2. Kinetic analysis of Aurora A-catalysed peptide phosphorylation (pmol phosphate/min) with increasing concentrations of ATP was performed with the indicated concentrations of H_2O_2. $K_{M[ATP]}$ values (± standard deviation) were calculated from two independent experiments using GraphPad Prism software. **(C)** Analysis of thermal shifts induced by 1 mM ATP and 100 µM MLN8237 in the presence of 1 mM of the indicated redox-reagent. Means of two independent experiments are shown.

Supplementary Figure 4. Analysis of Aurora A and a redox-resistant C290A mutant.

(A) Purified WT and C290A Aurora A (0.5 μg each) resolved by SDS-PAGE and visualised by Coomassie blue staining (top panel) and immunoblot (50 ng protein) using antibodies with specificity for Aurora A (middle panel) and site specific autophosphorylation at Thr 288 (bottom panel). **(B)** Thermal denaturation profiles of recombinant Aurora A proteins 5 μM. Representative unfolding profiles from two independent experiments are shown. **(C)** Thermal shifts induced by 1 mM ATP and 100 μM MLN8237. **(D)** Calculation of $K_{M[ATP]}$ values for WT (red) and C290A Aurora A (blue). ATP concentrations were varied in the presence of a fixed amount (6 nM) of Aurora A protein. The rate of peptide substrate phosphorylation (pmol phosphate/min) was calculated from two independent experiments using GraphPad Prism software. **(E)** Immunoblot of an *in vitro* kinase assay using recombinant GST-TACC3 as a substrate for C290A Aurora A. Aurora A (50 ng) was incubated with the indicated concentrations of H_2O_2 and DTT or 0.1 mM of the Aurora A-specific inhibitor MLN8237 for 30 mins at 20 °C. The kinase assay was initiated following the addition of GST-TACC3 (1 μg) and C290A Aurora A-dependent phosphorylation of TACC3 (pSer558, top panel) was detected after 15 mins. 0.5 mM ATP and 5 mM $MgCl_2$ were included in the reaction. Reactions were terminated by the addition of SDS loading buffer. Equal loading of TACC3 substrate was confirmed with anti-TACC3 antibody (second panel from top). Also shown is total (second panel from bottom) and phosphorylated C290A Aurora A (pThr 288, bottom panel).

Supplementary Figure 5. Analysis of C290S and C290D mutants.

(A) Purified WT, C290A, C290S, C290D and kinase-dead (D274N) Aurora A (50 ng each protein) were resolved by SDS-PAGE immunoblotted using antibodies with specificity for Aurora A (top panel) and site specific autophosphorylation at Thr 288 (bottom panel). **(B)** Thermal denaturation profiles of recombinant Aurora A proteins (5 μM). Representative unfolding profiles from two independent experiments are shown. **(C)** Thermal shifts induced by 1 mM Mg-ATP or 100 μM MLN8237. **(D)** Real-time kinase assays performed using a fluorescent peptide substrate performed with the indicated amounts of WT, C290S and C290D Aurora A proteins.

Supplementary Figure 6. WT and C290A Aurora A both bind to TPX2.

(A) Interaction of WT and C290A His-Aurora A with GST-TPX2 under oxidizing and reducing conditions. 5 μM WT Aurora A was incubated with the indicated concentrations of H_2O_2 or DTT for 5 mins at 20 °C and pulled down with GST-TPX2 glutathione beads (~1 μg GST-TPX2 per 10 μl bead volume). Protein was eluted with 10 mM GSH. Pull down assays with C290A Aurora A also shown. Control experiments used GST as a bait protein. **(B)** Redox regulation of TPX2-bound WT and C290A Aurora A. WT (red) and C290A (blue)

Aurora A proteins were incubated with TPX2 and then assayed in the presence of 1 mM DTT or 10 mM H_2O_2. Activity was calculated relative to a control containing buffer only after 5 mins assay time. In all assays described here, Aurora A proteins were incubated with TPX2 for 10 mins at 20 °C before the addition of redox reagent or ATP. The concentration of TPX2 in the final reaction mixture was fixed at 100 nM. **(C)** The activity of WT (red) and C290A (blue) Aurora A (6 nM, assayed with 1 mM ATP) was evaluated using peptide substrate in the presence or absence of GST-TPX2. GST at an equimolar concentration to TPX2 included as a control. **(D)** Activation of C290S (circles) but not C290D (squares) Aurora A (2.5 μM, with 1 mM ATP) in the presence or absence of TPX2 (20 μM) or DTT (10 mM). (**E)** Immunoblot of an *in vitro* kinase assay using recombinant GST-TACC3 (1 μg) as a substrate for WT, C290A and C290S Aurora A. Aurora A (100 ng) was incubated with a peptide derived from TPX2 (10 μM) and Aurora A-dependent phosphorylation of TACC3 (pSer558, top panel) was detected after 30 mins. 0.5 mM ATP and 5 mM $MgCl_2$ were included in the reaction. Reactions were terminated by the addition of SDS loading buffer. Equal loading of TACC3 substrate was confirmed with anti-TACC3 antibody (second panel from top). Also shown is total (second panel from bottom) and phosphorylated Aurora A (pThr 288, bottom panel).

Supplementary Figure 7. Reversible glutathionylation of Aurora A and AKT.

(A) Immunoblot demonstrating reversible glutathionylation of Aurora A. 1 μg of recombinant Aurora A protein was incubated in the presence or absence of 10 mM GSSG for 30 mins at 20°C. SDS-PAGE was performed under reducing and non-reducing conditions. Western blots were probed with an antibody with specificity towards glutathione-conjugated proteins. Equal loading of protein was confirmed using an antibody for Aurora A. PKA (1 μg) was also included as a positive control. **(B)** Inhibition of Aurora A by H_2O_2 is relieved by DTT but not GSH. Aurora A (12.5 nM) activity was assayed in the presence or absence of 1 mM H_2O_2 for 25 mins and the reactions were then supplemented (where indicated) with 2 mM GSH, followed by 2 mM DTT after 50 mins. Aurora A-dependent phosphorylation of the fluorescent peptide substrate was initiated by the addition of 1 mM ATP. **(C)** Aurora A (40 μM) was incubated in the presence or absence of 125 μM diamide or diamide with 100 μM GSH for 20 mins at 20 °C. Following this, reactions were supplemented with buffer control, 500 μM GSH and 0.16 mg/ml glutaredoxin-1 (GRX), or GSH and GRX in isolation for a further 20 mins. Reactions were then sampled for western blotting analysis (upper panel) or assayed using *in vitro* kinase assay (final Aurora A concentration was 200 nM, bottom panel). Data shown is mean and SD of two independent experiments. **(D)** AKT is potently activated by GSH. Activity of PDK1 phosphorylated S473D AKT (7 nM) was measured in the presence or absence of 2 mM GSH and 1 mM ATP.

Supplementary Figure 8. Taxonomic analysis of conserved Cys residues within the activation segment of ePKs.

(A) The distribution of Cys residues, and co-varying amino acids at all positions within the activation segment, located between the DFG and APE residues, are displayed using WebLogos. The percentage of ePKs containing the indicated Cys residues is indicated on the right. **(B)** Kinome group distribution of all ePKs containing a Cys 290 equivalent. The total number of kinases identified within each group is indicated. **(C)** Taxonomic distribution of T loop +2 Cys-containing sequences in all ePKs **(D)** Aurora kinases, **(E)** PKA and **(F)** PLK sub-families. Taxonomic groups are coloured as indicated and the total number of sequences identifiifed in each category are indicated within the pie chart.

Supplementary Figure 9. Biochemical analysis of Cys-containing protein kinases.

(A) Purified WT and Cys-Ala mutants kinases (0.5 μg each) resolved by SDS-PAGE and visualised by Coomassibe blue staining. **(B)** Detection of reactive cysteine oxidation in WT and Cys-Ala recombinant MELK proteins with an antibody with specificity towards cysteine sulfenic acids that have been derivatised by dimedone (SOH-MELK). GST-MELK (0.5 μg) was incubated in the presence of absence of 1 mM H_2O_2 for 10 min and then exposed to 1 mM dimedone for a further 20 mins (all incubations performed at 20°C). Total GST-MELK loading was visualised using ponceau staining (bottom panel).

Supplementary Figure 10. Thermal profiling and immunoblotting-based redox analysis of Aurora A 'DFG +2' kinase mutants.

(A) Bacterially expressed WT, S278A or S279C Aurora A (2 μg each) were purified in the absence of DTT, resolved by SDS-PAGE and visualised by Coomassie blue staining. **(B)** Thermal denaturation profiles of purified Aurora A proteins (5 μM). Representative unfolding profiles from three independent experiments are shown. Calculated T_m values are shown for each protein. **(C)** Change in Tm values (ΔT_m) induced by DTT or ATP/Mg incubation were determined from thermal melt curves. **(D)** DTT-dependent changes in the electrophoretic mobility of WT, S278A and S278C Aurora A were investigated in the presence and absence of H_2O_2. Aurora A (50 ng) was incubated with the indicated concentration of H_2O_2 for 10 mins at 20°C and analysed after non-reducing (-DTT) or reducing (+DTT) SDS-PAGE. Total Aurora A (upper panel) and pThr 288 Aurora A (lower panel) immunoblots are shown.

Supplementary Figure 11. Kinases possessing a T-loop +2 Cys residue that are insensitive to redox-dependent regulation.

A cohort of kinases with suspected redox sensitivity based on the presence of an analogous activation loop-located Cys residue were probed for reversible oxidation-dependent inhibition using real time phosphorylation of kinase specific peptide substrates (see Table 2). Assay conditions were as for Fig. 7 and the following concentrations of kinases were used: **(A)** 4 nM PHK, **(B, C)** 25 nM His-PKG1-1, and **(D,E)** 80 nM His-PKG1-2. Assays **(C)** and **(E)** were supplemented with 1 mM cGMP.

Supplementary Figure 12. Redox analysis of model Tyr kinases and Cys mutants.

Purified ABL and EPHA3 tyrosine kinases were assayed using the specified redox-dependent conditions described in Fig. 7 and Table 2. Final ABL or EPHA3 concentrations in the assay were: **(A)** 30 nM WT His-EPHA3, **(B)** 5 nM ABL and 30 nM of **(C)** G783C, **(D)** G784C or **(E)** G783C/G784C His-EPHA3

Supplementary Figure 13. Structural-models of disulphide-based mechanisms involving activation segment Cys in Ser/Thr kinases.

(A) Formation of an intramolecular disulfide in AKT between Cys residues in the activation segment. **(B)** Intermolecular disulfide between exchanged activation segments of MELK. Both events require the conservation of Cys residues in the activation segment.

REFERENCES AND NOTES:

1. Finkel, T., *Signal transduction by reactive oxygen species.* The Journal of cell biology, 2011. **194**(1): p. 7-15.
2. Dickinson, B.C. and C.J. Chang, *Chemistry and biology of reactive oxygen species in signaling or stress responses.* Nature chemical biology, 2011. **7**(8): p. 504-11.
3. Behring, J.B., et al., *Spatial and temporal alterations in protein structure by EGF regulate cryptic cysteine oxidation.* Science signaling, 2020. **13**(615).
4. Paulsen, C.E. and K.S. Carroll, *Orchestrating redox signaling networks through regulatory cysteine switches.* ACS chemical biology, 2010. **5**(1): p. 47-62.
5. Patterson, J.C., et al., *ROS and Oxidative Stress Are Elevated in Mitosis during Asynchronous Cell Cycle Progression and Are Exacerbated by Mitotic Arrest.* Cell systems, 2019. **8**(2): p. 163-167 e2.
6. Seo, Y.H. and K.S. Carroll, *Profiling protein thiol oxidation in tumor cells using sulfenic acid-specific antibodies.* Proceedings of the National Academy of Sciences of the United States of America, 2009. **106**(38): p. 16163-8.
7. Rhee, S.G., et al., *Intracellular messenger function of hydrogen peroxide and its regulation by peroxiredoxins.* Current opinion in cell biology, 2005. **17**(2): p. 183-9.
8. Gupta, V. and K.S. Carroll, *Sulfenic acid chemistry, detection and cellular lifetime.* Biochimica et Biophysica Acta (BBA)-General Subjects, 2014. **1840**(2): p. 847-875.
9. Salmeen, A., et al., *Redox regulation of protein tyrosine phosphatase 1B involves a sulphenyl-amide intermediate.* Nature, 2003. **423**(6941): p. 769-73.
10. van Montfort, R.L., et al., *Oxidation state of the active-site cysteine in protein tyrosine phosphatase 1B.* Nature, 2003. **423**(6941): p. 773-7.
11. Forman, H.J., et al., *Protein cysteine oxidation in redox signaling: caveats on sulfenic acid detection and quantification.* Archives of biochemistry and biophysics, 2017. **617**: p. 26-37.
12. Grek, C.L., et al., *Causes and consequences of cysteine S-glutathionylation.* The Journal of biological chemistry, 2013. **288**(37): p. 26497-504.
13. Anselmo, A.N. and M.H. Cobb, *Protein kinase function and glutathionylation.* The Biochemical journal, 2004. **381**(Pt 3): p. e1-2.
14. Schafer, F.Q. and G.R. Buettner, *Redox environment of the cell as viewed through the redox state of the glutathione disulfide/glutathione couple.* Free Radical Biology and Medicine, 2001. **30**(11): p. 1191-1212.
15. Owen, J.B. and D.A. Butterfield, *Measurement of oxidized/reduced glutathione ratio*, in *Protein Misfolding and Cellular Stress in Disease and Aging*2010, Springer. p. 269-277.
16. Maher, P., *The effects of stress and aging on glutathione metabolism.* Ageing research reviews, 2005. **4**(2): p. 288-314.
17. Dalle-Donne, I., et al., *S-glutathionylation in protein redox regulation.* Free Radical Biology and Medicine, 2007. **43**(6): p. 883-898.
18. Manning, G., et al., *Evolution of protein kinase signaling from yeast to man.* Trends in biochemical sciences, 2002. **27**(10): p. 514-20.
19. Nolen, B., S. Taylor, and G. Ghosh, *Regulation of protein kinases; controlling activity through activation segment conformation.* Molecular cell, 2004. **15**(5): p. 661-75.
20. Johnson, L.N., M.E. Noble, and D.J. Owen, *Active and inactive protein kinases: structural basis for regulation.* Cell, 1996. **85**(2): p. 149-58.
21. Kannan, N. and A.F. Neuwald, *Did protein kinase regulatory mechanisms evolve through elaboration of a simple structural component?* Journal of molecular biology, 2005. **351**(5): p. 956-72.
22. Tonks, N.K., *Redox redux: revisiting PTPs and the control of cell signaling.* Cell, 2005. **121**(5): p. 667-70.

23. Paulsen, C.E., et al., *Peroxide-dependent sulfenylation of the EGFR catalytic site enhances kinase activity.* Nature chemical biology, 2011. **8**(1): p. 57-64.
24. Truong, T.H. and K.S. Carroll, *Redox regulation of epidermal growth factor receptor signaling through cysteine oxidation.* Biochemistry, 2012. **51**(50): p. 9954-65.
25. Heppner, D.E., et al., *Direct cysteine sulfenylation drives activation of the Src kinase.* Nature communications, 2018. **9**(1): p. 4522.
26. Kemble, D.J. and G. Sun, *Direct and specific inactivation of protein tyrosine kinases in the Src and FGFR families by reversible cysteine oxidation.* Proceedings of the National Academy of Sciences of the United States of America, 2009. **106**(13): p. 5070-5.
27. Giannoni, E., et al., *Intracellular reactive oxygen species activate Src tyrosine kinase during cell adhesion and anchorage-dependent cell growth.* Molecular and cellular biology, 2005. **25**(15): p. 6391-403.
28. Cuello, F. and P. Eaton, *Cysteine-Based Redox Sensing and Its Role in Signaling by Cyclic Nucleotide-Dependent Kinases in the Cardiovascular System.* Annual review of physiology, 2019. **81**: p. 63-87.
29. Cross, J.V. and D.J. Templeton, *Oxidative stress inhibits MEKK1 by site-specific glutathionylation in the ATP-binding domain.* The Biochemical journal, 2004. **381**(Pt 3): p. 675-83.
30. Corcoran, A. and T.G. Cotter, *Redox regulation of protein kinases.* The FEBS journal, 2013. **280**(9): p. 1944-65.
31. Burgoyne, J.R., et al., *Cysteine redox sensor in PKGIa enables oxidant-induced activation.* Science, 2007. **317**(5843): p. 1393-1397.
32. Nadeau, P.J., S.J. Charette, and J. Landry, *REDOX reaction at ASK1-Cys250 is essential for activation of JNK and induction of apoptosis.* Molecular Biology of the Cell, 2009. **20**(16): p. 3628-3637.
33. Humphries, K.M., J.K. Pennypacker, and S.S. Taylor, *Redox regulation of cAMP-dependent protein kinase signaling: kinase versus phosphatase inactivation.* The Journal of biological chemistry, 2007. **282**(30): p. 22072-9.
34. Shao, D., et al., *A redox-dependent mechanism for regulation of AMPK activation by Thioredoxin1 during energy starvation.* Cell Metabolism, 2014. **19**(2): p. 232-245.
35. Cao, L.S., et al., *Structural basis for the regulation of maternal embryonic leucine zipper kinase.* PloS one, 2013. **8**(7): p. e70031.
36. Murata, H., et al., *Glutaredoxin exerts an antiapoptotic effect by regulating the redox state of Akt.* The Journal of biological chemistry, 2003. **278**(50): p. 50226-33.
37. Sjolander, J.J., et al., *A redox-sensitive thiol in Wis1 modulates the fission yeast MAPK response to H2O2 and is the target of a small molecule.* Molecular and cellular biology, 2020.
38. Kalyanaraman, H., et al., *The activity of cGMP-dependent protein kinase Ialpha is not directly regulated by oxidation-induced disulfide formation at cysteine 43.* The Journal of biological chemistry, 2017. **292**(20): p. 8262-8268.
39. Burgoyne, J.R., et al., *Hydrogen peroxide sensing and signaling by protein kinases in the cardiovascular system.* Antioxidants & redox signaling, 2013. **18**(9): p. 1042-52.
40. Sheehe, J.L., et al., *Oxidation of cysteine 117 stimulates constitutive activation of the type Ialpha cGMP-dependent protein kinase.* The Journal of biological chemistry, 2018. **293**(43): p. 16791-16802.
41. Cuello, F. and P. Eaton, *Cysteine-Based Redox Sensing and Its Role in Signaling by Cyclic Nucleotide-Dependent Kinases in the Cardiovascular System.* Annual review of physiology, 2018.

42. Prysyazhna, O., O. Rudyk, and P. Eaton, *Single atom substitution in mouse protein kinase G eliminates oxidant sensing to cause hypertension.* Nature medicine, 2012. **18**(2): p. 286-90.
43. Burgoyne, J.R., et al., *Cysteine redox sensor in PKGIa enables oxidant-induced activation.* Science, 2007. **317**(5843): p. 1393-7.
44. Butterworth, S., et al., *The structure-guided discovery of osimertinib: the first U.S. FDA approved mutant selective inhibitor of EGFR T790M.* MedChemComm, 2017. **8**(5): p. 820-822.
45. Zhao, Z., et al., *Determining Cysteines Available for Covalent Inhibition Across the Human Kinome.* Journal of medicinal chemistry, 2017. **60**(7): p. 2879-2889.
46. Liu, Q., et al., *Developing irreversible inhibitors of the protein kinase cysteinome.* Chemistry & biology, 2013. **20**(2): p. 146-59.
47. Byrne, D.P., D.M. Foulkes, and P.A. Eyers, *Pseudokinases: update on their functions and evaluation as new drug targets.* Future medicinal chemistry, 2017. **9**(2): p. 245-265.
48. Chaikuad, A., et al., *The Cysteinome of Protein Kinases as a Target in Drug Development.* Angewandte Chemie, 2018. **57**(16): p. 4372-4385.
49. Bischoff, J.R., et al., *A homologue of Drosophila aurora kinase is oncogenic and amplified in human colorectal cancers.* The EMBO journal, 1998. **17**(11): p. 3052-65.
50. Eyers, P.A., et al., *A novel mechanism for activation of the protein kinase Aurora A.* Current biology : CB, 2003. **13**(8): p. 691-7.
51. Bayliss, R., et al., *Structural basis of Aurora-A activation by TPX2 at the mitotic spindle.* Molecular cell, 2003. **12**(4): p. 851-62.
52. Eyers, P.A. and J.L. Maller, *Regulation of Xenopus Aurora A activation by TPX2.* The Journal of biological chemistry, 2004. **279**(10): p. 9008-15.
53. Burgess, S.G., et al., *Mitotic spindle association of TACC3 requires Aurora-A-dependent stabilization of a cryptic alpha-helix.* The EMBO journal, 2018. **37**(8).
54. Macurek, L., et al., *Polo-like kinase-1 is activated by aurora A to promote checkpoint recovery.* Nature, 2008. **455**(7209): p. 119-23.
55. Carmena, M. and W.C. Earnshaw, *The cellular geography of aurora kinases.* Nature reviews. Molecular cell biology, 2003. **4**(11): p. 842-54.
56. Hegarat, N., et al., *Aurora A and Aurora B jointly coordinate chromosome segregation and anaphase microtubule dynamics.* The Journal of cell biology, 2011. **195**(7): p. 1103-13.
57. Bertolin, G., et al., *Aurora kinase A localises to mitochondria to control organelle dynamics and energy production.* eLife, 2018. **7**.
58. Kosower, N.S. and E.M. Kosower, *[11] Diamide: An oxidant probe for thiols.* Methods in Enzymology, 1995. **251**: p. 123-133.
59. Humphries, K.M., C. Juliano, and S.S. Taylor, *Regulation of cAMP-dependent protein kinase activity by glutathionylation.* Journal of Biological Chemistry, 2002. **277**(45): p. 43505-43511.
60. Littlepage, L.E., et al., *Identification of phosphorylated residues that affect the activity of the mitotic kinase Aurora-A.* Proceedings of the National Academy of Sciences, 2002. **99**(24): p. 15440-15445.
61. Walter, A.O., et al., *The mitotic serine/threonine kinase Aurora2/AIK is regulated by phosphorylation and degradation.* Oncogene, 2000. **19**(42): p. 4906.
62. Rudyk, O. and P. Eaton, *Biochemical methods for monitoring protein thiol redox states in biological systems.* Redox biology, 2014. **2**: p. 803-813.
63. Sheehan, D., *Detection of redox-based modification in two-dimensional electrophoresis proteomic separations.* Biochemical and biophysical research communications, 2006. **349**(2): p. 455-62.

64. Chung, H.S., et al., *Cysteine Oxidative Posttranslational Modifications.* Circulation Research, 2013. **112**(2): p. 382-392.
65. Maller, C., E. Schröder, and P. Eaton, *Glyceraldehyde 3-phosphate dehydrogenase is unlikely to mediate hydrogen peroxide signaling: studies with a novel anti-dimedone sulfenic acid antibody.* Antioxidants & redox signaling, 2011. **14**(1): p. 49-60.
66. Soylu, İ. and S.M. Marino, *Cy-preds: An algorithm and a web service for the analysis and prediction of cysteine reactivity.* Proteins: Structure, Function, and Bioinformatics, 2016. **84**(2): p. 278-291.
67. Humphries, K.M., M.S. Deal, and S.S. Taylor, *Enhanced dephosphorylation of cAMP-dependent protein kinase by oxidation and thiol modification.* Journal of Biological Chemistry, 2005. **280**(4): p. 2750-2758.
68. Byrne, D.P., et al., *cAMP-dependent protein kinase (PKA) complexes probed by complementary differential scanning fluorimetry and ion mobility-mass spectrometry.* The Biochemical journal, 2016. **473**(19): p. 3159-75.
69. Foulkes, D.M., et al., *Covalent inhibitors of EGFR family protein kinases induce degradation of human Tribbles 2 (TRIB2) pseudokinase in cancer cells.* Science signaling, 2018. **11**(549).
70. Burgess, S.G. and R. Bayliss, *The structure of C290A: C393A Aurora A provides structural insights into kinase regulation.* Acta Crystallographica Section F: Structural Biology Communications, 2015. **71**(3): p. 315-319.
71. Humphries, K.M., J.K. Pennypacker, and S.S. Taylor, *Redox Regulation of cAMP-dependent Protein Kinase Signaling KINASE VERSUS PHOSPHATASE INACTIVATION.* Journal of Biological Chemistry, 2007. **282**(30): p. 22072-22079.
72. Kufer, T.A., et al., *Human TPX2 is required for targeting Aurora-A kinase to the spindle.* Journal of Cell Biology, 2002. **158**(4): p. 617-623.
73. Zorba, A., et al., *Molecular mechanism of Aurora A kinase autophosphorylation and its allosteric activation by TPX2.* Elife, 2014. **3**: p. e02667.
74. Dodson, C.A. and R. Bayliss, *Activation of Aurora-A kinase by protein partner binding and phosphorylation are independent and synergistic.* Journal of Biological Chemistry, 2012. **287**(2): p. 1150-1157.
75. Ruff, E.F., et al., *A dynamic mechanism for allosteric activation of Aurora kinase A by activation loop phosphorylation.* Elife, 2018. **7**: p. e32766.
76. Kinoshita, K., et al., *Aurora A phosphorylation of TACC3/maskin is required for centrosome-dependent microtubule assembly in mitosis.* Journal of Cell Biology, 2005. **170**(7): p. 1047-1055.
77. Tyler, R.K., et al., *VX-680 inhibits Aurora A and Aurora B kinase activity in human cells.* Cell cycle, 2007. **6**(22): p. 2846-54.
78. Criddle, D.N., et al., *Menadione-induced reactive oxygen species generation via redox cycling promotes apoptosis of murine pancreatic acinar cells.* Journal of Biological Chemistry, 2006. **281**(52): p. 40485-40492.
79. Askoxylakis, V., et al., *Investigation of tumor hypoxia using a two-enzyme system for in vitro generation of oxygen deficiency.* Radiation oncology, 2011. **6**(1): p. 35.
80. Mueller, S., G. Millonig, and G. Waite, *The GOX/CAT system: a novel enzymatic method to independently control hydrogen peroxide and hypoxia in cell culture.* Advances in Medical Sciences (De Gruyter Open), 2009. **54**(2).
81. Truong, T.H., et al., *Molecular basis for redox activation of epidermal growth factor receptor kinase.* Cell chemical biology, 2016. **23**(7): p. 837-848.
82. van der Reest, J., et al., *Proteome-wide analysis of cysteine oxidation reveals metabolic sensitivity to redox stress.* Nature communications, 2018. **9**(1): p. 1581.
83. Go, Y.M., J.D. Chandler, and D.P. Jones, *The cysteine proteome.* Free radical biology & medicine, 2015. **84**: p. 227-245.

84. Eyers, P.A., K. Keeshan, and N. Kannan, *Tribbles in the 21st Century: The Evolving Roles of Tribbles Pseudokinases in Biology and Disease.* Trends in cell biology, 2017. **27**(4): p. 284-298.
85. Smith, D.A., et al., *The Srk1 protein kinase is a target for the Sty1 stress-activated MAPK in fission yeast.* The Journal of biological chemistry, 2002. **277**(36): p. 33411-21.
86. Stokoe, D., et al., *MAPKAP kinase-2; a novel protein kinase activated by mitogen-activated protein kinase.* The EMBO journal, 1992. **11**(11): p. 3985-94.
87. Smith, F.D., et al., *Local protein kinase A action proceeds through intact holoenzymes.* Science, 2017. **356**(6344): p. 1288-1293.
88. Gupta, D.R., et al., *Multistep regulation of protein kinase A in its localization, phosphorylation and binding with a regulatory subunit in fission yeast.* Current genetics, 2011. **57**(5): p. 353-65.
89. Lopez-Aviles, S., et al., *Inactivation of the Cdc25 phosphatase by the stress-activated Srk1 kinase in fission yeast.* Molecular cell, 2005. **17**(1): p. 49-59.
90. Leroux, A.E., J.O. Schulze, and R.M. Biondi. *AGC kinases, mechanisms of regulation and innovative drug development*. in *Seminars in Cancer Biology*. 2018. Elsevier.
91. Combes, G., et al., *Playing polo during mitosis: PLK1 takes the lead.* Oncogene, 2017. **36**(34): p. 4819.
92. Scutt, P.J., et al., *Discovery and exploitation of inhibitor-resistant aurora and polo kinase mutants for the analysis of mitotic networks.* The Journal of biological chemistry, 2009. **284**(23): p. 15880-93.
93. Caron, D., et al., *Mitotic phosphotyrosine network analysis reveals that tyrosine phosphorylation regulates Polo-like kinase 1 (PLK1).* Sci. Signal., 2016. **9**(458): p. rs14-rs14.
94. Bettencourt-Dias, M., et al., *SAK/PLK4 is required for centriole duplication and flagella development.* Current Biology, 2005. **15**(24): p. 2199-2207.
95. Habedanck, R., et al., *The Polo kinase Plk4 functions in centriole duplication.* Nature Cell Biology, 2005. **7**(11): p. 1140.
96. Manning, G., et al., *The protein kinase complement of the human genome.* Science, 2002. **298**(5600): p. 1912-1934.
97. Wang, Y., et al., *MELK is an oncogenic kinase essential for mitotic progression in basal-like breast cancer cells.* Elife, 2014. **3**: p. e01763.
98. Beullens, M., et al., *Substrate specificity and activity regulation of protein kinase MELK.* Journal of Biological Chemistry, 2005. **280**(48): p. 40003-40011.
99. Huang, X., et al., *Crystal structure of an inactive Akt2 kinase domain.* Structure, 2003. **11**(1): p. 21-30.
100. Zmijewski, J.W., et al., *Exposure to hydrogen peroxide induces oxidation and activation of AMP-activated protein kinase.* Journal of Biological Chemistry, 2010: p. jbc. M110. 143685.
101. Bright, N., C. Thornton, and D. Carling, *The regulation and function of mammalian AMPK-related kinases.* Acta physiologica, 2009. **196**(1): p. 15-26.
102. Kambe, T., et al., *Inactivation of Ca2+/calmodulin-dependent protein kinase I by S-glutathionylation of the active-site cysteine residue.* FEBS Letters, 2010. **584**(11): p. 2478-2484.
103. Erickson, J.R., et al., *A dynamic pathway for calcium-independent activation of CaMKII by methionine oxidation.* Cell, 2008. **133**(3): p. 462-474.
104. Leonberg, A.K. and Y.-C. Chai, *The functional role of cysteine residues for c-Abl kinase activity.* Molecular and cellular biochemistry, 2007. **304**(1-2): p. 207-212.
105. Brandes, N., S. Schmitt, and U. Jakob, *Thiol-based redox switches in eukaryotic proteins.* Antioxidants & redox signaling, 2009. **11**(5): p. 997-1014.

106. Tsuchiya, Y., *Covalent Aurora A regulation by the metabolic integrator coenzyme A.* BioRxiv, 2018. **PrePrint**.
107. Beenstock, J., N. Mooshayef, and D. Engelberg, *How do protein kinases take a selfie (autophosphorylate)?* Trends in Biochemical Sciences, 2016. **41**(11): p. 938-953.
108. Pearce, L.R., D. Komander, and D.R. Alessi, *The nuts and bolts of AGC protein kinases.* Nature reviews. Molecular cell biology, 2010. **11**(1): p. 9-22.
109. Murata, H., et al., *Glutaredoxin exerts an anti-apoptotic effect by regulating the redox state of Akt.* Journal of Biological Chemistry, 2003.
110. Tavender, T.J. and N.J. Bulleid, *Peroxiredoxin IV protects cells from oxidative stress by removing H2O2 produced during disulphide formation.* Journal of cell science, 2010. **123**(Pt 15): p. 2672-9.
111. Burhans, W.C. and N.H. Heintz, *The cell cycle is a redox cycle: linking phase-specific targets to cell fate.* Free Radical Biology and Medicine, 2009. **47**(9): p. 1282-1293.
112. Chiu, J. and I.W. Dawes, *Redox control of cell proliferation.* Trends in cell biology, 2012. **22**(11): p. 592-601.
113. Wang, G.-F., et al., *Oxidative stress induces mitotic arrest by inhibiting Aurora A-involved mitotic spindle formation.* Free Radical Biology and Medicine, 2017. **103**: p. 177-187.
114. Shagisultanova, E., R.L. Dunbrack Jr, and E.A. Golemis, *Issues in interpreting the in vivo activity of Aurora-A.* Expert Opinion on Therapeutic Targets, 2015. **19**(2): p. 187-200.
115. Walter, A.O., et al., *The mitotic serine/threonine kinase Aurora2/AIK is regulated by phosphorylation and degradation.* Oncogene, 2000. **19**(42): p. 4906-16.
116. Zhao, Z.-s., et al., *The GIT-associated kinase PAK targets to the centrosome and regulates Aurora-A.* Molecular Cell, 2005. **20**(2): p. 237-249.
117. Willems, E., et al., *The functional diversity of Aurora kinases: a comprehensive review.* Cell Division, 2018. **13**(1): p. 7.
118. Tsuchiya, Y., et al., *Covalent Aurora A regulation by the metabolic integrator coenzyme A.* Redox biology, 2020. **28**: p. 101318.
119. Corcoran, A. and T.G. Cotter, *Redox regulation of protein kinases.* FEBS Journal, 2013. **280**(9): p. 1944-1965.
120. Truong, T.H. and K.S. Carroll, *Redox regulation of protein kinases.* Critical Reviews in Biochemistry and Molecular Biology, 2013. **48**(4): p. 332-356.
121. Saitoh, M., et al., *Mammalian thioredoxin is a direct inhibitor of apoptosis signal-regulating kinase (ASK) 1.* The EMBO journal, 1998. **17**(9): p. 2596-606.
122. Park, H.-S., et al., *Inhibition of apoptosis signal-regulating kinase 1 by nitric oxide through a thiol redox mechanism.* Journal of Biological Chemistry, 2004. **279**(9): p. 7584-7590.
123. Janet, V. and D.J. Templeton, *Oxidative stress inhibits MEKK1 by site-specific glutathionylation in the ATP-binding domain.* Biochemical Journal, 2004. **381**(3): p. 675-683.
124. Diao, Y., et al., *Oxidation-induced intramolecular disulfide bond inactivates mitogen-activated protein kinase kinase 6 by inhibiting ATP binding.* Proceedings of the National Academy of Sciences, 2010. **107**(49): p. 20974-20979.
125. Wilhelm, D., et al., *The level of intracellular glutathione is a key regulator for the induction of stress-activated signal transduction pathways including Jun N-terminal protein kinases and p38 kinase by alkylating agents.* Molecular and cellular biology, 1997. **17**(8): p. 4792-800.
126. Jarvis, R.M., S.M. Hughes, and E.C. Ledgerwood, *Peroxiredoxin 1 functions as a signal peroxidase to receive, transduce, and transmit peroxide signals in mammalian cells.* Free radical biology & medicine, 2012. **53**(7): p. 1522-30.

127. Stocker, S., et al., *A role for 2-Cys peroxiredoxins in facilitating cytosolic protein thiol oxidation.* Nature chemical biology, 2018. **14**(2): p. 148-155.
128. Peralta, D., et al., *A proton relay enhances H2O2 sensitivity of GAPDH to facilitate metabolic adaptation.* Nature chemical biology, 2015. **11**(2): p. 156-63.
129. Poole, L.B., *The basics of thiols and cysteines in redox biology and chemistry.* Free radical biology & medicine, 2015. **80**: p. 148-57.
130. McSkimming, D.I., et al., *KinView: a visual comparative sequence analysis tool for integrated kinome research.* Molecular bioSystems, 2016. **12**(12): p. 3651-3665.
131. Caron, D., et al., *Mitotic phosphotyrosine network analysis reveals that tyrosine phosphorylation regulates Polo-like kinase 1 (PLK1).* Science signaling, 2016. **9**(458): p. rs14.
132. Wilson, L.J., et al., *New Perspectives, Opportunities, and Challenges in Exploring the Human Protein Kinome.* Cancer research, 2018. **78**(1): p. 15-29.
133. Cobbaut, M., et al., *Differential regulation of PKD isoforms in oxidative stress conditions through phosphorylation of a conserved Tyr in the P+1 loop.* Scientific reports, 2017. **7**(1): p. 887.
134. Levinson, N.M., *The multifaceted allosteric regulation of Aurora kinase A.* The Biochemical journal, 2018. **475**(12): p. 2025-2042.
135. Dodson, C.A., et al., *Crystal structure of an Aurora-A mutant that mimics Aurora-B bound to MLN8054: insights into selectivity and drug design.* Biochemical journal, 2010. **427**(1): p. 19-28.
136. McIntyre, P.J., et al., *Characterization of three druggable hot-spots in the aurora-A/TPX2 interaction using biochemical, biophysical, and fragment-based approaches.* ACS Chemical Biology, 2017. **12**(11): p. 2906-2914.
137. Pitsawong, W., et al., *Dynamics of human protein kinase Aurora A linked to drug selectivity.* Elife, 2018. **7**: p. e36656.
138. Lake, E.W., et al., *Quantitative conformational profiling of kinase inhibitors reveals origins of selectivity for Aurora kinase activation states.* Proceedings of the National Academy of Sciences, 2018. **115**(51): p. E11894-E11903.
139. Gilburt, J.A., et al., *Dynamic Equilibrium of the Aurora A Kinase Activation Loop Revealed by Single-Molecule Spectroscopy.* Angewandte Chemie International Edition, 2017. **56**(38): p. 11409-11414.
140. Cao, L.-S., et al., *Structural basis for the regulation of maternal embryonic leucine zipper kinase.* PloS One, 2013. **8**(7): p. e70031.
141. Shrestha, S., *Identification of a novel redox-active switch in Fructosamine-3-kinases expands the regulatory repertoire of the protein kinase fold family of enzymes.* BioRxiv, 2019.
142. Bharadwaj, M.S., et al., *Relationships between mitochondrial content and bioenergetics with obesity, body composition and fat distribution in healthy older adults.* BMC obesity, 2015. **2**(1): p. 40.
143. Wallace, D.C., *Mitochondria and cancer.* Nature Reviews Cancer, 2012. **12**(10): p. 685.
144. Arun, S., L. Liu, and G. Donmez, *Mitochondrial biology and neurological diseases.* Current Neuropharmacology, 2016. **14**(2): p. 143-154.
145. Gill, J.G., E. Piskounova, and S.J. Morrison. *Cancer, oxidative stress, and metastasis*. in *Cold Spring Harbor Symposia on Quantitative Biology*. 2016. Cold Spring Harbor Laboratory Press.
146. Singh, M. and H.R. Jadhav, *Targeting non-small cell lung cancer with small-molecule EGFR tyrosine kinase inhibitors.* Drug discovery today, 2018. **23**(3): p. 745-753.

147. Leproult, E., et al., *Cysteine mapping in conformationally distinct kinase nucleotide binding sites: application to the design of selective covalent inhibitors.* Journal of Medicinal Chemistry, 2011. **54**(5): p. 1347-1355.
148. Bain, J., et al., *The selectivity of protein kinase inhibitors: a further update.* The Biochemical journal, 2007. **408**(3): p. 297-315.
149. Mohanty, S., et al., *Hydrophobic Core Variations Provide a Structural Framework for Tyrosine Kinase Evolution and Functional Specialization.* PLoS genetics, 2016. **12**(2): p. e1005885.
150. Byrne, D.P., et al., *New tools for evaluating protein tyrosine sulfation: tyrosylprotein sulfotransferases (TPSTs) are novel targets for RAF protein kinase inhibitors.* The Biochemical journal, 2018. **475**(15): p. 2435-2455.
151. Murphy, J.M., et al., *A robust methodology to subclassify pseudokinases based on their nucleotide-binding properties.* The Biochemical journal, 2014. **457**(2): p. 323-34.
152. Lu, S., et al., *Mapping disulfide bonds from sub-micrograms of purified proteins or micrograms of complex protein mixtures.* Biophysics reports, 2018. **4**(2): p. 68-81.
153. Mormann, M., et al., *Fragmentation of intra-peptide and inter-peptide disulfide bonds of proteolytic peptides by nanoESI collision-induced dissociation.* Analytical and bioanalytical chemistry, 2008. **392**(5): p. 831-8.
154. Neuwald, A.F., *Rapid detection, classification and accurate alignment of up to a million or more related protein sequences.* Bioinformatics, 2009. **25**(15): p. 1869-75.
155. Kannan, N., et al., *Structural and functional diversity of the microbial kinome.* PLoS biology, 2007. **5**(3): p. e17.
156. Finn, R.D., et al., *The Pfam protein families database.* Nucleic acids research, 2010. **38**(Database issue): p. D211-22.
157. Talevich, E., A. Mirza, and N. Kannan, *Structural and evolutionary divergence of eukaryotic protein kinases in Apicomplexa.* BMC evolutionary biology, 2011. **11**: p. 321.
158. consortium, U., *UniProt: a hub for protein information.* Nucleic acids research, 2015. **43**(Database issue): p. D204-12.
159. Sayers, E.W., et al., *Database resources of the National Center for Biotechnology Information.* Nucleic acids research, 2009. **37**(Database issue): p. D5-15.
160. Schneider, T.D. and R.M. Stephens, *Sequence logos: a new way to display consensus sequences.* Nucleic acids research, 1990. **18**(20): p. 6097-100.
161. Craven, R.A., et al., *Vectors for the expression of tagged proteins in Schizosaccharomyces pombe.* Gene, 1998. **221**(1): p. 59-68.
162. Day, A.M. and E.A. Veal, *Hydrogen peroxide-sensitive cysteines in the Sty1 MAPK regulate the transcriptional response to oxidative stress.* The Journal of biological chemistry, 2010. **285**(10): p. 7505-16.
163. Day, A.M. and E.A. Veal, *Hydrogen Peroxide-sensitive Cysteines in the Sty1 MAPK Regulate the Transcriptional Response to Oxidative Stress.* J Biol Chem, 2010. **285**(10): p. 7505-16.
164. Wolfe, B.A. and K.L. Gould, *Fission yeast Clp1p phosphatase affects G2/M transition and mitotic exit through Cdc25p inactivation.* The EMBO journal, 2004. **23**(4): p. 919-29.
165. Higuchi, T., Y. Watanabe, and M. Yamamoto, *Protein kinase A regulates sexual development and gluconeogenesis through phosphorylation of the Zn finger transcriptional activator Rst2p in fission yeast.* Molecular and cellular biology, 2002. **22**(1): p. 1-11.

ACKNOWLEDGEMENTS:

We thank Professor Kathy Gould and Professor Masayuki Yamamoto for *S. pombe* strains and Dr James Hastie and Dr Hilary McLauchlan for help with reagents. The authors also thank Sam Evans for media preparation and outstanding technical support**.**

FUNDING:

This work was funded by a Royal Society Research Grant (to PAE), BBSRC TRDF grant B/N021703/1 (to PAE), BBSRC DTP studentship (MG), BBSRC project grant BH181282 (to EV) and North West Cancer Research grants CR1097 and CR1208 (to DPB and PAE). Funding for NK from the National Institutes of Health (R01GM114409) is also gratefully acknowledged.

AUTHOR CONTRIBUTIONS:

PAE, CEE and EAV obtained funding and designed experiments collaboratively alongside DPB, MG, MC AEC and LD, who performed the experiments. SS and NK performed bioinformatics analysis, and DPB and PAE wrote the paper, with contributions from all authors, who also approved the final version prior to submission.

COMPETING INTERESTS:

There are no perceived conflicts of interest from any authors.

DATA AND MATERIALS AVAILABILITY:

All data needed to evaluate conclusions made are available in the main or supplementary sections of the paper.

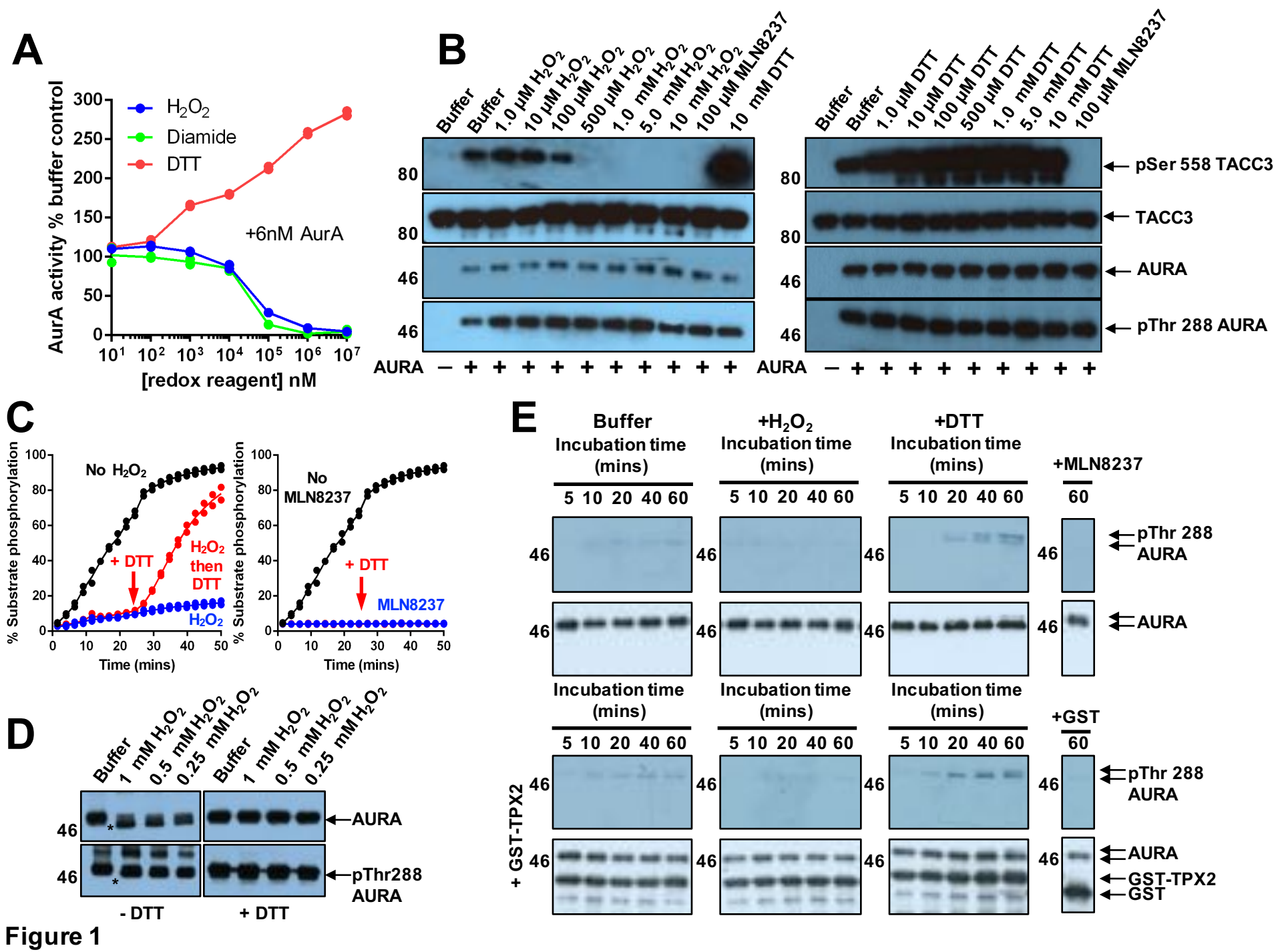
A
AurA activity % buffer control
[redox reagent] nM
H2O2
Diamide
DTT
+6nM AurA
B
Buffer
1.0 µM H2O2
10 µM H2O2
100 µM H2O2
500 µM H2O2
1.0 mM H2O2
5.0 mM H2O2
10 mM H2O2
100 µM MLN8237
10 mM DTT
1.0 µM DTT
10 µM DTT
100 µM DTT
500 µM DTT
1.0 mM DTT
5.0 mM DTT
10 mM DTT
100 µM MLN8237
pSer 558 TACC3
TACC3
AURA
pThr 288 AURA
AURA
C
% Substrate phosphorylation
Time (mins)
No H2O2
+ DTT
H2O2 then DTT
H2O2
No MLN8237
+ DTT
MLN8237
D
Buffer
1 mM H2O2
0.5 mM H2O2
0.25 mM H2O2
AURA
pThr288 AURA
- DTT
+ DTT
E
Buffer
+H2O2
+DTT
Incubation time (mins)
5 10 20 40 60
+MLN8237
60
pThr 288 AURA
AURA
+GST
+ GST-TPX2
GST-TPX2
GST

Figure 1

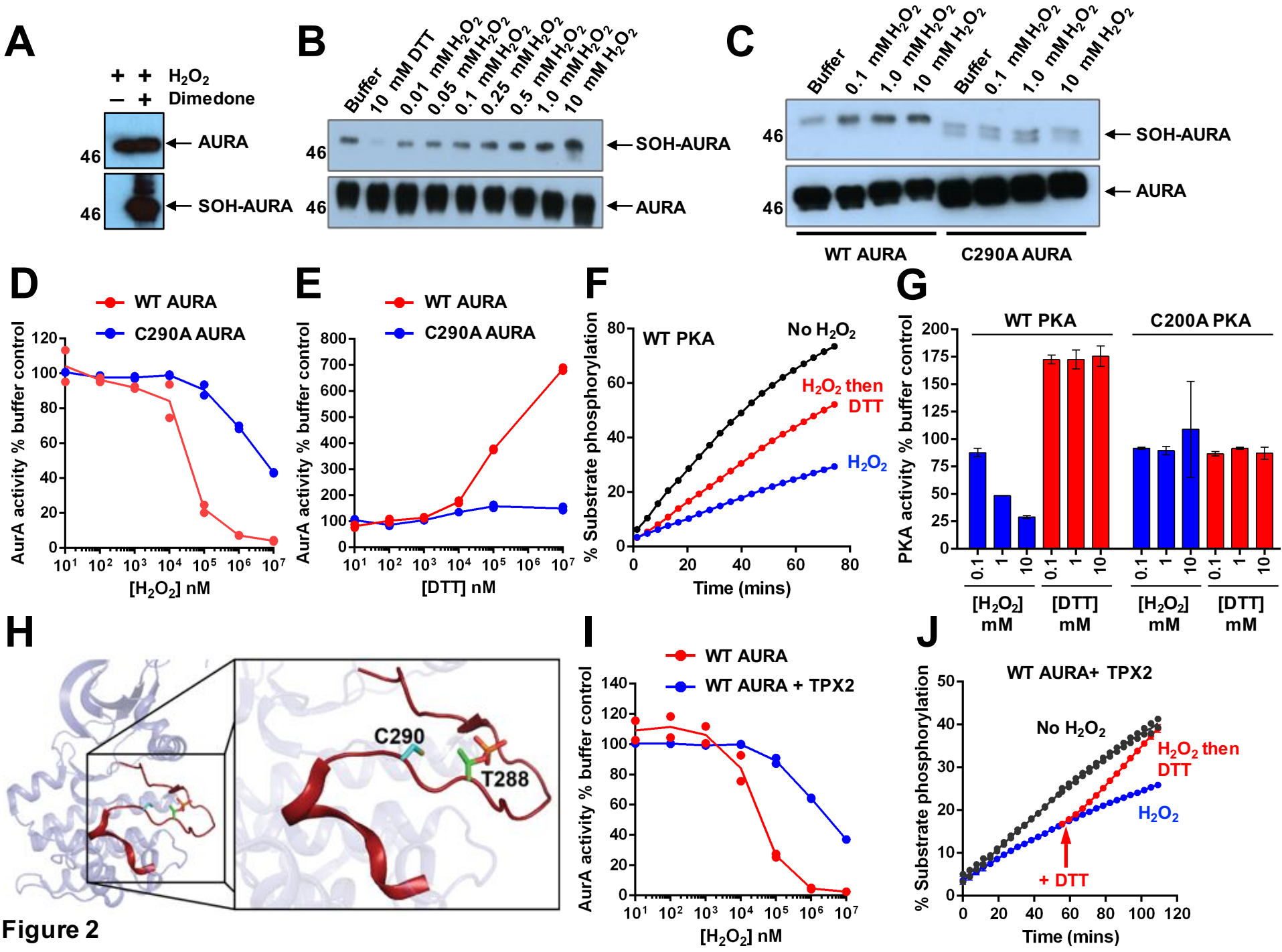
A
+ + H2O2
– + Dimedone
46
AURA
46
SOH-AURA
B
Buffer
10 mM DTT
0.01 mM H2O2
0.05 mM H2O2
0.1 mM H2O2
0.25 mM H2O2
0.5 mM H2O2
1.0 mM H2O2
10 mM H2O2
46
SOH-AURA
46
AURA
C
Buffer
0.1 mM H2O2
1.0 mM H2O2
10 mM H2O2
Buffer
0.1 mM H2O2
1.0 mM H2O2
10 mM H2O2
46
SOH-AURA
46
AURA
WT AURA
C290A AURA
D
WT AURA
C290A AURA
AurA activity % buffer control
[H2O2] nM
E
WT AURA
C290A AURA
AurA activity % buffer control
[DTT] nM
F
WT PKA
No H2O2
H2O2 then DTT
H2O2
% Substrate phosphorylation
Time (mins)
G
WT PKA
C200A PKA
PKA activity % buffer control
[H2O2] mM
[DTT] mM
[H2O2] mM
[DTT] mM
H
C290
T288
I
WT AURA
WT AURA + TPX2
AurA activity % buffer control
[H2O2] nM
J
WT AURA+ TPX2
No H2O2
H2O2 then DTT
H2O2
+ DTT
% Substrate phosphorylation
Time (mins)

Figure 2

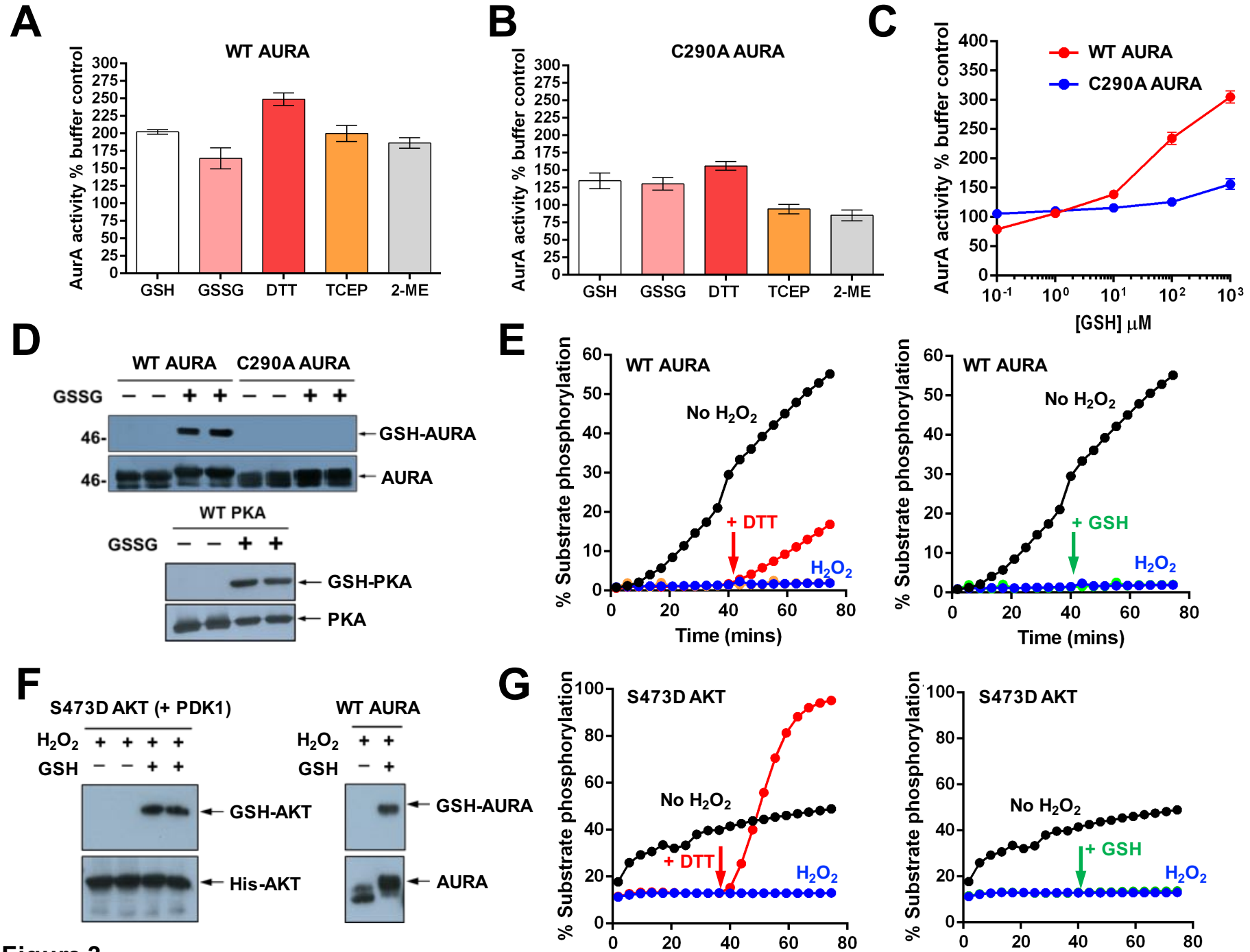
A
WT AURA
AurA activity % buffer control
GSH
GSSG
DTT
TCEP
2-ME
B
C290A AURA
C
WT AURA
C290A AURA
[GSH] μM
D
WT AURA
C290A AURA
GSSG
GSH-AURA
AURA
WT PKA
GSH-PKA
PKA
E
% Substrate phosphorylation
Time (mins)
No H2O2
+ DTT
+ GSH
H2O2
F
S473D AKT (+ PDK1)
WT AURA
H2O2
GSH
GSH-AKT
His-AKT
GSH-AURA
AURA
G
S473D AKT

Figure 3

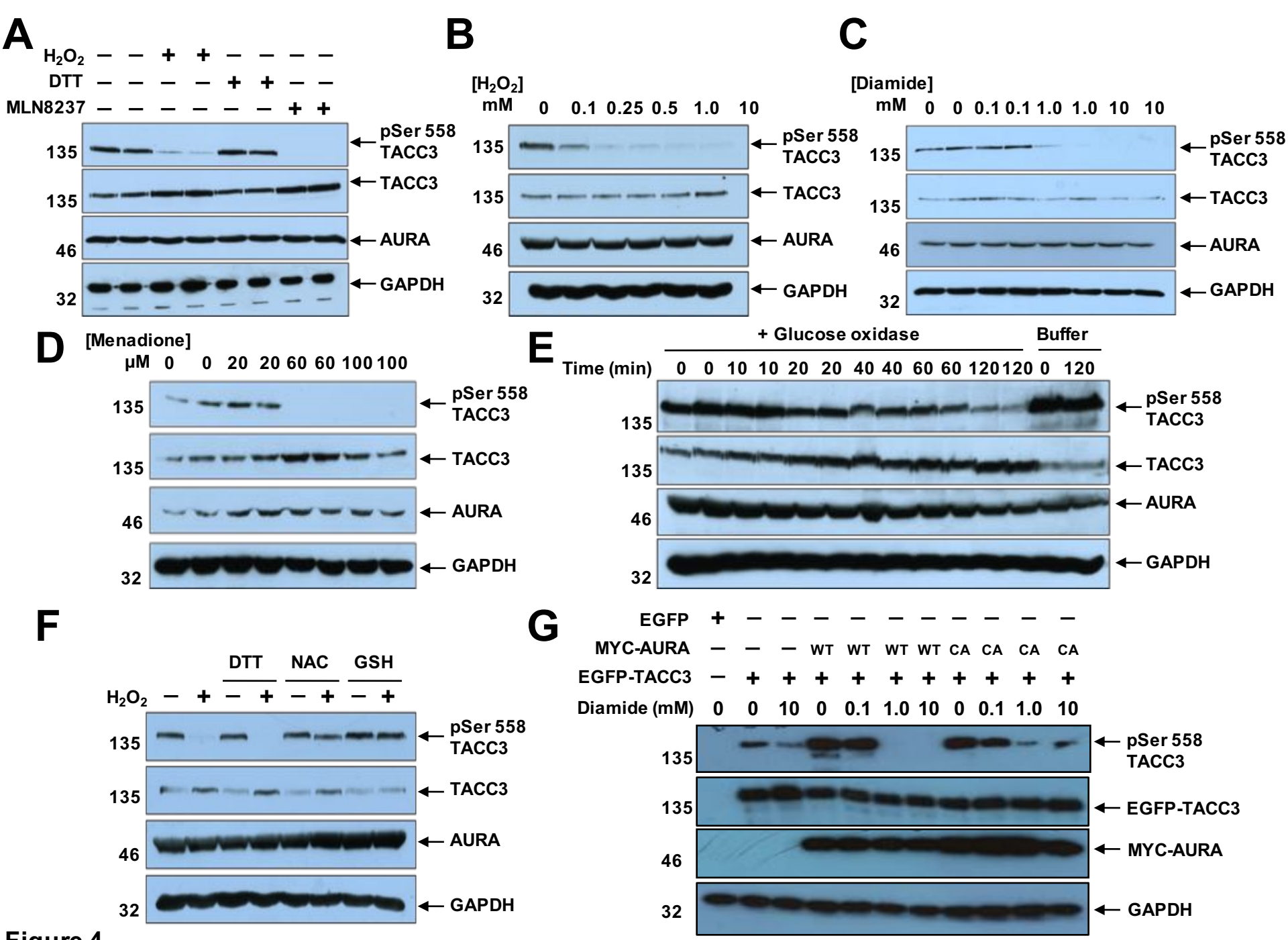
A
H2O2 – – + + – – – –
DTT – – – – + + – –
MLN8237 – – – – – – + +
135
135
46
32
pSer 558 TACC3
TACC3
AURA
GAPDH
B
[H2O2]
mM 0 0.1 0.25 0.5 1.0 10
135
135
46
32
pSer 558 TACC3
TACC3
AURA
GAPDH
C
[Diamide]
mM 0 0 0.1 0.1 1.0 1.0 10 10
135
135
46
32
pSer 558 TACC3
TACC3
AURA
GAPDH
D
[Menadione]
μM 0 0 20 20 60 60 100 100
135
135
46
32
pSer 558 TACC3
TACC3
AURA
GAPDH
E
+ Glucose oxidase
Buffer
Time (min) 0 0 10 10 20 20 40 40 60 60 120 120 0 120
135
135
46
32
pSer 558 TACC3
TACC3
AURA
GAPDH
F
DTT NAC GSH
H2O2 – + – + – + – +
135
135
46
32
pSer 558 TACC3
TACC3
AURA
GAPDH
G
EGFP + – – – – – – – – – –
MYC-AURA – – – WT WT WT WT CA CA CA CA
EGFP-TACC3 – + + + + + + + + + +
Diamide (mM) 0 0 10 0 0.1 1.0 10 0 0.1 1.0 10
135
135
46
32
pSer 558 TACC3
EGFP-TACC3
MYC-AURA
GAPDH

Figure 4

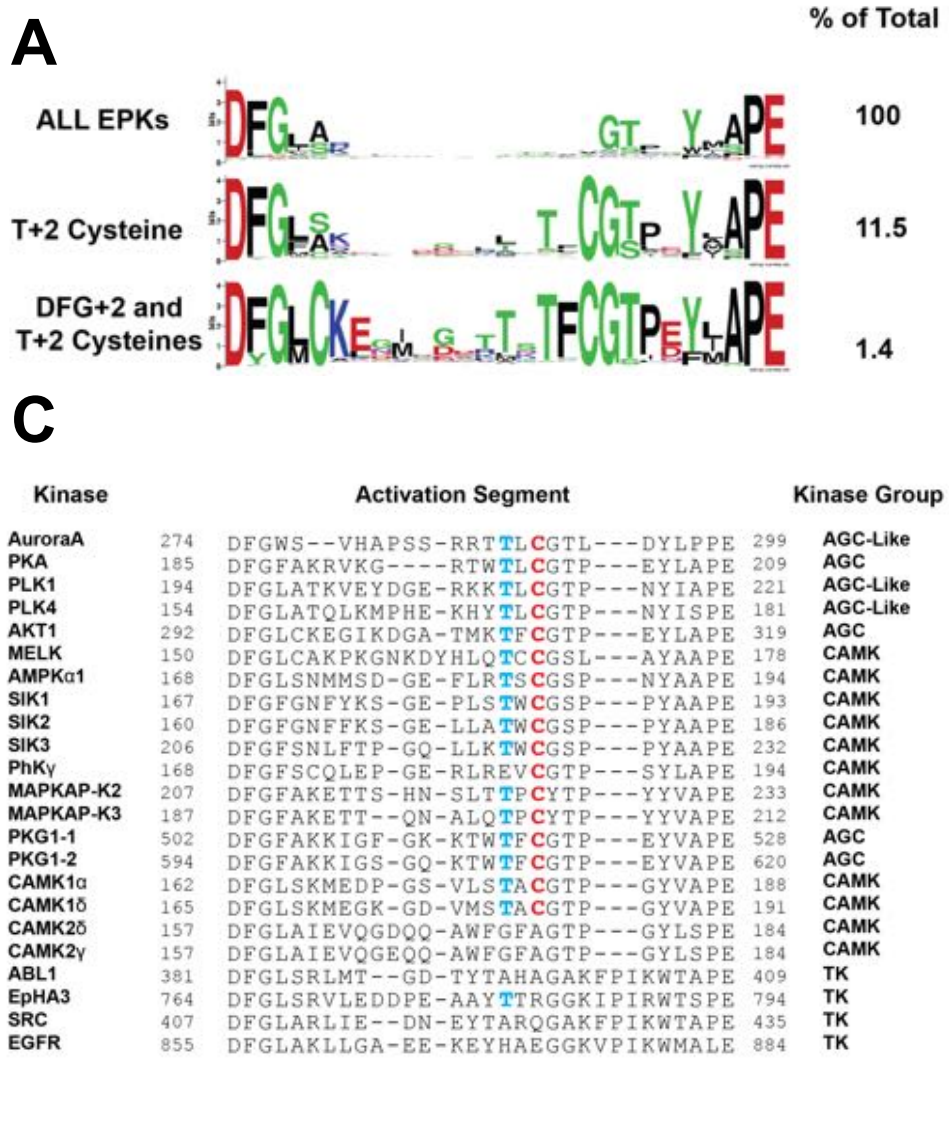
A
% of Total
ALL EPKs
100
T+2 Cysteine
11.5
DFG+2 and
T+2 Cysteines
1.4
C
Kinase
Activation Segment
Kinase Group
AuroraA 274 DFGWS--VHAPSS-RRTTLCGTL---DYLPPE 299 AGC-Like
PKA 185 DFGFAKRVKG----RTWTLCGTP---EYLAPE 209 AGC
PLK1 194 DFGLATKVEYDGE-RKKTLCGTP---NYIAPE 221 AGC-Like
PLK4 154 DFGLATQLKMPHE-KHYTLCGTP---NYISPE 181 AGC-Like
AKT1 292 DFGLCKEGIKDGA-TMKTFCGTP---EYLAPE 319 AGC
MELK 150 DFGLCAKPKGNKDYHLQTCCGSL---AYAAPE 178 CAMK
AMPKα1 168 DFGLSNMMSD-GE-FLRTSCGSP---NYAAPE 194 CAMK
SIK1 167 DFGFGNFYKS-GE-PLSTWCGSP---PYAAPE 193 CAMK
SIK2 160 DFGFGNFFKS-GE-LLATWCGSP---PYAAPE 186 CAMK
SIK3 206 DFGFSNLFTP-GQ-LLKTWCGSP---PYAAPE 232 CAMK
PhKγ 168 DFGFSCQLEP-GE-RLREVCGTP---SYLAPE 194 CAMK
MAPKAP-K2 207 DFGFAKETTS-HN-SLTTPCYTP---YYVAPE 233 CAMK
MAPKAP-K3 187 DFGFAKETT--QN-ALQTPCYTP---YYVAPE 212 CAMK
PKG1-1 502 DFGFAKKIGF-GK-KTWTFCGTP---EYVAPE 528 AGC
PKG1-2 594 DFGFAKKIGS-GQ-KTWTFCGTP---EYVAPE 620 AGC
CAMK1α 162 DFGLSKMEDP-GS-VLSTACGTP---GYVAPE 188 CAMK
CAMK1δ 165 DFGLSKMEGK-GD-VMSTACGTP---GYVAPE 191 CAMK
CAMK2δ 157 DFGLAIEVQGDQQ-AWFGFAGTP---GYLSPE 184 CAMK
CAMK2γ 157 DFGLAIEVQGEQQ-AWFGFAGTP---GYLSPE 184 CAMK
ABL1 381 DFGLSRLMT--GD-TYTAHAGAKFPIKWTAPE 409 TK
EpHA3 764 DFGLSRVLEDDPE-AAYTTRGGKIPIRWTSPE 794 TK
SRC 407 DFGLARLIE--DN-EYTARQGAKFPIKWTAPE 435 TK
EGFR 855 DFGLAKLLGA-EE-KEYHAEGGKVPIKWMALE 884 TK
B
Human Kinome:
Cys Activation Segment
TK
TKL
STE
CMGC
CK1
AGC
CAMK
Cys-residue
TK pseudokinase Cys-residue
"Illustration reproduced courtesy of Cell Signaling Technology, Inc. (www.cellsignal.com)"

Figure 5

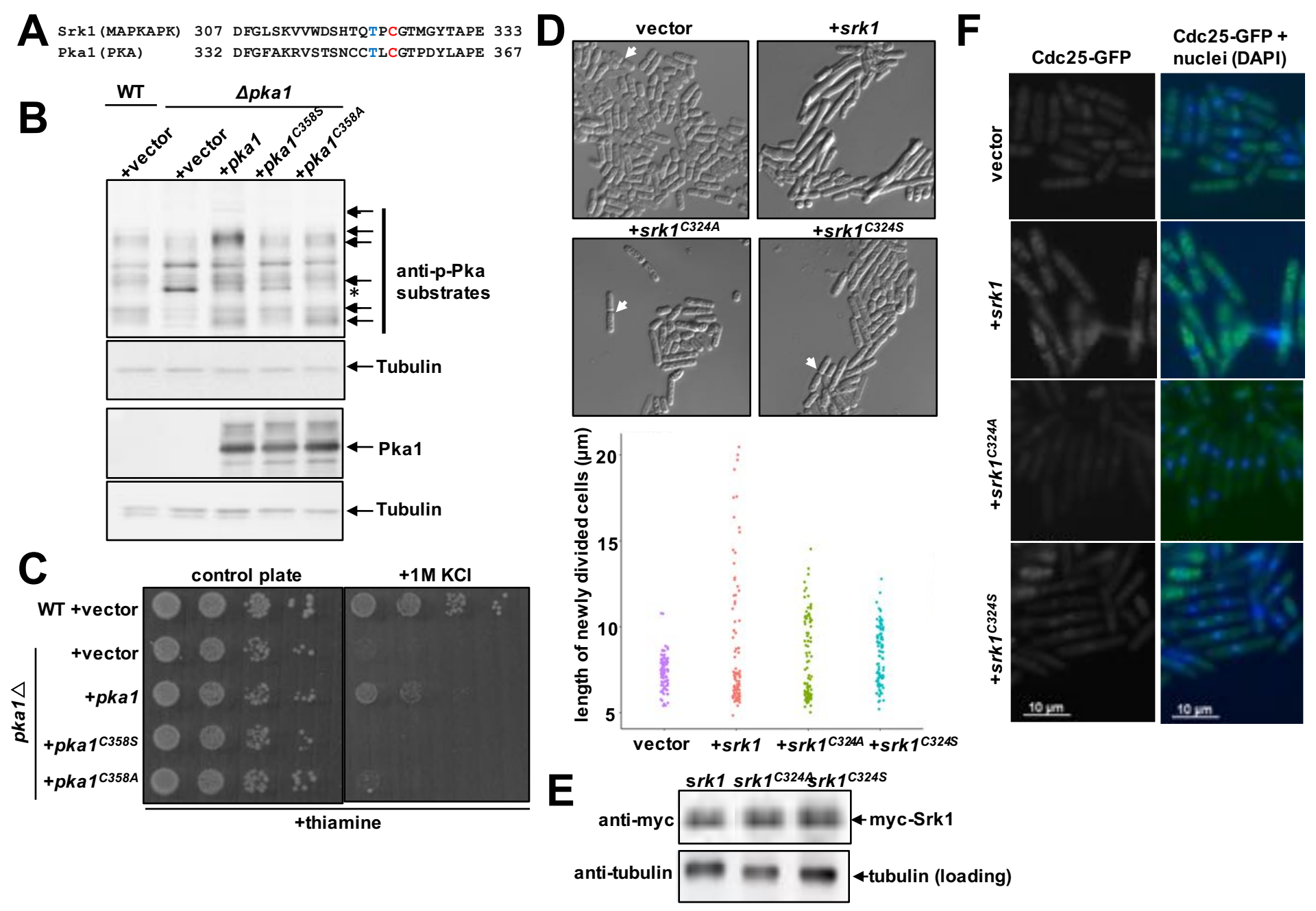
A
Srk1(MAPKAPK) 307 DFGLSKVVWDSHTQTPCGTMGYTAPE 333
Pka1(PKA) 332 DFGFAKRVSTSNCCTLCGTPDYLAPE 367
B
WT
Δpka1
+vector
+vector
+pka1
+pka1C358S
+pka1C358A
anti-p-Pka substrates
Tubulin
Pka1
Tubulin
C
control plate
+1M KCl
WT +vector
+vector
+pka1
+pka1C358S
+pka1C358A
pka1△
+thiamine
D
vector
+srk1
+srk1C324A
+srk1C324S
length of newly divided cells (μm)
20
15
10
5
vector
+srk1
+srk1C324A
+srk1C324S
E
srk1 srk1C324A srk1C324S
anti-myc
myc-Srk1
anti-tubulin
tubulin (loading)
F
Cdc25-GFP
Cdc25-GFP + nuclei (DAPI)
vector
+srk1
+srk1C324A
+srk1C324S
10 μm
10 μm

Figure 6

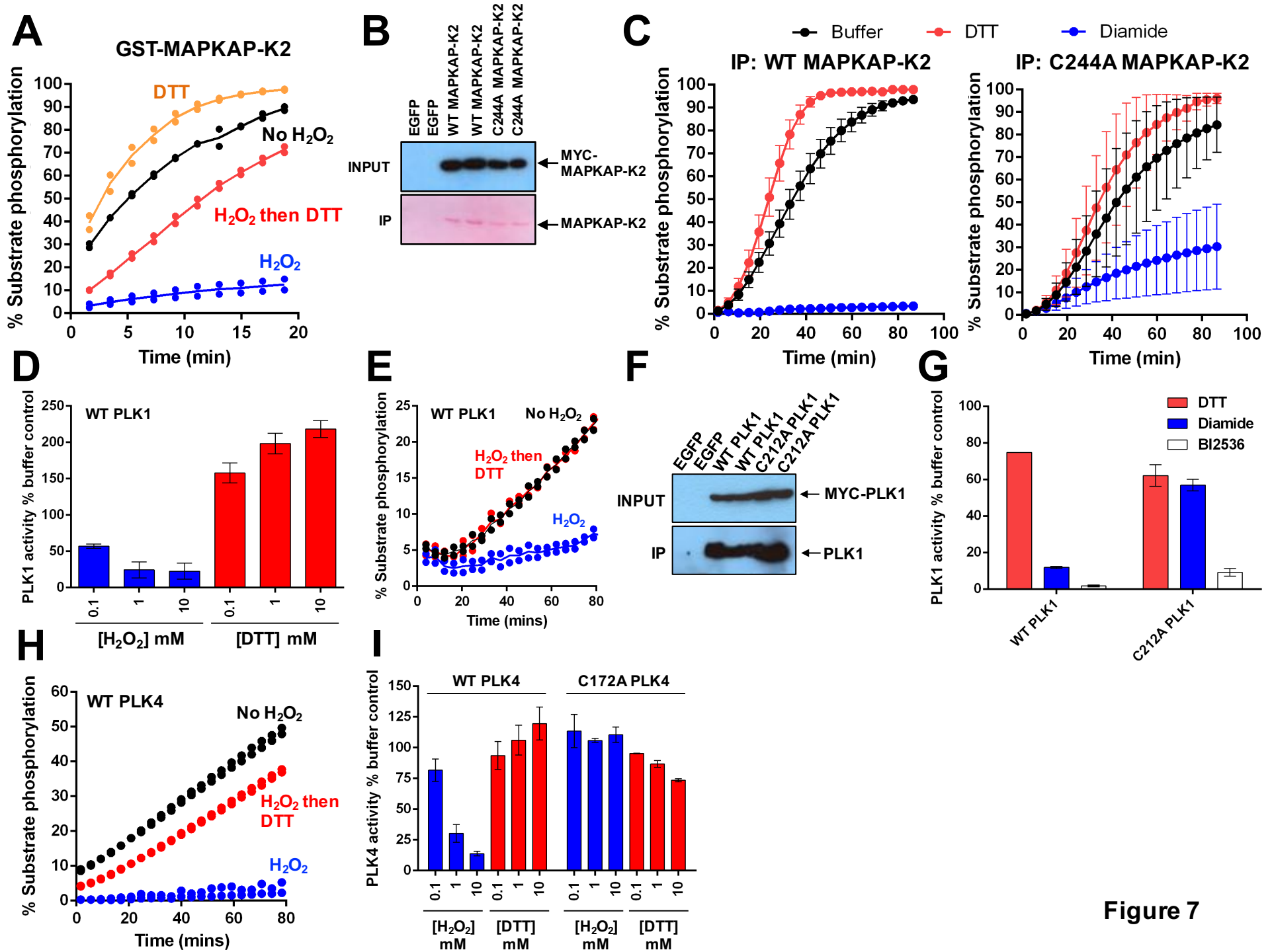
A
GST-MAPKAP-K2
% Substrate phosphorylation
Time (min)
DTT
No H2O2
H2O2 then DTT
H2O2
B
EGFP
EGFP
WT MAPKAP-K2
WT MAPKAP-K2
C244A MAPKAP-K2
C244A MAPKAP-K2
INPUT
IP
MYC-MAPKAP-K2
MAPKAP-K2
C
Buffer
DTT
Diamide
IP: WT MAPKAP-K2
IP: C244A MAPKAP-K2
% Substrate phosphorylation
Time (min)
D
WT PLK1
PLK1 activity % buffer control
[H2O2] mM
[DTT] mM
E
WT PLK1
No H2O2
H2O2 then DTT
H2O2
% Substrate phosphorylation
Time (mins)
F
EGFP
EGFP
WT PLK1
WT PLK1
C212A PLK1
C212A PLK1
INPUT
IP
MYC-PLK1
PLK1
G
DTT
Diamide
BI2536
PLK1 activity % buffer control
WT PLK1
C212A PLK1
H
WT PLK4
No H2O2
H2O2 then DTT
H2O2
% Substrate phosphorylation
Time (mins)
I
WT PLK4
C172A PLK4
PLK4 activity % buffer control
[H2O2] mM
[DTT] mM
[H2O2] mM
[DTT] mM

Figure 7

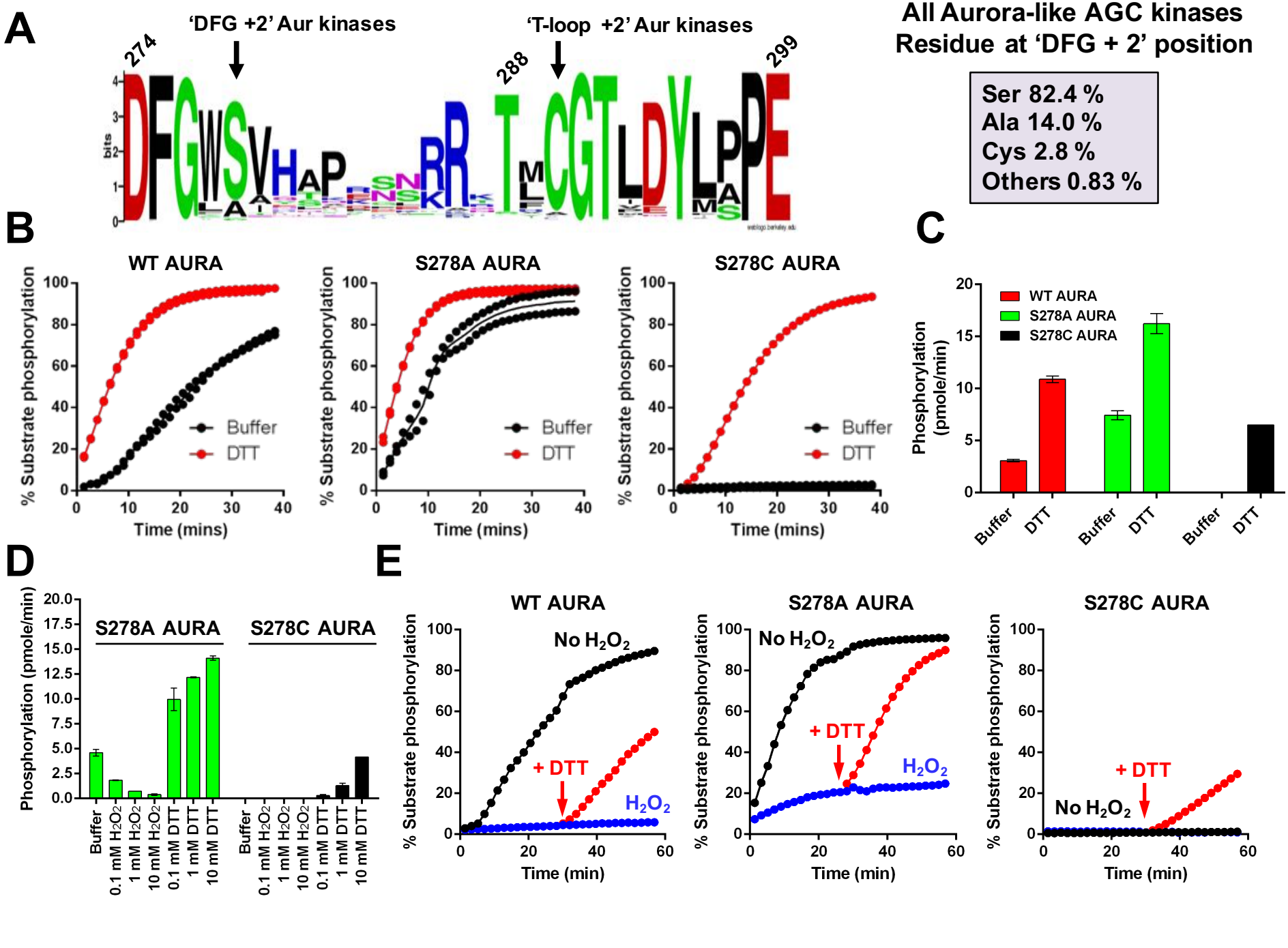
A
'DFG +2' Aur kinases
'T-loop +2' Aur kinases
274
288
299
bits
All Aurora-like AGC kinases
Residue at 'DFG + 2' position
Ser 82.4 %
Ala 14.0 %
Cys 2.8 %
Others 0.83 %
B
WT AURA
S278A AURA
S278C AURA
% Substrate phosphorylation
Time (mins)
Buffer
DTT
C
Phosphorylation (pmole/min)
WT AURA
S278A AURA
S278C AURA
Buffer
DTT
D
S278A AURA
S278C AURA
Phosphorylation (pmole/min)
Buffer
0.1 mM H2O2
1 mM H2O2
10 mM H2O2
0.1 mM DTT
1 mM DTT
10 mM DTT
E
WT AURA
S278A AURA
S278C AURA
% Substrate phosphorylation
Time (min)
No H2O2
+ DTT
H2O2

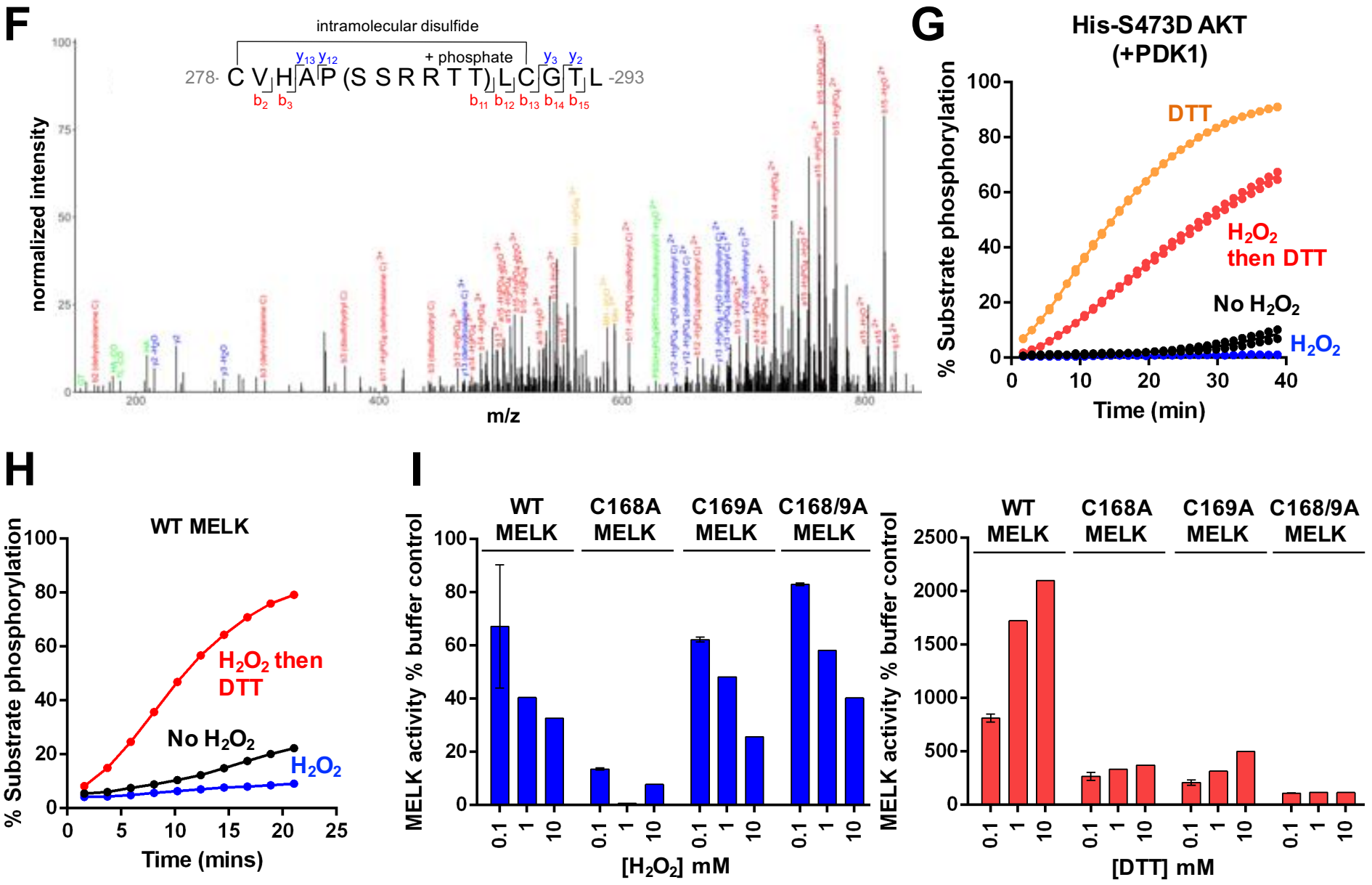
F
intramolecular disulfide
+ phosphate
278- C V H A P (S S R R T T) L C G T L -293
normalized intensity
m/z
G
His-S473D AKT
(+PDK1)
% Substrate phosphorylation
DTT
H2O2 then DTT
No H2O2
H2O2
Time (min)
H
WT MELK
% Substrate phosphorylation
H2O2 then DTT
No H2O2
H2O2
Time (mins)
I
WT MELK
C168A MELK
C169A MELK
C168/9A MELK
MELK activity % buffer control
[H2O2] mM
[DTT] mM

Figure 8

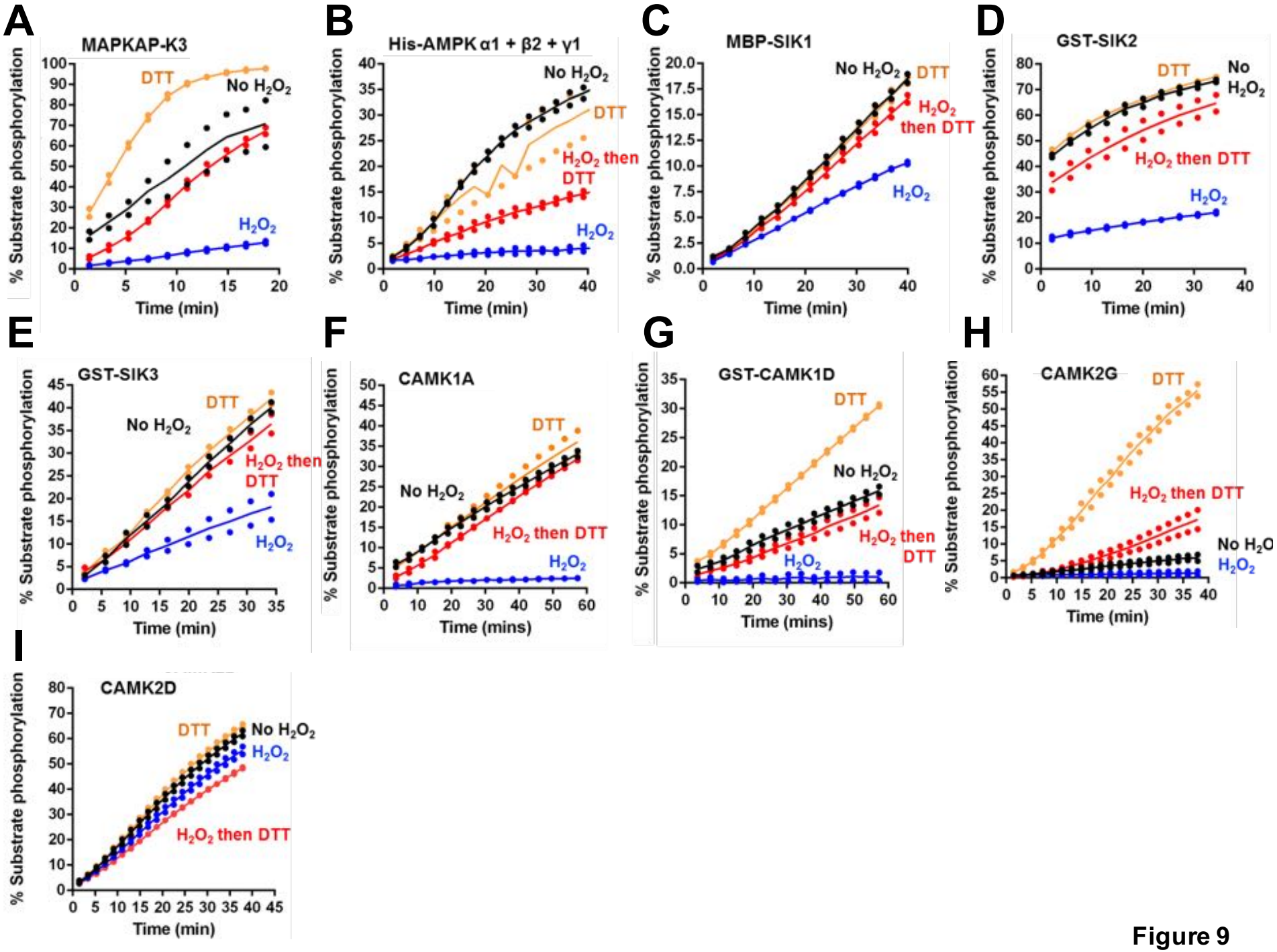
A
MAPKAP-K3
% Substrate phosphorylation
Time (min)
DTT
No H_2O_2
H_2O_2
B
His-AMPK α1 + β2 + γ1
% Substrate phosphorylation
Time (min)
No H_2O_2
DTT
H_2O_2 then DTT
H_2O_2
C
MBP-SIK1
% Substrate phosphorylation
Time (min)
No H_2O_2
DTT
H_2O_2 then DTT
H_2O_2
D
GST-SIK2
% Substrate phosphorylation
Time (min)
DTT
No H_2O_2
H_2O_2 then DTT
H_2O_2
E
GST-SIK3
% Substrate phosphorylation
Time (min)
DTT
No H_2O_2
H_2O_2 then DTT
H_2O_2
F
CAMK1A
% Substrate phosphorylation
Time (mins)
DTT
No H_2O_2
H_2O_2 then DTT
H_2O_2
G
GST-CAMK1D
% Substrate phosphorylation
Time (mins)
DTT
No H_2O_2
H_2O_2 then DTT
H_2O_2
H
CAMK2G
% Substrate phosphorylation
Time (min)
DTT
H_2O_2 then DTT
No H_2O
H_2O_2
I
CAMK2D
% Substrate phosphorylation
Time (min)
DTT
No H_2O_2
H_2O_2
H_2O_2 then DTT

Figure 9